



# HHS Public Access

Author manuscript

*IEEE Trans Ultrason Ferroelectr Freq Control*. Author manuscript; available in PMC 2020 March 02.

Published in final edited form as:

*IEEE Trans Ultrason Ferroelectr Freq Control*. 2020 March ; 67(3): 454–482. doi:10.1109/TUFFC.2019.2947755.

## Mechanisms of Interaction of Ultrasound with Cancellous Bone: A Review

**Keith A. Wear [Senior Member, IEEE]**

U.S. Food and Drug Administration, Silver Spring, MD, 20993

### Abstract

Ultrasound is now a clinically-accepted modality in the management of osteoporosis. The most common commercial clinical devices assess fracture risk from measurements of attenuation and sound speed in cancellous bone. This review discusses fundamental mechanisms underlying the interaction between ultrasound and cancellous bone. Because of its two-phase structure (mineralized trabecular network embedded in soft tissue—marrow), its anisotropy, and its inhomogeneity, cancellous bone is more difficult to characterize than most soft tissues. Experimental data for the dependences of attenuation, sound speed, dispersion, and scattering on ultrasound frequency, bone mineral density, composition, microstructure, and mechanical properties are presented. The relative roles of absorption, scattering, and phase cancellation in determining attenuation measurements *in vitro* and *in vivo* are delineated. Common speed of sound metrics, which entail measurements of transit times of pulse leading edges (to avoid multipath interference), are greatly influenced by attenuation, dispersion, and system properties including center frequency and bandwidth. However, a theoretical model has been shown to be effective for correction for these confounding factors *in vitro* and *in vivo*. Theoretical and phantom models are presented to elucidate why cancellous bone exhibits negative dispersion, unlike soft tissue, which exhibits positive dispersion. Signal processing methods are presented for separating “fast” and “slow” waves (predicted by poro-elasticity theory and supported in cancellous bone) even when the two waves overlap in time and frequency domains. Models to explain dependences of scattering on frequency and mean trabecular thickness are presented and compared with measurements. Anisotropy, the effect of the fluid filler medium (marrow *in vivo* or water *in vitro*), phantoms, computational modeling of ultrasound propagation, acoustic microscopy, and nonlinear properties in cancellous bone are also discussed.

### Keywords

cancellous bone; ultrasound; bone sonometry; osteoporosis

### I. INTRODUCTION

IN 1984, Langton *et al.* published the finding that ultrasonic attenuation in calcaneus (heel bone) *in vivo* has a strong correlation with bone mineral content, an important determinant of fracture risk [1]. This seminal finding launched a worldwide effort to investigate the

characterization of cancellous bone with ultrasound. Cancellous bone (a.k.a. trabecular bone or spongy bone) consists of a mineralized, porous trabecular network embedded in bone marrow, with filament-like trabeculae tending to align roughly along loading directions. It is mostly found in calcaneus, vertebrae, and in medullary cavities near the ends of tubular bones. Cancellous bone is surrounded by a denser, less-porous shell of cortical bone. Fig. 1 shows a human calcaneus with lateral cortical endplates removed. Fig. 2 shows human cancellous femur.

Early ultrasound studies in bone focused on the calcaneus rather than other skeletal sites such as hip and spine, where the most serious osteoporotic fractures occur. There are many reasons to support this approach.

First, the calcaneus is accessible to interrogation from two opposite sides, has relatively simple shape, and has minimal surrounding soft tissue. These features make it a more practical target for through-transmission measurements than other skeletal sites. (Through-transmission measurements use one transducer as a transmitter and a second, opposing, co-axially-aligned transducer on the other side of the bone as a receiver.)

Second, the calcaneus contains approximately 90% cancellous bone and 10% cortical bone [2] (see Fig. 1). Because of high surface area to bone matrix volume ratio, cancellous bone exhibits faster loss than cortical bone at the onset of unbalanced bone remodeling associated with osteoporosis [3]. Therefore, skeletal sites rich in cancellous bone would be expected to reflect changes due to osteoporosis earlier than other skeletal sites.

Third, the calcaneus is a weight-bearing bone that is thought to experience a mechanical environment similar to clinically important sites such as hip and spine [2].

Finally, an important prospective x-ray study involving 8134 women established that bone density at the calcaneus is a strong indicator of risk of hip fracture (the most debilitating kind of osteoporotic fracture), superior to bone density at the radius and spine (but of course inferior to bone density at the proximal femur) [4].

Clinical utility for through-transmission ultrasound to assess hip fracture risk was established by studies in the mid-1990s [5, 6]. This led to the development of commercial, clinical bone sonometers based on the through-transmission geometry. Now, calcaneal bone sonometry is recognized by major professional organizations as effective in the management of osteoporosis [7, 8].

Future development of medical ultrasound technology involving bone (including but not limited to devices for measuring fracture risk) would benefit from a comprehensive understanding of the mechanisms of the interaction between ultrasound and cancellous bone. With this motivation, the present paper attempts to summarize the current state of knowledge on physical interpretation of ultrasound measurements in cancellous bone. The emphasis is on human cancellous bone, but examples in other species are considered. This topic is more than vast enough to fill a review paper of this size. Therefore, the interaction of ultrasound with cortical bone [9–11] and skull [12–14] is left to others. In addition, comprehensive

discussions of clinical diagnostic findings [15] and therapeutic applications [16, 17] in bone may be found elsewhere.

## II. ATTENUATION

### A. Metrics for Attenuation

Attenuation coefficient is a frequency-dependent material property that describes losses due to absorption and scattering. Attenuation coefficient and speed of sound (SOS) are usually measured in through-transmission. One transducer transmits a broadband pulse into the bone. A second, opposing, co-axially-aligned transducer receives the attenuated signal that passed through the bone. In addition, a calibration measurement is performed with only water between the two transducers. Complex amplitude spectra are usually obtained by applying the Fast Fourier Transform (FFT) to digitized radio-frequency (RF) signals. If  $f$  is frequency,  $X(f)$  is the calibration amplitude spectrum,  $Y(f)$  is the amplitude spectrum of the signal propagated through bone, and attenuation in water is neglected, then [18]

$$20\log\left|\frac{X(f)}{Y(f)}\right| = \alpha_s(f)d - 10\log\left|T_{ws}^I(f)\right| \left|T_{sw}^I(f)\right| \quad (1)$$

where  $T_{ws}(f)$  and  $T_{sw}(f)$  are intensity transmission coefficients at water-sample and sample-water interfaces,  $\alpha_s(f)$  is the attenuation coefficient in dB per unit length, and  $d$  is the sample thickness.

This substitution technique assumes that the effects of beam diffraction are identical for the two measurements and therefore cancel out when the spectral ratio is taken. This assumption gets weaker as the difference in sound speed between the bone sample and water increases. A diffraction correction method to account for sound speed mismatch has been developed [19, 20]. This effect has been shown to be significant for attenuation and velocity metrics in samples with velocity exceeding 2000 m/s [19–21] but small for attenuation ( $\pm 0.05$  dB/cm) and phase velocity ( $\pm 1$  m/s) in typical cancellous bone samples [21].

The slope of a linear fit of  $20\log[X(f)/Y(f)]$  vs.  $f$  over the usable frequency band of the ultrasound measurement system (*e.g.*, 300 kHz – 700 kHz) is known as broadband ultrasound attenuation (BUA) [22]. Normalized BUA or nBUA is BUA divided by sample thickness  $d$  [22]. Typical units for BUA and nBUA are dB/MHz and dB/cmMHz respectively.

Often the frequency dependences of transmission coefficients may be neglected over the experimental frequency band, especially for *in vitro* experiments in which the surfaces of pure cancellous bone samples are machined to be approximately planar. With this assumption, nBUA gives the slope of the attenuation coefficient, which is an intrinsic material property. BUA is not an intrinsic material property because it is the product of nBUA and bone thickness  $d$ . However, since fracture risk is negatively correlated with both nBUA and bone thickness, the product makes an effective clinical fracture risk predictor.

The range of frequencies for the BUA measurement may be enhanced using coded excitation [23]. BUA images of calcaneus *in vivo* have been shown to be feasible [24–27].

Cortical endplates have been reported to increase nBUA by an average of 13% [22] and BUA by an average of 15% [28] in human calcaneus. Algorithms have been proposed to compensate for the effects of cortical endplates [28–30].

While calcaneus is the most straightforward site for measurement of BUA, BUA can also be measured at the femur [31–33]. Many commercial clinical devices measure BUA in calcaneus [2, 9, 34].

An alternative attenuation metric, frequency-modulated attenuation (FMA) is also measured in through-transmission mode. Instead of using broadband ultrasound pulses, FMA uses linear-frequency-swept signals.  $FMA = 10 \log (E_r / E_b)$  where  $E_r$  and  $E_b$  are time-integrals for the squared through-transmission signal envelopes for reference (*i.e.*, water-only) and bone measurements [35, 36].

For *in vivo* measurements, there is uncertainty in  $d$  because bones (*e.g.*, calcaneus) are surrounded by soft tissue. However,  $d$  can be estimated by performing pulse-echo measurements with both transducers in addition to through-transmission measurements [37–40].

## B. Attenuation vs. Frequency

Many publications have reported that attenuation coefficient in human calcaneus varies approximately linearly with frequency in a clinical range of about 300–600 kHz [1, 41–44]. Over broader frequency ranges, attenuation coefficient can show deviations from linear frequency dependence in human cancellous calcaneus *in vitro* [45–48], as shown in Fig. 3. For example, attenuation coefficient from 0.2–1.7 MHz has been reported to be proportional to  $f^{1.09 \pm 0.3}$  in 14 human cancellous calcaneus specimens *in vitro* [45]. Even over a clinical range (300–700 kHz), polynomial fits of attenuation coefficients as functions of frequency showed quadratic coefficients statistically different from zero in 12 of 30 human cancellous calcaneus samples *in vitro* [48]. A higher degree of nonlinearity has been reported in human cancellous femur and tibia, with rate of change of attenuation coefficient (dB/cmMHz) higher below 1 MHz and lower above 1 MHz [49].

## C. Attenuation vs. BMD and Composition

In studies on human cancellous calcaneus [50–54], vertebrae [55], femur [49, 56, 57] and tibia [49, 58] *in vitro*, the median and mean  $\pm$  standard deviation of the squared correlation coefficient between nBUA and site-matched, volumetric bone mineral density (BMD) near the clinical range of frequencies are  $r^2 = 0.71$ ,  $0.67 \pm 0.10$ . A similar value,  $r^2 = 0.69$ , has been reported for intact human femur *in vitro* [59, 60].

In studies in human calcaneus *in vivo* [43, 44, 61–64], the median and mean  $\pm$  standard deviation of the squared correlation coefficient between BUA and site-matched, areal BMD (volumetric BMD multiplied by thickness) near the clinical range of frequencies are  $r^2 = 0.53$ ,  $0.56 \pm 0.08$ .

In another study in human calcaneus *in vivo*, BUA correlated positively and linearly with areal BMD only in calcanei of low or moderate density ( $r^2 = 0.72$ ). At high levels of BMD,

BUA plateaued or possibly declined with increasing BMD, as shown in Fig. 4. When calcaneal areas of low and high areal BMD were included, the relationship between BMD and BUA was best described by a second-order polynomial ( $r^2 = 0.62$ ) [65]. This behavior is consistent with earlier measurements of nBUA in human and bovine cancellous bone *in vitro*, which exhibited a parabolic relationship with porosity with a maximum value near 75% [66–68].

Two studies found that demineralization (by treating bone with nitric acid [42] or EDTA [58]) significantly reduced bovine cancellous femur BUA (300–800 kHz) [42] and human cancellous tibia nBUA (0.5–2 MHz) [58] *in vitro*. However, another study, in which no active demineralization was applied, found no significant correlation between nBUA (1–2.8 MHz) and bone mineral content (normalized to the calcified matrix volume) in human cancellous tibia and femur *in vitro* [69]. The lack of significant correlation may have been partially due to the relatively low natural variation of mineral content in the samples (8.8%) [69] and also to the complex parabolic relationship between BUA/nBUA and BMD mentioned above [65].

One study found that decollagenization (by treating bone with sodium hypochlorite) significantly increased nBUA (0.5–2 MHz) in human cancellous tibia *in vitro* [58]. However, another study, in which no active decollagenization was applied, found no significant correlation between nBUA (1–2.8 MHz) and calcified matrix collagen (normalized to the calcified matrix volume) in human cancellous tibia and femur *in vitro* [69]. The lack of significant correlation may have been partially due to the relatively low natural variation of collagen content in the samples (11.2%) [69].

One study found a significant negative correlation ( $r = -0.47$ ) between nBUA (1–2.8 MHz) and fat content in human cancellous tibia and femur *in vitro* but no significant correlations between nBUA and water content or proteoglycan content [69].

The studies discussed in this section and throughout this review paper include measurements on human and animal cancellous bone. Animal cancellous bone studies provide a useful complement to human cancellous bone studies because they extend ranges of BMD and bone volume fraction to higher values than found in humans. However, because animal bone (particularly bovine bone) can be considerably denser than human bone, trends observed in animal bone do not always exactly match trends observed in human bone.

#### D. Attenuation vs. Microstructure

Histomorphometric analysis of 3D micro-computed tomography ( $\mu$ CT) scans of cancellous bone samples can provide descriptive parameters such as the ratio of bone volume to total volume (BV/TV), mean trabecular thickness (Tb.Th), mean trabecular separation (Tb.Sp), trabecular number (Tb.N), degree of anisotropy (DA), and structural model index (SMI) [70, 71]. While BV/TV is mostly an indication of bone quantity, the other parameters describe trabecular microstructure. Fig. 5 shows steps involved in analyzing human cancellous calcaneus with ultrasound and  $\mu$ CT. Fig. 6 shows a  $\mu$ CT reconstruction of a rectangular volume from a human calcaneus sample. High resolution peripheral CT (HR-pQCT) may be used to analyze microstructure in the distal radius and tibia *in vivo* [72–74].

Investigators have found many significant correlations between QUS parameters and histomorphometric parameters in human cancellous bone. In addition, many have compared univariate regression models of QUS vs. a measure of bone quantity (*e.g.*, apparent density, BMD, or BV/TV) with multiple regression models of QUS vs. bone quantity and histomorphometric parameters. This analysis offers insight into the added variance of QUS parameters explained by microstructure beyond that explained by bone quantity alone. This has implications regarding additional diagnostic information that QUS could provide beyond BMD, the standard clinical measurement.

In multiple regression studies on human cancellous vertebrae [55, 75], calcaneus [52, 53, 75, 76], tibia [77] and femur [57, 77], the median for the squared correlation coefficient between nBUA and site-matched, bone quantity (*e.g.*, BV/TV) near the clinical range of frequencies is  $r^2 = 0.75$ . In these studies, the median value for the added variance of nBUA,  $\Delta r^2$ , explained by microstructure is 0.07.

FMA has been shown to be useful for investigating microstructure of ovine [35] and bovine [36] cancellous femur.

### E. Attenuation vs. Mechanical Properties

Mechanical properties of cancellous bone are important because they are closely related to fracture risk, the primary clinical endpoint [78–82]. Cancellous bone contains hydroxyapatite mineral and fibrous collagen components that team up to create an adaptive and flexible structure to withstand a variety of loading conditions. Correlations between QUS parameters (which may be measured *in vivo*) and mechanical properties in cancellous bone (which are usually measured *ex vivo*) are of interest for diagnostic applications.

Mechanical testing is the most widely-accepted method for measuring mechanical properties on specimens but is impractical *in vivo*. Mechanical testing of cancellous bone specimens often entails preconditioning with low-amplitude cyclic compression followed by compression to approximately 5% strain in order to generate a stress-strain curve, from which mechanical parameters such as Young's modulus, yield stress, yield strain and ultimate strength, may be derived [49, 83].

Finite element analysis (FEA) based on high-resolution 3D image data is also effective for estimating mechanical properties on bone specimens [80, 84]. (Although  $\mu$ CT is the most common imaging modality to provide input data for FEA, ultrasound tomography has also been shown to be effective for estimating stiffness in cancellous bone replica models [85].)

In studies on human cancellous calcaneus [22, 86, 87], femur [49, 88] and tibia [49, 88] specimens, the median and mean  $\pm$  standard deviation of the squared correlation coefficient between nBUA and mechanical parameters (*e.g.*, Young's modulus, ultimate strength) are  $r^2 = 0.60, 0.57 \pm 0.14$ . Fig. 7 shows a scatter plot of log strength vs. log nBUA in human calcaneus *in vitro*. Lower correlations have been reported for bovine cancellous femur [83].

In order to investigate the sensitivity of BUA to elastic properties, BUA was measured with 1 MHz transducers in human cancellous calcaneus cores before and after destructive testing that reduced elastic modulus without significant changes to porosity or microstructure [89].

BUA decreased by less than 2% despite decreases in elastic modulus greater than 75%. The investigators concluded that BUA is not directly sensitive to elastic properties of human calcaneus and therefore empirical correlations between BUA and elastic properties must be due to correlations among microstructure, porosity, elastic properties and BUA in undamaged cancellous bone [89, 90].

## F. Mechanisms of Attenuation

Sources of measured attenuation (*e.g.*, BUA or nBUA) include absorption, longitudinal-longitudinal (LL) scattering, longitudinal-shear (LS) scattering, and phase cancellation. A discussion of the role of scattering in determining attenuation is deferred to the section on scattering (Sec. V). However, phase cancellation can be treated here.

The importance of phase cancellation can be assessed by comparing measurements of attenuation performed using phase sensitive (PS) and phase insensitive (PI) methods [18, 44, 91–95]. Fig. 8 shows measurements of BUA assessed by PS and PI methods in 73 women [44]. For BUA < 75 dB/MHz, the two measures are approximately equal, suggesting that phase cancellation at the receiving transducer is negligible. However, for BUA > 75 dB/MHz, the PS values are much greater than PI values, suggesting the phase cancellation at the receiving transducer is substantial. A similar trend has been reported for nBUA in human calcaneus *in vitro*, with a break point near 15 dB/cmMHz [94]. As BUA (or nBUA) increases, scattering also increases and creates more opportunity for phase cancellation and therefore greater discrepancy between PS and PI BUA (or nBUA). Phase cancellation has also been demonstrated in sheep femoral trabecular bone by comparing PS and PI BUA [95] with difference increasing with frequency.

One model for phase cancellation represents the ultrasound beam as a set of parallel “sonic rays,” propagating through a medium with two components with contrasting sound speeds (trabecular bone and marrow) [96]. The transit time of each ray is determined by the proportion of bone and marrow in the path of the ray. The transit time spectrum describes the proportion of sonic rays at a particular transit time [97]. Phase cancellation in this model results from sonic rays with different transit times and therefore different phase shifts. A deconvolution algorithm to recover transit time spectra has been validated in cancellous bone replica samples [98, 99]. The transit time spectrum has been shown to be very effective for predicting solid volume fraction of simplified bone / marrow replica models consisting of acrylic and water [100]. In addition, bone volume fraction obtained from the transit time spectrum has been shown to be effective for estimation of mechanical stiffness and failure load in human cancellous femur *in vitro* [101].

## III. SPEED OF SOUND

### A. Metrics for Speed of Sound

In general, velocity may be described by phase velocity (velocity of a single-frequency component as a function of frequency), group velocity (velocity of the center of a pulse), and signal velocity (velocity of the leading edge of a pulse) [102]. “Speed of sound” (SOS) is measured in through-transmission. One transducer transmits a broadband pulse into the

bone. A second, opposing, co-axially-aligned transducer receives the attenuated signal that passed through the bone. In addition, a calibration measurement is performed with only water between the two transducers. SOS is often computed from

$$SOS = \frac{c_w}{1 + \frac{c_w \Delta t}{d}} \quad (2)$$

where  $c_w$  is the acoustic velocity in water.  $\Delta t$  is the difference in transit times of the two pulses, and  $d$  is the thickness of the sample. As mentioned in Sec. II, diffraction-related errors due to speed-of-sound mismatch [20] in the substitution experiment are small for typical cancellous bone samples ( $\pm 1$  m/s) [21].

A marker on the pulse (*e.g.*, a zero crossing) is chosen to measure transit times. The same marker is chosen for bone measurement and calibration (*i.e.*, water only) measurement. Markers are often chosen near the leading edge in order to avoid multipath interference (*e.g.*, forward scattering, refraction, reverberations in cortical plates, multiple scattering). Several investigators have reported that the SOS measurement in cancellous bone depends on marker location with higher values near the leading edge and lower values near the trailing edge *in vitro* [103–107], *in vivo* [108], and in simulation [109]. The main reason for this is that frequency-dependent attenuation (which is a low-pass filter) stretches the attenuated signal in time and causes  $\Delta t$  to depend on marker choice and the extent of pulse spreading [106, 110], as shown in Fig. 9. This is a small effect in soft tissues but a much bigger effect in bone because the attenuation coefficient is much larger, leading to greater pulse spreading [106]. This phenomenon has been studied theoretically in soft tissues that were assumed to be non-dispersive [110] and more generally in dispersive media including bone [106]. In Fig. 9, the black bar on the time axis represents the mean  $\pm$  one standard deviation of marker locations from 43 studies that used the following markers: first detectable deviation from zero (L3) [53, 58, 88, 104, 105, 111–119], thresholding at 3 times the noise standard deviation [120], thresholding at 10–20% of the first rising half cycle [49, 69, 77, 105, 119, 121–123], thresholding at 10% of maximum amplitude [124], first maximum [40, 124–126], “first” zero crossing (L2) [31, 32, 55, 75, 76, 89, 104, 105, 119, 122, 124, 127–131], “second” zero crossing (L1) [39, 51, 83, 104, 132], and envelope maximum [51, 83, 124, 130, 133–135]. See Table II.

It can be shown that the dependence of SOS on marker choice and other experimental parameters is approximately given by [107, 108]

$$SOS_n - c_g \approx - \frac{\tau_n c_g^2 \sigma_f^2 \beta}{f_0^2} \frac{1}{1 - (\sigma_f^2 \beta d / f_0)} \quad (3)$$

where the subscript  $n$  denotes a transit-time marker choice (*e.g.*, a zero crossing such as L3 in Fig. 9),  $c_g$  is the group velocity,  $\beta$  is the slope of attenuation coefficient with respect to frequency (analogous to *nBUA*),  $f_0$  is the center frequency, and the calibration signal is assumed to have a Gaussian amplitude spectrum proportional to  $\exp[-(f - f_0)^2 / 2\sigma_f^2]$ . The time variable  $\tau_n$  is the time lag between the transit-time marker ( $n$ ) and the envelope



maximum measured in units of the calibration waveform period ( $T_0 = 1/f_0$ ) (see Table I and Fig. 9).

Eq. (3) suggests that SOS depends not only on a true velocity property ( $c_g$ ) but also on confounding variables such as  $\tau_n$ ,  $f_0$ ,  $\sigma_f$ ,  $\beta$ , and  $d$ . These confounding variables complicate the physical interpretation of SOS measurements and cause difficulties in comparisons of data from different investigations. This likely contributes to the disparity in SOS measurements seen in clinical bone sonometers [136, 137], suggesting the potential benefit of standardization [34, 108, 137].

Fig. 10 shows how (3) applied to data from 73 women *in vivo* compensates for confounding variables to provide more consistent SOS measurements [108]. Since  $\beta$  increases with BMD (see Section II), (3) shows that differences between SOS measurements and group velocity increase with BMD. Therefore, Eq. (3) explains why the correlation between SOS and BMD has been found to increase as marker location moves from the center of the pulse toward the leading edge in human femur [124, 130]. A more general formula than (3) that includes the effects of dispersion is available [106, 138].

Cortical endplates have been reported to introduce a 2% increase in SOS measurements in human calcaneus [112].

## B. Model for Velocity

At 50 kHz, measurements of SOS in bovine cancellous femur have been shown to be predicted well (correlation coefficient squared  $r^2 = 0.94$ ) by bar wave theory [139–141], which is valid at low frequencies such that the wavelength is much greater than both the pore size and the lateral dimensions of the specimen [90, 111]

$$SOS_{bar} = \sqrt{\frac{E}{\rho}} \quad (4)$$

where  $SOS_{bar}$  is the bar wave velocity,  $E$  is Young's modulus, and  $\rho$  is mass density. At a more clinically relevant frequency of 1 MHz, SOS in 18 bovine cancellous femur samples (if longitudinal waves are measured instead of bar waves) has been fit to a linear function of the form  $SOS = A + B(E/\rho)^{1/2}$  with a squared correlation coefficient of  $r^2 = 0.85$  but with a nonzero intercept  $A$  near 1400 m/s [111]. Similarly, at 1.25 MHz, SOS in equine cancellous vertebrae,  $r^2 = 0.94$  and an intercept  $A$  also near 1400 m/s have been reported [126].

## C. Phase Velocity vs. Frequency (Dispersion)

Like SOS, phase velocity,  $c(f)$ , is often measured in through-transmission experiments. Unlike SOS, phase velocity measurement requires Fourier transformation of the digitized through-transmission signals. Phase velocity is computed from [142, 143]

$$c(f) = \frac{c_w}{1 - \frac{c_w \Delta\phi(f)}{2\pi f d}} \quad (5)$$

where  $f$  = frequency, and  $\Delta\phi(f)$  is the phase shift between the bone measurement and the calibration measurement. The equation for phase velocity (5) is often reported with a plus sign instead of a minus sign in the denominator. The ambiguity arises from ambiguity in  $\Delta\phi(f)$ , which may be computed as  $\phi(f) - \phi_w(f)$  or  $\phi_w(f) - \phi(f)$ . Phase velocity has also been measured in cancellous bone using a phase tracking method [144].

The frequency dependence of phase velocity is called dispersion. Dispersion is generally positive in soft tissues. (That is, phase velocity increases with frequency). For media with attenuation coefficients that vary linearly with frequency, the Kramers-Kronig relations (which are required for causal systems) imply that [145–147]

$$c(f) = c(f_0) + [c(f_0)]^2 \frac{\beta}{\pi^2} \ln\left(\frac{f}{f_0}\right) \quad (6)$$

Eq. (6) predicts that linearly-attenuating media will exhibit positive dispersion with a logarithmic frequency dependence, consistent with empirical evidence for soft tissues [145].

Unlike soft tissues, cancellous bone exhibits negative dispersion [21, 105, 148–153]. Two explanations for this have been proposed. The first explanation is that apparent negative dispersion arises from the interference of two waves, each of which is positively dispersive [154–157]. The two waves could be the fast and slow waves predicted for poro-elastic media by Biot theory [158, 159] (see Section IV). The second explanation is multiple scattering, which also results in interference of waves. This has been demonstrated analytically [160] and experimentally [161, 162] in phantoms with cylindrical scatterers representing trabeculae. It has also been demonstrated analytically and experimentally using a one-dimensional multiple scattering model called the stratified model in bovine tibia and femur [163], ovine femur [164], and human calcaneus *in vitro* [165]. The “restricted-bandwidth form” of the Kramers-Kronig dispersion relations may be used to improve agreement between measured and theoretical phase velocities in cancellous bone [143].

#### D. SOS vs. BMD and Composition

In studies on human cancellous calcaneus [50–53], vertebrae [6, 55], femur [49, 56, 57] and tibia [49, 58] *in vitro*, the median and mean  $\pm$  standard deviation of the squared correlation coefficient between SOS and site-matched, volumetric BMD near the clinical range of frequencies are  $r^2 = 0.77$ ,  $0.72 \pm 0.12$ . A similar value,  $r^2=0.71$ , has been reported for intact human femur *in vitro* [59, 60]. Fig. 11 shows SOS vs apparent density in bovine cancellous tibia *in vitro* in three orientations.

Three studies found that demineralization (by treating bone with nitric acid [42] or EDTA [58, 126]) significantly reduced bovine cancellous femur SOS (600 kHz) [42], human cancellous tibia SOS (2.25 MHz) [58], and equine cancellous vertebrae (1.25 MHz) [126] *in vitro*. However, another study, in which no active demineralization was applied, found no significant correlation between SOS (2.25 MHz) and bone mineral content (normalized to the calcified matrix volume) in human cancellous tibia and femur *in vitro* [69]. The lack of significant correlation may have been partially due to the relatively low natural variation of mineral content in the samples (8.8%) [69].

One study found that decollagenization (by treating bone with sodium hypochlorite) significantly decreased SOS (2.25 MHz) in human cancellous tibia *in vitro* [58]. However, another study, in which no active decollagenization was applied, found no significant correlation between SOS (2.25 MHz) and calcified matrix collagen (normalized to the calcified matrix volume) in human cancellous tibia and femur *in vitro* [69]. The lack of significant correlation may have been partially due to the relatively low natural variation of collagen content in the samples (11.2%) [69].

One study found a significant negative correlation ( $r = -0.43$ ) between SOS (2.25 MHz) and fat content in human cancellous tibia and femur *in vitro* but no significant correlations between SOS and water content or proteoglycan content [69].

Experiments comparing phase velocity measurements in human cancellous femur *in vitro* obtained using marrow, water, and alcohol as fluid fillers suggest that the phase velocity of the saturating fluid is a primary determinant of phase velocity of the composite structure [166].

#### E. SOS vs. Microstructure

In multiple regression studies on human cancellous vertebrae [55, 75], calcaneus [52, 53, 75, 76], tibia [77] and femur [57, 77], the median for the squared correlation coefficient between SOS and site-matched bone quantity (*e.g.*, BV/TV) near the clinical range of frequencies is  $r^2 = 0.78$ . In these studies, the median for the added variance of SOS,  $\Delta r^2$ , explained by microstructure is 0.04.

#### F. SOS vs. Mechanical Properties

In studies on human cancellous vertebra [167], calcaneus [22, 86, 87], femur [49, 88] and tibia [49, 88] *in vitro*, the median and mean  $\pm$  standard deviation of the squared correlation coefficient between SOS and mechanical parameters (*e.g.*, Young's modulus, ultimate strength) are  $r^2 = 0.46$ ,  $0.48 \pm 0.10$ . In studies in bovine [83, 111, 116] and ovine [132] femur, the median and mean  $\pm$  standard deviation of the squared correlation coefficient between SOS and mechanical parameters are  $r^2 = 0.79$ ,  $0.71 \pm 0.20$ .

In order to investigate the sensitivity of SOS to elastic properties, SOS (1 MHz) was measured in human cancellous calcaneus cores before and after destructive testing that reduced elastic modulus without significant changes to porosity or microstructure [89]. SOS decreased by less than 0.25% despite decreases in elastic modulus greater than 75%. The investigators concluded that SOS is not directly sensitive to elastic properties of human calcaneus and therefore empirical correlations between SOS and elastic properties must be due to correlations among microstructure, porosity, elastic properties and SOS in undamaged cancellous bone [89, 90]. These experiments illustrate limitations in applying the bar equation to cancellous bone at clinical frequencies near 1 MHz [89].

In order to assess mechanical integrity of vertebral cancellous bone *in vivo*, investigators have developed a method to measure SOS from reflections from metallic pins inserted during surgery [168].

## IV. TWO-WAVE PHENOMENON

### A. Biot Theory and Evidence for Fast and Slow Waves

Biot theory predicts that fluid-saturated porous solids can support two longitudinal waves that travel with different velocities [158, 159]. The fast wave is associated with the fluid (blood and marrow) moving in phase with the solid (mineralized trabeculae), and the slow wave is associated with the fluid moving out of phase with the solid [169–172].

Many authors have demonstrated the existence of two longitudinal waves that may correspond to Biot's predictions in bovine cancellous bone in through-transmission experiments *in vitro*, as shown in Fig. 12. Bovine cancellous femur [173] and tibia [114] specimens *in vitro* can support a low-amplitude fast wave and a higher amplitude slow wave when ultrasound propagates approximately parallel to the predominant trabecular orientation. Similarly, human cancellous vertebrae can support fast and slow waves *in vitro* when propagation is along the craniocaudal axis [55]. Human cancellous femur can support fast and slow waves *in vitro* in the main load direction [122]. Temporal separation between fast and slow waves can be increased if alcohol is substituted for water as the filling fluid *in vitro* [174].

Properties of fast and slow waves are anisotropic [175, 176], with fast wave velocity achieving its maximum value when propagation is parallel to the predominant trabecular orientation [119, 123, 177], as shown in Fig. 12. Fast and slow waves can be identified even when cortical plates are attached to equine cancellous bone specimens *in vitro* [178, 179]. When ultrasound is transmitted through the radius *in vitro*, three waves can propagate and be distinguished: circumferential wave through radial cortex and surrounding soft tissue, fast and slow waves due to cancellous bone in radial interior [180, 181]. The evolution of fast and slow waves as they propagate through cancellous bone has been investigated *in vitro* by alternately performing through-transmission measurements and cutting thin slices from bone samples [182, 183], as shown in Fig. 13. Fast and slow waves have been observed in 3D printed cancellous bone phantoms based on  $\mu$ CT reconstructions of equine femur [184]. Detection of fast and slow waves can be improved through the use of coded excitation based on Golay code modulation [185].

Fast and slow waves have also been identified *in vivo*, in the human distal radius. It has been reported that fast and slow wave properties *in vivo* yield information regarding cancellous bone microstructure and elasticity [186–188].

There have many studies to test variants of Biot theory and related theories for prediction of fast and slow wave properties in cancellous bone. A complete accounting of these investigations [135, 170, 171, 173–175, 189–220] is beyond the scope of this paper, but a thorough review is available elsewhere [169].

Separation of fast and slow waves can be more difficult in human cancellous calcaneus than other species / skeletal sites mentioned above because it is less anisotropic (and separation is maximum when ultrasound propagates along a clearly-defined trabecular orientation). In addition, human calcaneus has a lower bone volume fraction than found in many animal

skeletal sites (and separation increases with BV/TV as shown in Fig. 8 in [122]). However, Biot theory accurately predicts the dependence of velocity on porosity in human calcaneus [221].

## B. Signal Processing for Separation of Fast and Slow Waves

Separate reconstruction of individual fast and slow waves is challenging when the two waves overlap in time and frequency domains. Several methods proposed for this decomposition, including Bayesian [146, 222–224], modified least-squares Prony’s (MLSP) [225], space alternating generalized expectation maximization (SAGE) [226], MLSP plus curve fitting (MLSP+CF) [227, 228], and adaptive beamforming [229, 230] algorithms, are predicated on a model for the transfer function of the bone specimen that contains terms for fast and slow waves [156, 222]

$$Y(f) = X(f)[H_{fast}(f) + H_{slow}(f)] \quad (7)$$

where  $Y(f)$  and  $X(f)$  are complex amplitude spectra of the signals passing through bone and water-path-only respectively. For the Bayesian and MLSP+CF algorithms, the fast and slow wave transfer functions are

$$H_k(f) = A_k \exp[-\beta_k f d] \exp\left[\frac{i2\pi f d}{c_k(f)}\right] \quad (8)$$

where  $k$  can be “fast” or “slow.”  $A_k$  are frequency-independent wave amplitudes,  $\beta_k$  are slopes of attenuation coefficients (with respect to frequency),  $c_k(f)$  are phase velocities, and  $d$  is the sample thickness [154]. Causality implies that frequency-dependent phase velocities  $c_k(f)$  obey (6). The adaptive beamforming method assumes similar transfer functions  $H_k(f)$  that are augmented with phase rotation parameters that compensate for wave propagation through inhomogeneous media [229].

The Bayesian method maximizes the joint posterior probability for all the wave parameters (magnitudes, attenuation slopes, velocities) given the measured waveform using Markov chain Monte Carlo with simulated annealing [222]. The Bayesian method provides estimates not just of wave parameters but also of probability density functions for those parameters.

The MLSP method employs Prony’s method, which fits a signal (in this case, the sum of fast- and slow-wave transfer functions) to the sum of complex exponentially-modulated sinusoids [225]. The MLSP method assumes nondispersive waves. However, if the outputs of the MLSP method are used as inputs to a curve-fitting routine (MLSP+CF method), then the solution can be constrained to obey the dispersion relation (6) given above [227]. Consequently, the MLSP+CF method has superseded the MLSP method.

The SAGE algorithm begins with “dictionaries” for amplitude and phase that are constructed from the Fourier transform of the reference signal and used to form a good initial guess for the solution. Then, an iterative nonlinear optimization scheme based on the Levenberg-Marquardt algorithm is used to obtain a final solution [226].

Generalized harmonic analysis begins by finding the frequency, amplitude, and phase of the sine wave that best matches the measured signal. It repeats this process on the residual and on subsequent residuals to generate a set of complex sine waves to approximate the measured signal [231].

The multi-channel instantaneous frequency method applies a filter bank to the measured signal and then computes the time-dependent phase of each filter output using a Hilbert transform. The instantaneous frequency is the time derivative of the phase. The multi-channel approach is more stable than the single channel approach when the waveform contains multiple components and/or background noise [232].

The adaptive beam forming method is a two-step process. First, initial estimates of fast and slow waves are performed using frequency-domain interferometry. Second, final estimates are obtained by performing least-squares fitting in the time domain [229, 230].

Although bandlimited deconvolution is not restricted to attenuation coefficients that vary linearly with frequency, it has recovered highly linear attenuation coefficients in bovine cancellous femur as reflected by average correlation coefficients between attenuation coefficients and frequency:  $0.997 \pm 0.002$  (fast wave) and  $0.986 \pm 0.013$  (slow wave) [233]. This finding provides substantial support for the two-wave model (8), which assumes attenuation coefficients that vary linearly with frequency.

There have not been many side-by-side comparisons of the various algorithms applied to the same experimental data. However, bandlimited deconvolution, MLSP+CF, and Bayesian methods gave similar results in bovine cancellous femur samples [228]. In addition, the Bayesian and MLSP+CF algorithms gave similar results in equine cancellous radius [146]. Simulations suggest that the relative performances of MLSP and SAGE depend on parameters of the experiment modeled, with MLSP having a comparative advantage in high signal-to-noise ratio (SNR) conditions and small temporal separation of waves but SAGE having a comparative advantage in low SNR conditions [226].

Most methods require less than 5 s on an ordinary laptop computer [142, 225, 226, 228, 229, 233]. The Bayesian method is more computationally intensive, requiring 100 min on a Sun Enterprise 250 dual 400-MHz workstation or 3 min using 32 processors of an SGI Altix 3000 with Itanium2 processors running at 900 MHz [222]. However, computation times would be expected to decrease as computer technology evolves. In addition, as mentioned previously, the Bayesian method provides estimates not just of wave parameters but also of probability density functions for those parameters.

## V. SCATTERING

### A. Metrics for Scattering

Comprehensive discussions of scattering from cancellous bone have been published previously [234, 235]. Here a more concise presentation (with some recent updates and added emphasis on mechanisms underlying scattering) is given. Fig. 14 shows acquisition of ultrasonic backscatter data from human calcaneus *in vivo* [236].

Scattering from cancellous bone arises from interfaces between the solid mineralized trabecular network and the fluid filler, which is marrow *in vivo* or water *in vitro*. Backscattering may be described quantitatively by the backscatter coefficient, which is defined as follows. If a plane wave  $P_{inc}(f)$  is incident upon a scatterer with backscattering amplitude  $\Phi_b(f)$ , then the scattered wave  $P_{scat}(f)$  measured a distance  $r$  away from the scatterer may be described by [237–241]

$$P_{scat}(r, f) = P_{inc}(f)\Phi_b(f)e^{ikr}/r \quad (9)$$

if  $kr \gg 1$ ,  $ka_s \ll 1$ , and  $a_s$  is the scatterer radius. The backscatter coefficient  $\eta(f)$  from a volume of unresolved scatterers is given by [241]

$$\eta(f) = n_0 |\Phi_b(f)|^2 \quad (10)$$

where  $n_0$  is the number of scatterers per unit volume. It has been assumed that the scatterers are positioned sufficiently randomly in space that phase differences between scattered signals from pairs of scatterers are uniformly distributed between 0 and  $2\pi$  radians. Backscatter measurements are inherently noisier than attenuation and sound speed measurements because they are impacted by varying degrees of constructive and destructive interference from signals scattered by randomly-positioned scatterers [242–244], as is the case with speckle noise in ultrasound B-mode scans [245, 246]. When the number of scatterers (*i.e.* trabeculae) per resolution cell is large enough (so that the central limit theorem applies), it can be shown that the envelope of the backscattered signal obeys a Rayleigh distribution with a characteristic mean to standard deviation ratio of 1.91 [245, 246], which is consistent with measurements in human calcaneus *in vivo* [247] and a model for scattering from thin cylindrical scatterers with randomly varying diameters [248].

Like attenuation coefficient and phase velocity, backscatter coefficient is an intrinsic material property and, if measured properly, exhibits minimal dependence on the measurement system. There are many methods for measurement of ultrasonic backscatter coefficient [237–241, 249, 250]. The average backscatter coefficient over a band of frequencies (usually centered about the transducer resonance frequency) is sometimes called broadband ultrasonic backscatter (BUB).

The backscatter coefficient provides insight into the size and distribution of scatterers. For spherical scatterers that are much smaller than the wavelength, the backscatter coefficient is proportional to frequency to the fourth power [102]. For cylindrical scatterers that are much thinner than a wavelength, the backscatter coefficient is proportional to frequency to the third power [251].

Although the backscatter coefficient is useful for elucidating physical mechanisms underlying the scattering process, it is difficult to measure *in vivo*. Other metrics may not be measurement-system-independent descriptions of scattering properties but still may provide useful diagnostic information. Scattering indexes may be obtained from the apparent backscatter transfer function (ABTF), which is the ratio of the spectrum of backscatter from a gated volume of cancellous bone to the spectrum of an echo from a planar reflector

(usually expressed in dB) [252]. The adjective “apparent” refers to the fact that the signal is not corrected for attenuation or diffraction [253]. Apparent integrated backscatter (AIB) is the average of the ABTF over a band of frequencies that usually corresponds to the usable band of the transducer. The frequency slope of apparent backscatter (FSAB) is the slope of a linear regression of ABTF vs. frequency [253]. AIB and FSAB depend on two time-gate parameters that affect the volume within the tissue that is selected for analysis: gate delay (from the beginning of the bone signal) and gate width, both of which may be optimized [88, 252, 254]. Autoregressive spectral estimation (instead of the Fast Fourier Transform) may be used to improve estimation of ABTF [255]. ABTF has been measured in human cancellous femur at frequencies from 0.6 – 15 MHz [256]. Usage of backscatter difference measurements (that is, differences in parameters derived from near and far windows in the gated backscatter signal) can reduce dependence on transducer properties, beam properties, and the effects of intervening tissues (soft tissue and cortical plates) [257–260]. The integrated reflection coefficient (IRC) is the mean of the frequency-dependent energy reflection coefficient over the range of frequencies corresponding to the usable frequency band of the transducer [49, 69, 83, 88, 261–263]. The backscattered spectral centroid shift (BSCS) describes the frequency downshift in backscattered signals due to the low-pass filter effect of attenuation in cancellous bone [264, 265].

The effects of overlying tissues on scattering metrics can be suppressed using dual-frequency ultrasound measurements [261, 262, 266–268]. The effects of the cortical shell on scattering metrics can be suppressed by estimation of and compensation for the integrated transmission coefficient through the cortex [269]. The presence of cortex has been reported to have a small effect on correlations between backscatter parameters and BMD in human femoral heads [270].

## B. Models for Scattering

While several models for scattering from cancellous bone have been proposed [271–278], two models have received far more experimental validation than the others: the incoherent scattering cylinder model [274] and the weak scattering model [275].

Two variants of cylinder scattering models, based on theory for scattering from a solid cylinder [279], were developed independently. One variant assumes coherent scattering from a two-dimensional array of regularly-spaced, parallel cylinders. Cylinder spacing and diameter could be estimated from measurements of scattering as a function of angle and frequency. Because only two or three bone samples were interrogated (one bovine and one or two human), it is difficult to assess the robustness of the model and method.

Another variant of the cylinder scattering model assumes that trabeculae are positioned sufficiently randomly that the incoherent contribution to scattering dominates the coherent contribution (*i.e.*, the phase differences between scattered signals from pairs of trabeculae are uniformly distributed between 0 and  $2\pi$  radians) [251, 274]. In the incoherent limit, the dependence of scattering on frequency and cylinder diameter is the same for a single scatterer or an ensemble of unresolved scatterers [251, 274]. When the cylinder diameter (mean value of 127  $\mu\text{m}$  in human calcaneal trabeculae [70]) is much smaller than a wavelength (about 3 mm at 500 kHz), the cylinder model predicts that backscatter should be



proportional to frequency cubed, which is consistent with measurements in the clinical frequency range ( $< 1$  MHz) as shown in Fig. 15. The cylinder model has been extended to include cylinders with finite lengths [280], quasi-periodic positions [281, 282], and randomly-varying diameters [248]. As mentioned in Section III. E, the cylinder scattering model also explains the dependence of phase velocity and dispersion on trabecular thickness and trabecular spacing in cancellous bone mimicking phantoms.

The incoherent assumption explains measurements of backscattered envelope mean-to-standard deviation ratio in human calcaneus *in vivo* of  $1.81 \pm 0.08$  (2.25 MHz) [247],  $1.92 \pm 0.12$  (580 kHz) [283] and  $1.73 \pm 0.12$  (1.3 MHz) [283], which are close to the theoretical Rayleigh distribution value of 1.91 for purely incoherent scattering [245, 246]. The fact that experimental values tend to be a little lower than 1.91 can be explained by a mixed model composed of long, thick trabeculae and short, thin trabeculae [283].

The other scattering model that has received extensive experimental validation is the weak scattering model [275, 284]. This model predicts the backscatter coefficient based on the structural autocorrelation function, which may be measured from cancellous bone samples using  $\mu$ CT. Like the incoherent cylinder model, the weak scattering model considers only the incoherent component of scattering [284]. This model has been extended to a 2-component form [285]. Substantial agreement between the incoherent scattering cylinder model and the weak scattering model in human cancellous femur *in vitro* has been reported [234, 235, 286].

The binary (marrow fat and bone matrix) mixture model [273, 276], which has received less experimental validation than the models discussed above, predicts a scattering coefficient that is proportional to mean fluctuations in velocity, neglecting contributions due to fluctuations in density as has been done with soft tissue scattering models [287, 288].

### C. Backscatter vs. Frequency

Fig. 15 shows means and standard errors for backscatter coefficient as a function of frequency from 16 human cancellous calcaneus samples *in vitro* [274]. Fig. 15 also shows the prediction of the incoherent scattering cylinder model. At low frequencies ( $< 1$  MHz), backscatter is approximately proportional to frequency cubed, as predicted by the incoherent scattering cylinder model [251, 274]. Several studies support this approximate cubic frequency dependence in human cancellous calcaneus *in vitro* [152, 274, 275, 289, 290] and bovine cancellous femur *in vitro* [291] at low frequencies. Values of the exponent of frequency dependence of slightly greater than 3 in human cancellous calcaneus may be explained by finite effective cylinder lengths [280], combined contributions from cylinders (trabeculae) and point-like scatterers (plates), multiple scattering [274], or some combination. The dependence of backscatter coefficient on frequency deviates from the cubic behavior for frequencies above 1 MHz [49, 274, 281], with some studies suggesting that backscatter coefficient from human cancellous calcaneus *in vitro* hits a plateau between 2 and 2.5 MHz [274, 281]. Studies in bovine cancellous bone *in vitro* suggest backscatter coefficient increases approximately monotonically with frequency below 1 MHz [281, 285, 291] and can be shown to be consistent with a binary mixture model [273, 276, 291].

Theoretically, the far field scattering response of a thin cylinder to an incident plane wave varies as frequency cubed when the wavelength is much bigger than the cylinder diameter [279]. An experimental study indicates that the theoretical far field scattering response from a single cylinder has the same dependences on frequency and diameter as the backscatter coefficient measured with a focused transducer from an ensemble of cylindrical scatterers [251].

The incoherent cylinder scattering model and the weak scattering model have been shown to exhibit very similar predictions of backscatter coefficient in 26 human cancellous femur samples *in vitro* [286].

The ABTF (in dB) usually decreases with frequency over the range from 0.6 MHz to 9.1 MHz in human cancellous femur *in vitro* [253], except when gate delay is very short (< about 1 or 2  $\mu$ s) [252].

#### D. Backscatter vs. BMD and Composition

In studies on human cancellous calcaneus [50–53, 247, 292, 293], femur [49, 56, 57] and tibia [49] *in vitro*, the median and mean  $\pm$  standard deviation of the squared correlation coefficient between BUB and site-matched, volumetric BMD near the clinical range of frequencies are  $r^2 = 0.66$ ,  $0.65 \pm 0.13$ .

In human spine *in vivo*, the square of the correlation coefficient between the BSCS at 2.5 MHz and volumetric BMD has been reported to be  $r^2 = 0.37$  [294]. BSCS and AIB at 3.5 MHz and 5.0 MHz measured in human calcaneus *in vivo* exhibit squared correlation coefficients with areal BMD measured at the hip and spine in the range of  $0.41 < r^2 < 0.61$  [295, 296]. AIB measured in intact human proximal femur *ex vivo* exhibits squared correlation coefficient with areal BMD in the femoral neck of  $r^2 = 0.44$  [297].

Low correlations have been reported ( $r^2 = 0.01$  and  $r^2 = 0.23$ ) in transverse and longitudinal orientations between AIB and volumetric BMD in bovine cancellous tibiae *in vitro* near 1 MHz, but higher correlations ( $r^2 = 0.82$  and  $r^2 = 0.49$ ) have been reported in transverse and longitudinal orientations near 5 MHz [298]. In cases of significant correlation, AIB usually decreases with BMD, except when gate delay is very short (< 1  $\mu$ s) [252]. The opposite trends of backscatter coefficient and AIB as BMD increases may be attributable to the fact that AIB includes the effects of attenuation (which increases with BMD) while backscatter coefficient does not.

The correlation between BUB (200–600 kHz) and volumetric BMD in bovine cancellous femur *in vitro* has been reported to be  $r^2 = 0.37$  [83]. Correlations in the range  $0.48 < r^2 < 0.66$  between BUB and volumetric BMD in human cancellous femur and tibia *in vitro* have been reported for measurements with five transducers with center frequencies ranging from 0.5–5 MHz [49]. The correlation between BUB (1.5–3.8 MHz) and bone volume fraction (which, like BMD, is a good indicator of bone quantity) in human cancellous femur and tibia *in vitro* has been reported to be  $r^2 = 0.76$  [69].

One study found that demineralization (by treating bone with EDTA [58]) significantly reduced AIB in human cancellous tibia *in vitro* (1–3 MHz) [58] in the superoinferior (SI)

direction but not in mediolateral (ML) or anteroposterior (AP) directions *in vitro*. However, another study, in which no active demineralization was applied, found no significant correlation between BUB (2.25 MHz) and mineral content (normalized to the calcified matrix volume) in human cancellous tibia and femur *in vitro* [69]. The lack of significant correlation may have been partially due to the relatively low natural variation of mineral content in the samples (8.8%) [69].

One study found that decollagenization (by treating bone with sodium hypochlorite) significantly increased AIB (1–3 MHz) in all three directions in human cancellous tibia *in vitro* [58]. Another study, in which no active decollagenization was applied, found a significant negative correlation ( $r = -0.50$ ) between BUB (1–2.8 MHz) and calcified matrix collagen (normalized to the calcified matrix volume) in human cancellous tibia and femur *in vitro* [69], as shown in Fig. 16. A follow-up study found similar significant negative correlations ( $-0.46 > r > -0.75$ ) between BUB/AIB and calcified matrix collagen in human cancellous tibia and femur *in vitro* for transducers with center frequencies of 1, 2.25, 3.5, and 5 MHz [263].

One study found a significant negative correlation ( $r = -0.55$ ) between BUB (1–2.8 MHz) and fat content in human cancellous tibia and femur *in vitro* but no significant correlations between BUB and water content or proteoglycan content [69].

#### E. Backscatter vs. Microstructure

In multiple regression studies on human cancellous calcaneus [52, 53], tibia [77] and femur [57, 77] specimens *in vitro*, the median for the squared correlation coefficient between BUB and bone quantity (*e.g.*, BV/TV) near the clinical range of frequencies is  $r^2 = 0.63$ . In these studies, the median for the added variance of BUB,  $\Delta r^2$ , explained by microstructure is 0.07. Similar results have been reported for backscatter difference parameters in human cancellous femur *in vitro* at 3.5 MHz (although  $r^2$  values were sometimes higher when measurements were averaged over 6 orthogonal directions) [260] and multiple backscatter parameters in bovine cancellous femur at 2.25 MHz [299].

Fig. 17 shows a scatter plot of backscatter coefficient vs. mean trabecular thickness (Tb.Th) in 43 human calcaneus samples *in vitro*. Fig. 17 also shows a power law fit in which backscatter coefficient at 500 kHz is proportional to trabecular thickness to the 2.8 power. (95% confidence interval: 1.7 – 3.9). This dependence is very close to the prediction of the incoherent scattering cylinder model (2.9) [300]. The weak scattering model has been shown to be effective for estimating trabecular thickness from ultrasonic backscatter measurements in cancellous bone specimens [243, 244, 284].

#### F. Backscatter vs. Mechanical Properties

In studies on human cancellous calcaneus [22, 87], femur [49, 88, 263] and tibia [49, 88, 263] *in vitro*, the median and mean  $\pm$  standard deviation of the squared correlation coefficient between BUB and mechanical parameters (*e.g.*, Young's modulus, ultimate strength) are  $r^2 = 0.51$ ,  $0.46 \pm 0.09$ .

## G. Multiple Scattering

Scattering models that ignore multiple scattering are consistent with measurements of frequency dependence of backscatter in the clinical frequency range [274, 275]. Therefore, multiple scattering is usually assumed to be small compared to single scattering in this range.

However, indirect evidence for multiple scattering exists in the clinical frequency range. A theoretical model for multiple scattering from cylinders [160] has been shown to be accurate for predicting negative dispersion observed in the clinical frequency range in cancellous bone *in vitro* [21, 105, 148, 149], *in vivo* [150] and cancellous bone-mimicking phantoms [161, 162]. Another model provides additional insight into multiple scattering processes in cancellous bone [277, 278].

A theoretical model based on cylindrical trabeculae predicts that multiple scattering in cancellous bone is relatively small below 1.5 MHz but is substantial above 1.5 MHz [301]. Direct evidence for multiple scattering from human cancellous femur has been observed *in vitro* at 3 MHz [302]. Multiple scattering may be inferred from the angular dependence of backscattered intensity, which may be measured using a linear array. A single element is used for transmission while all elements are used for reception. The process is repeated using a different transmit element each time to acquire the complete dataset. At short times, the angular dependence of backscattered intensity is nearly flat, but at later times there is an enhancement in the backscattering direction that is a signature of multiple scattering [302]. Such measurements from human cancellous femur *in vitro* indicate scattering mean-free path between 2.3 and 8 mm [302]. The method may be used to measure diffusion constant, which characterizes the rate of growth of the diffusive halo due to multiple scattering. Measurements at 3 MHz in human cancellous femur *in vitro* suggest that the diffusion constant may have diagnostic value [303]. Simulations at 5 MHz in equine cancellous femur suggest that the diffusion constant is effective for quantifying anisotropy [117].

## H. Scattering as a Component of Attenuation

Potential sources of measured attenuation (*e.g.*, BUA or nBUA) include absorption, longitudinal-longitudinal (LL) scattering, longitudinal-shear (LS) scattering, and phase cancellation. These sources are not mutually exclusive. For example, some ultrasound energy can be initially scattered (LL or LS) at a trabecular interface and then subsequently absorbed as it propagates away from the trabecula. Phase cancellation was considered in Section II.F.

In the clinical frequency range ( $< 1$  MHz), LL scattering would not seem to be a significant component of attenuation [274, 304] because it is highly nonlinear with frequency [251, 274, 275, 284, 289, 304] while attenuation is quasi-linear with frequency [1, 41–43].

One finite difference time domain (FDTD) simulation solved the 2D viscoelastic wave equation with and without viscous loss terms set to zero and found little difference (4.4%) in attenuation (300-900 kHz) in the two cases for a human cancellous calcaneus sample subjected to computational erosions and dilations [305]. This result suggested that direct absorption is a small component of attenuation. Another FDTD simulation solved the 3D

linear elastic wave propagation equation without taking absorption into account and was able predict magnitude and frequency dependence of attenuation (0.4-1.2 MHz) for 31 human cancellous femur samples consistent with measurements on cancellous bone (*e.g.*, quasi-linear frequency dependence) [306]. This finding led the investigators to suggest that LS scattering could be a significant contribution to attenuation [306]. Subsequent paired comparison of this simulation approach with measurements on 28 human cancellous femur samples *in vitro* showed that the simulation correctly predicted experimental attenuation (0.4-1.2 MHz) values for low BV/TV, but tended to underestimate experimental attenuation magnitude and frequency dependence for higher BV/TV [307]. The authors concluded that the relative contribution of scattering to attenuation increases with frequency, becoming predominant (>50%) over absorption for frequencies above 600 kHz [307]. This simulation and another simulation (3D FDTD simulation based on 11  $\mu$ CT images of cancellous bone from human cadaver knees) suggest that the importance of absorption relative to scattering increases as BV/TV increases [307, 308].

If, in the clinical range of frequencies, 1) attenuation varies quasi-linearly with frequency, 2) scattering is a significant component of attenuation, and 3) LL scattering varies highly nonlinearly with frequency, then LS scattering must vary quasi-linearly with frequency and dominate LL scattering. In order to investigate these mechanisms experimentally, attenuation and backscattering were measured over a broad range of frequencies on cancellous-bone-mimicking phantoms containing nylon wires (simulating trabeculae) in a soft tissue-mimicking medium (simulating marrow) [309]. Frequency-dependent attenuation coefficients,  $\alpha(f)$ , were decomposed into three components as illustrated in Fig. 18:

$$\alpha(f) = \alpha_{FL}(f) + \alpha_{L2}(f) + \alpha_{NL}(f) \quad (11)$$

The first component,  $\alpha_{FL}(f)$ , corresponds to absorption in the fluid medium (*e.g.*, marrow). It varies approximately linearly with frequency and may be measured in a phantom containing only soft tissue-mimicking medium without nylon wires. The second linear component,  $\alpha_{L2}(f)$ , contains absorption in the wires (trabeculae) and LS scattering by the wires, which was hypothesized [309] to vary quasi-linearly with frequency based on previous studies of suspensions of particles in fluids [310–312] (see Fig. 8 in [313]). The second linear component,  $\alpha_{L2}(f)$ , may be measured by performing a linear fit to low-frequency attenuation measurements and then subtracting  $\alpha_{FL}(f)$  as shown in Fig. 18. The nonlinear component,  $\alpha_{NL}(f)$ , was hypothesized to be due to LL scattering [309].

Fig. 18 shows measurements of total attenuation ( $\alpha$ , left column), nonlinear attenuation ( $\alpha_{NL}$ , middle column), and LL backscatter coefficient ( $\eta$ , right column) in five phantoms with different nylon wire thicknesses [309]. For each row (*i.e.*, each phantom) in Fig. 18, the frequencies at which nonlinear attenuation (middle column) and LL backscatter coefficient (right column) become non-negligible are approximately equal (increasing from 1 MHz in the top row to 2.5 MHz in the bottom row), supporting the association of  $\alpha_{NL}(f)$  with LL scattering. The two functions are similar in shape but not identical because  $\alpha_{NL}(f)$  corresponds to the integral of LL scattering over all solid angles while LL backscatter corresponds only to LL scattering in the reverse direction. Linear regression analysis of low-frequency (clinical range) attenuation coefficient slope (due to  $\alpha_{FL}$  and  $\alpha_{L2}$ ) vs. volume

fraction occupied by nylon filaments yielded a correlation coefficient of  $r = 0.96$  (95% confidence interval: 0.82–0.99), supporting the relevance of the phantom model to cancellous bone [309].

Another experimental investigation into sources of attenuation compared attenuation measurements performed on 26 human cancellous femur samples *in vitro* with three different filling fluids: marrow, water, and alcohol [166]. No significant influence of the fluid choice on attenuation was observed despite a wide variety of fluid viscosity and acoustic impedance mismatch between fluid and trabeculae. This led the investigators to conclude that LS scattering and absorption in the trabeculae were candidates as main sources for attenuation [166].

Shear waves due to mode conversion at scatterer interfaces are likely to be transient. For example, shear waves generated from graphite particles suspended in gelatin are described as “evanescent” because they are quickly absorbed [313]. Similar rapid absorption is likely in cancellous bone. Shear attenuation coefficients in bovine cancellous bone are approximately 17 dB/imm at 1 MHz [314], which means that shear wave power decreases by 98% for each mm of propagation. Therefore, characterization of LS-scattering from trabeculae as an absorption mechanism is not unreasonable, although it overlooks a brief, highly-confined, transitional phase of energy in the form of a transient shear wave that propagates on the order of 1 mm prior to nearly-complete absorption [304].

## VI. ADDITIONAL TOPICS

### A. Anisotropy

QUS parameters depend on the orientation of ultrasound propagation relative to the predominant trabecular orientation. Regarding BUA and nBUA, results are mixed with one study in bovine radius [315] indicating higher BUA in the parallel orientation and studies in human vertebrae [55] and bovine tibia [114] indicating lower nBUA in the parallel orientation. Studies in bovine femur [111], human vertebrae [55, 167] and bovine tibia [114] consistently indicate that SOS is faster in the parallel orientation, as shown in Fig. 11. One study in human calcaneus [304] indicates that backscatter coefficient is higher in the perpendicular (ML) orientation. This is plausible because echoes tend to be stronger when ultrasound strikes a target from the perpendicular direction. In bovine tibia, the difference in AIB between parallel and perpendicular orientations has been found to be small, perhaps due to increases in both nBUA and backscatter coefficient in the perpendicular orientation cancelling each other out to produce little change in AIB [114]. In human distal femur, for short gate delays ( $< 2 \mu\text{s}$ ) AIB is significantly larger in the perpendicular orientation while for longer delays AIB is similar in perpendicular and parallel orientations [252].

In bovine femur, the fast wave speed has been found to be maximum along the main trabecular orientation [119, 216] while the slow wave speed was relatively isotropic [119]. The fast wave can exhibit significant refraction when the propagation direction is not coincident with the main trabecular alignment [176, 316]. The attenuation coefficient of the fast wave has also been found to be maximum along the main trabecular orientation [216].

## B. The Effect of Fluid Filler

For convenience, many *in vitro* experiments are conducted in defatted (marrow removed) cancellous bone samples immersed in water. This raises the question of the effects of substituting water for marrow on QUS parameters. Measurements of nBUA and SOS in human cancellous calcaneus / femur at 1 MHz suggest that replacing marrow with water has anywhere from no statistically significant effect on either parameter [22, 112] to a mean decrease of nBUA of 5.6 dB/cmMHz [317] and a mean increase of SOS of 20-43 m/s [166, 317]. Measurements in bovine cancellous femur at 500 kHz and 1 MHz suggest a mean decrease of nBUA of 2 - 10 dB/cmMHz and mean increases of SOS of 35 – 48 m/s [120, 133, 318]. Measurements in bovine tibia at 2.25 MHz suggest no significant change in either parameter [115]. A simulation study suggests that these effects depend on BV/TV [308]. Replacing marrow with water was found not to have a big effect on dispersion or frequency dependence of backscatter in bovine cancellous femur [152]. The ultrasonic properties of human [319] and bovine [320] marrow samples have been studied extensively.

## C. Cancellous Bone-mimicking Phantoms

Experiments on bone-mimicking phantoms are useful for modeling the interaction between ultrasound and cancellous bone. An early phantom design, based on epoxy mixed with cubic granules of gelatin, exhibits nBUA values consistent with the clinical range and negative dispersion similar to cancellous bone [321, 322].

Phantoms consisting of light-cured resin manufactured using stereo lithography, with silicone rubber as a marrow mimic, exhibit values of BUA and SOS consistent with cancellous bone [194, 323]. Water-saturated stereo-lithographical bone replicas of cancellous bone have been used to perform measurements of through-transmission ultrasound with values similar to predictions based on modified anisotropic Biot-Allard theory for porous media [204, 205]. Three-dimensional printed phantoms generated from synchrotron x-ray  $\mu$ CT images of equine cancellous femur have been interrogated at 1 MHz and exhibit both fast and slow longitudinal waves [184].

Phantoms consisting of alternating parallel layers of water and polystyrene (simulating marrow and trabecular material) exhibit negative dispersion similar to cancellous bone and consistent with the analytic stratified model [165].

Nylon wires exhibit frequency-dependent scattering similar to cancellous bone [251]. Phantoms consisting of parallel nylon wires in two-dimensional arrays immersed in water exhibit dependences of phase velocity and dispersion on bone volume fraction similar to cancellous bone [161]. Phantoms that use nylon wire segments in random orientations immersed in tissue-mimicking gel also exhibit dependences of phase velocity and dispersion on bone volume fraction similar to cancellous bone [162]. Phantoms that use nylon wire segments in random orientation immersed in tissue-mimicking gel are useful for elucidating the relative roles of absorption, LS scattering, and LL scattering in cancellous bone [309].

Polyacetal cuboid bone-mimicking phantoms exhibit dependences of phase velocity and nBUA on porosity and dependence of attenuation coefficient on frequency consistent with cancellous bone and cancellous-bone-mimicking phantoms [324].

Water-saturated metal foams have been shown to be useful for mimicking some properties of cancellous bone. Aluminum foams (see Fig. 19) can exhibit slow wave phase velocity consistent with Biot theory [325–327]. A study on one set of aluminum foams indicates that SOS increases with porosity, but nBUA decreases with porosity [328]. Studies on nickel foams [329] and copper foams [330] indicate several properties that are consistent with cancellous bone: attenuation coefficient varies approximately as frequency to the first power [1], phase velocity exhibits negative dispersion [21, 105, 148–150], and backscatter coefficient varies approximately as frequency cubed [274, 275]. Water-saturated polymer foams exhibit values of nBUA, SOS, and backscatter parameters consistent with cancellous bone [118].

Phantoms consisting of a custom composite material using an epoxy resin, alumina powder, and inclusions (poppy seeds or hemp seeds) to control porosity can exhibit BUA and SOS in the range of values reported for cancellous bone [331].

#### D. Simulations

Simulations are helpful for elucidating mechanisms underlying the interaction of ultrasound with cancellous bone. A previous review discusses simulation examples from cortical bone, cancellous bone, whole bones, skull, and therapeutic applications [332]. The present section provides developments since the previous review and places greater emphasis on cancellous bone.

A pioneering FDTD simulation based on the 2D elastic wave equation predicted dependences of ultrasound velocity and mean frequency in cancellous human calcaneus (derived from  $\mu$ CT) on bone volume fraction consistent with experimental results [134]. The same simulation was used to investigate the relative roles of absorption and scattering in cancellous human calcaneus [305]. A 3D version of this simulation was used to validate net time delay (difference between transit time through cancellous bone and transit time through hypothetical object of equal thickness containing soft tissue only) as an effective index of BMD [333]. The 3D version has also been used to investigate the effect of bone marrow on attenuation and speed in cancellous bone [308], Fig. 20 shows snapshots of waves propagating through cancellous bone, showing ballistic and scattered components.

FDTD simulation based on 3D linear elastic wave propagation predicts several phenomena in cancellous human femur samples (derived from synchrotron  $\mu$ CT) that are consistent with experimental evidence: attenuation varies approximately linearly with frequency, nBUA and SOS increase with bone volume fraction, and most samples exhibit negative dispersion [306, 334]. It can reveal fast and slow waves when the ultrasound propagation direction is aligned with the predominant trabecular orientation. It predicts that mode conversion of incident longitudinal waves to shear waves is a significant contributor to attenuation [306] and that the dependence of nBUA on BV/TV can be mostly explained by scattering [307]. Using image processing to induce “virtual osteoporosis” in  $\mu$ CT data, it predicts that nBUA and SOS are mostly determined by volume fraction but that material properties and microstructure also play roles [131, 335]. 3D FDTD simulations indicate that except when BV/TV is high, variations of BUA induced purely by changes in BV/TV exceed technique imprecision and therefore can be detected [336]. However, variations of QUS properties



induced by changes in compressive or shear stiffness are more difficult to model due to sparse description of elastic properties at the tissue level [336].

A one-dimensional finite difference approach has been applied to model velocity in cancellous bone [337], but this approach has some limitations [338].

FDTD simulation based on the elastic wave equation has been studied extensively on bovine cancellous bone models (usually measured with  $\mu$ CT), which are more anisotropic than human cancellous bone and therefore elucidate the effects of trabecular orientation. In two-dimensions, FDTD simulation based on Biot theory is better for identifying fast and slow waves than FDTD simulation based on the elastic wave equation because of the limitations of the 2D elastic model [314]. However, viscoelastic FDTD simulation has closer agreement to experiment than Biot's FDTD for single wave propagation perpendicular to the trabeculae [339]. The effects of porosity on amplitude and speed of fast and slow waves have been elucidated by performing 3D FDTD solution of the viscoelastic wave equation on 3D  $\mu$ CT images of cancellous bone subjected to varying degrees of erosion [340, 341] or, alternatively, with a simplified model for cancellous bone consisting of spherical pores in otherwise solid bone [342]. Similarly, the effects of orientation of the ultrasound beam relative to the trabecular direction has been investigated by digitally rotating the  $\mu$ CT cancellous bone image [316]. This FDTD method suggests that reflection coefficients of fast and slow waves at the boundary between cancellous bone and cortical bone increase with porosity [343]. Finally, this approach has been used to characterize reflected and backscattered waves from cancellous bone [344, 345].

FDTD simulation based on the 3D elastic wave equation shows that the attenuation of the fast wave is higher in the early state of propagation and gradually decreases as the wave propagates in bovine cancellous bone [183]. It also predicts dependences of fast wave speed and fast and slow wave amplitudes on bone volume fraction similar to measurements in bovine cancellous bone [346, 347]. It has been used to investigate the effect of surrounding cortical bone on fast and slow waves propagating through equine cancellous radius [178, 179].

A 3D mixture model, in which each point in the cancellous bone has both fluid and solid phases coexisting has been used to predict attenuation monotonically increasing with frequency as has been observed experimentally [348].

3D FDTD simulation has been used to model and compensate for the effects of the cortical layer on cancellous bone backscatter metrics [269].

3D FDTD simulation using randomly distributed clusters of ellipsoidal scatterers in a fluid can predict the propagation of fast and slow waves, as in Biot theory [349]. Under the independent scattering approximation (ISA), this approach successfully predicts the attenuation coefficient (unlike Biot's theory) and the existence of negative dispersion [215]. However, the ISA does not model wave speeds in two-wave propagation as well as Biot's theory [215].

3D Finite element modeling (FEM), in which only the solid part of the bone was considered (*i.e.*, vacuum filler), suggests that the bar equation successfully predicts *SOS* near 50 kHz but does not perform as well at a more clinical frequency of 1 MHz [125]. 3D Finite element analysis of models based on a weak variational formulation of the equations of motions in solid and neighboring fluid media that simulate elastic scattering, refraction, and mode conversion have been shown to predict the linear dependence of attenuation with frequency and increases in nBUA and *SOS* with BV/TV consistent with reported experimental measurements for cancellous bone [350]. FEM that considered reflection, refraction, elastic scattering and mode conversion has been shown to be accurate for predicting frequency-dependent attenuation and phase velocity of water-saturated aluminum foam cancellous-bone-mimicking phantoms [351]. FEM based on Biot's model has been used to investigate anisotropy of reflection and transmission of plane waves in a human cancellous bone specimen [203].

A 2D pseudo-spectral time domain numerical model has been developed to investigate effects of microcracks in cancellous bone [352].

Nonlinear propagation through cancellous bone has been modeled using the Khokhlov–Zabolotskaya–Kuznetsov (KZK) equation and suggests challenges associated with detecting harmonics of the fundamental frequency [353].

## E. Acoustic Microscopy

Discussions of acoustic microscopy for both cortical and cancellous bone may be found elsewhere [11, 354], but the present discussion focuses on applications in cancellous bone. Scanning acoustic microscopy (SAM) is possible at frequencies of 0.1-1 GHz. Due to high absorption at such high frequencies, only surface or subsurface images are obtained [355]. For a flat sample, the reflected signal depends on the reflection coefficient at the sample surface  $r = (Z_2 - Z_1) / (Z_2 + Z_1)$  where  $Z = \rho v$ ,  $\rho$  is the material density,  $v$  is the longitudinal velocity, and the indexes 1 and 2 refer to the sample medium and coupling medium. A SAM system may be calibrated by scanning a set of materials with known physical properties so that both density and elasticity may be obtained [355,356].

SAM has been used to measure Young's moduli of human trabeculae of 17.5 GPa (400 MHz, femur) [355,357] and 19.9 GPa (100 MHz, pelvis) [356]. Both of these values are close to the measurement obtained with nanoindentation, 18.1 GPa [355]. SAM at 200 MHz has been used to measure Young's moduli of murine trabeculae of  $12.9 \pm 2.0$  GPa and  $17.7 \pm 1.4$  GPa in B6 and C3H mice respectively [358].

SAM at 200 MHz was used to study the effects of dynamic compressive strain loading in bovine cancellous sternum and ulna [359], Fig. 21 shows a close relationship between acoustic impedance measured with acoustic microscopy and degree of bone mineralization measured with synchrotron radiation  $\mu$ CT.

Ultrasound longitudinal wave velocity in an individual trabecula may be inferred from measurements of Brillouin scattering, which is the interaction between light and thermally excited acoustic phonons [360]. Micro-Brillouin scattering has been used to measure

longitudinal wave velocities in bovine femoral trabecula with a spatial resolution of 10  $\mu\text{m}$  and to study the dependence of elastic properties on trabecular type (rod-like vs. plate-like) and direction of trabecular alignment [360, 361]. The squared correlation coefficient between acoustic impedance measured with 200 MHz SAM and longitudinal wave velocity measured with micro-Brillouin scattering has been reported to be  $R^2 = 0.63 - 0.67$  [362].

The effects of sample preparation for acoustic microscopy have been characterized [363].

## F. Nonlinear Properties of Cancellous Bone

Linear acoustics is valid at low pressures and based on an equation of state for which variations of pressure are directly proportional to variations in density. At higher pressures, the quadratic term in a Taylor series for the equation of state cannot be neglected. The ratio of quadratic to linear terms in the equation of state is denoted by  $B/A$ , which may be used to describe nonlinear behavior of media [364].

The ratio of the amplitudes of second harmonic relative to the fundamental (236 kHz) has been shown to be sensitive to BMD in through-transmission measurements in human calcaneus *in vivo* in seven volunteers [365]. Correlation coefficients of  $B/A$  with apparent bone density ( $r = 0.95$ ), BMD ( $r = 0.77$ ), BV/TV ( $r = 0.80$ ), and Tb.Th ( $r = 0.44$ ) have been reported in bovine cancellous femur (0.5 MHz transmitter, 0.5 or 1 MHz receiver) [366–368]. Similar findings have been reported in aluminum-foam cancellous-bone-mimicking phantoms [328].

Vibroacoustography is a nonlinear imaging method that has been demonstrated to be sensitive to porosity of phosphocalcic ceramic samples (that simulate bone) and also to be capable of generating images of human calcaneus *in vitro* that reveal spatial distribution of mineralization [369]. Nonlinear measurement methods that use a mechanical vibrator to shake samples during acoustic measurement have been shown to be sensitive to bone density in human calcaneus samples *in vitro* [370] and to distinguish between healthy and osteoporotic human cancellous femur samples *in vitro* [371].

## VII. CONCLUSION

Experimental, computational, and theoretical analysis elucidates mechanisms underlying the interaction between ultrasound and cancellous bone.

Attenuation at clinical frequencies in cancellous bone is primarily determined by bone quantity but is also influenced by composition, microstructure, and mechanical properties. Attenuation usually varies quasi-linearly with frequency in the clinical range. Phase cancellation (especially for denser bones) and longitudinal-shear scattering make important contributions to attenuation at clinical frequencies.

Speed of sound at clinical frequencies in cancellous bone is primarily determined by bone quantity but is also influenced by composition, microstructure, and mechanical properties. Common speed of sound metrics, which entail measurements of transit times of pulse leading edges (to avoid multipath interference), are greatly influenced by attenuation, dispersion, and system properties including center frequency and bandwidth. A formula has

been derived to accurately account for these distortions. Unlike soft tissue, which exhibits positive dispersion, cancellous bone tends to exhibit negative dispersion, which may be understood using theoretical and phantom models.

Cancellous bone supports two longitudinal waves (“fast” and “slow” waves), as predicted from poro-elasticity theory. Fast wave velocity is highest when ultrasound propagates parallel to the predominant trabecular orientation. Signal processing methods have been developed to separate fast and slow waves in cancellous bone even when they overlap in time and frequency domains.

Backscatter at clinical frequencies in cancellous bone is primarily determined by bone quantity but is also influenced by composition, microstructure, and mechanical properties. Backscatter coefficient from cancellous bone at clinical frequencies varies approximately as frequency to the third power and mean trabecular thickness to the third power, which may be explained by cylinder or weak-scattering models.

## Acknowledgment

The mention of commercial products, their sources, or their use in connection with material reported herein is not to be construed as either an actual or implied endorsement of such products by the Department of Health and Human Services. The author is grateful for funding support from the FDA Office of Women’s Health. The author thanks all the researchers who have contributed to this field and are cited in this review. The author gives special thanks to Pascal Laugier. Without his contributions, this review would have been much shorter.

This work was supported by the U.S. Food and Drug Administration Office of Women’s Health.

## REFERENCES

- [1]. Langton CM, Palmer SB, and Porter RW, “The measurement of broadband ultrasonic attenuation in cancellous bone,” *Eng Med*, vol. 13, no. 2, pp. 89–91, 4 1984. [PubMed: 6540216]
- [2]. Langton CM and Njeh CF, “The measurement of broadband ultrasonic attenuation in cancellous bone--a review of the science and technology,” *IEEE Trans Ultrason Ferroelectr Freq Control*, vol. 55, no. 7, pp. 1546–54, 7 2008. [PubMed: 18986945]
- [3]. Seeman E, “Age- and menopause-related bone loss compromise cortical and trabecular microstructure,” *J Gerontol A Biol Sci Med Sci*, vol. 68, no. 10, pp. 1218–25, 10 2013. [PubMed: 23833200]
- [4]. Cummings SR et al., “Bone density at various sites for prediction of hip fractures. The Study of Osteoporotic Fractures Research Group,” *Lancet*, vol. 341, no. 8837, pp. 72–5, 1 9 1993. [PubMed: 8093403]
- [5]. Gluer CC et al., “Osteoporosis: association of recent fractures with quantitative US findings,” *Radiology*, vol. 199, no. 3, pp. 725–32, 6 1996. [PubMed: 8637996]
- [6]. Hans D et al., “Ultrasonographic heel measurements to predict hip fracture in elderly women: the EPIDOS prospective study,” *Lancet*, vol. 348, no. 9026, pp. 511–4, 8 24 1996. [PubMed: 8757153]
- [7]. Krieg MA et al., “Quantitative ultrasound in the management of osteoporosis: the 2007 ISCD Official Positions,” *J Clin Densitom*, vol. 11, no. 1, pp. 163–87, Jan-Mar 2008. [PubMed: 18442758]
- [8]. U. S. P. S. T. Force, “Screening for osteoporosis: U.S. preventive services task force recommendation statement,” *Ann Intern Med*, vol. 154, no. 5, pp. 356–64, 3 1 2011. [PubMed: 21242341]
- [9]. Wear KA, Hoffmeister BK, and Laugier P, “Quantitative Ultrasound and the Management of Osteoporosis,” *Acoustics Today*, vol. 14, no. 2, pp. 34–42, 2018.

- [10]. Grimal Q and Laugier P, "Quantitative ultrasound assessment of cortical bone properties beyond bone mineral density," *IRBM*, vol. 40, pp. 16–24, 2019.
- [11]. Raum K, Grimal Q, Varga P, Barkmann R, Gluer CC, and Laugier P, "Ultrasound to assess bone quality," *Curr Osteoporos Rep*, vol. 12, no. 2, pp. 154–62, 6 2014. [PubMed: 24652476]
- [12]. Fry FJ and Barger JE, "Acoustical properties of the human skull," *J Acoust Soc Am*, vol. 63, no. 5, pp. 1576–90, 5 1978. [PubMed: 690336]
- [13]. Clement GT and Hynynen K, "A non-invasive method for focusing ultrasound through the human skull," *Phys Med Biol*, vol. 47, no. 8, pp. 1219–36, 4 21 2002. [PubMed: 12030552]
- [14]. Pinton G, Aubry JF, Bossy E, Muller M, Pernot M, and Tanter M, "Attenuation, scattering, and absorption of ultrasound in the skull bone," *Med Phys*, vol. 39, no. 1, pp. 299–307, 1 2012. [PubMed: 22225300]
- [15]. Moayyeri A et al., "Quantitative ultrasound of the heel and fracture risk assessment: an updated meta-analysis," *Osteoporos Int*, vol. 23, no. 1, pp. 143–53, 1 2012. [PubMed: 22037972]
- [16]. Padilla F, Puts R, Vico L, and Raum K, "Stimulation of bone repair with ultrasound: a review of the possible mechanic effects," *Ultrasonics*, vol. 54, no. 5, pp. 1125–45, 7 2014. [PubMed: 24507669]
- [17]. Huisman M et al., "International consensus on use of focused ultrasound for painful bone metastases: Current status and future directions," *Int J Hyperthermia*, vol. 31, no. 3, pp. 251–9, 5 2015. [PubMed: 25677840]
- [18]. Bauer AQ, Anderson CC, Holland MR, and Miller JG, "Bone sonometry: reducing phase aberration to improve estimates of broadband ultrasonic attenuation," *J Acoust Soc Am*, vol. 125, no. 1, pp. 522–9, 1 2009. [PubMed: 19173437]
- [19]. Xu W and Kaufman JJ, "Diffraction correction methods for insertion ultrasound attenuation estimation," *IEEE Trans BiomedEng*, vol. 40, no. 6, pp. 563–70, 6 1993.
- [20]. Kaufman JJ, Xu W, Chiabrera E, and Siffert RS, "Diffraction effects in insertion mode estimation of ultrasonic group velocity," *IEEE Trans Biomed Eng*, vol. 42, no. 2, pp. 232–242, 1995.
- [21]. Droin P, Berger G, and Laugier P, "Velocity dispersion of acoustic waves in cancellous bone," *IEEE Trans Ultrason Ferroelectr Freq Control*, vol. 45, no. 3, pp. 581–92, 1998. [PubMed: 18244210]
- [22]. Langton CM, Njeh CF, Hodgskinson R, and Currey JD, "Prediction of mechanical properties of the human calcaneus by broadband ultrasonic attenuation," *Bone*, vol. 18, no. 6, pp. 495–503, 6 1996. [PubMed: 8805988]
- [23]. Nowicki A, Litniewski J, Secomski W, Lewin PA, and Trots I, "Estimation of ultrasonic attenuation in a bone using coded excitation," *Ultrasonics*, vol. 41, no. 8, pp. 615–21, 11 2003. [PubMed: 14585473]
- [24]. Laugier P, Giat P, and Berger G, "Broadband ultrasonic attenuation imaging: a new imaging technique of the os calcis," *Calcif Tissue Int*, vol. 54, no. 2, pp. 83–6, 2 1994. [PubMed: 8012875]
- [25]. Laugier P, Fournier B, and Berger G, "Ultrasound parametric imaging of the calcaneus: in vivo results with a new device," *Calcif Tissue Int*, vol. 58, no. 5, pp. 326–31, 5 1996. [PubMed: 8661966]
- [26]. Laugier P, Novikov V, Elmann-Larsen B, and Berger G, "Quantitative ultrasound imaging of the calcaneus: precision and variations during a 120-Day bed rest," *Calcif Tissue Int*, vol. 66, no. 1, pp. 16–21, 1 2000. [PubMed: 10602839]
- [27]. Defontaine M et al., "2D arrays device for calcaneus bone transmission: an alternative technological solution using crossed beam forming," *Ultrasonics*, vol. 42, no. 1–9, pp. 745–52, 4 2004. [PubMed: 15047377]
- [28]. Xia Y, Lin W, and Qin YX, "The influence of cortical end-plate on broadband ultrasound attenuation measurements at the human calcaneus using scanning confocal ultrasound," *J Acoust Soc Am*, vol. 118, no. 3 Pt 1, pp. 1801–7, 9 2005.
- [29]. Alomari AH, Wille ML, and Langton CM, "The dependence of broadband ultrasound attenuation on phase interference in thin plates of variable thickness and curvature: a comparison of experimental measurement and computer simulation," *Proc Inst Mech Eng H*, vol. 232, no. 5, pp. 468478, 5 2018.

- [30]. Tasinkevych Y, Falinska K, Lewin PA, and Litniewski J, "Improving broadband ultrasound attenuation assessment in cancellous bone by mitigating the influence of cortical bone: Phantom and in-vitro study," *Ultrasonics*, vol. 94, pp. 382–390, 4 2019. [PubMed: 30001852]
- [31]. Barkmann R et al., "A method for the estimation of femoral bone mineral density from variables of ultrasound transmission through the human femur," *Bone*, vol. 40, no. 1, pp. 37–44, 1 2007. [PubMed: 16949896]
- [32]. Barkmann R et al., "In vivo measurements of ultrasound transmission through the human proximal femur," *Ultrasound Med Biol*, vol. 34, no. 7, pp. 1186–90, 7 2008. [PubMed: 18294756]
- [33]. Barkmann R et al., "Femur ultrasound (FemUS)--first clinical results on hip fracture discrimination and estimation of femoral BMD," *Osteoporos Int*, vol. 21, no. 6, pp. 969–76, 6 2010. [PubMed: 19693640]
- [34]. Laugier P, "Instrumentation for in vivo ultrasonic characterization of bone strength," *IEEE Trans Ultrason Ferroelectr Freq Control*, vol. 55, no. 6, pp. 1179–96, 2008. [PubMed: 18599407]
- [35]. Lin W, Xia Y, and Qin YX, "Characterization of the trabecular bone structure using frequency modulated ultrasound pulse," *J Acoust Soc Am*, vol. 125, no. 6, pp. 4071–7, 6 2009. [PubMed: 19507988]
- [36]. Lin W, Serra-Hsu F, Cheng J, and Qin YX, "Frequency specific ultrasound attenuation is sensitive to trabecular bone structure," *Ultrasound Med Biol*, vol. 38, no. 12, pp. 2198–207, 12 2012. [PubMed: 22975035]
- [37]. Chen T, Tzeng JS, and Lin CJ, "A novel method to measure acoustic speed of bone tissue," *Ultrasound Med Biol*, vol. 23, no. 9, pp. 1337–41, 1997. [PubMed: 9428133]
- [38]. Chen P, Chen T, Lu M, and Yao W, "The measurements of ultrasound parameters on calcaneus by two-sided interrogation techniques," *Meas. Sci. Tech*, vol. 16, pp. 1349–1354, 2005.
- [39]. Xia Y, Lin W, and Qin YX, "Bone surface topology mapping and its role in trabecular bone quality assessment using scanning confocal ultrasound," *Osteoporos Int*, vol. 18, no. 7, pp. 905–13, 7 2007. [PubMed: 17361323]
- [40]. Lin L, Lin W, and Qin YX, "Enhanced correlation between quantitative ultrasound and structural and mechanical properties of bone using combined transmission-reflection measurement," *J Acoust Soc Am*, vol. 137, no. 3, pp. 1144–52, 3 2015. [PubMed: 25786930]
- [41]. Rossman P, Zagzebski J, Mesina C, Sorenson J, and Mazess R, "Comparison of speed of sound and ultrasound attenuation in the os calcis to bone density of the radius, femur and lumbar spine," *Clin Phys Physiol Meas*, vol. 10, no. 4, pp. 353–60, 11 1989. [PubMed: 2698780]
- [42]. Tavakoli MB and Evans JA, "Dependence of the velocity and attenuation of ultrasound in bone on the mineral content," *Phys Med Biol*, vol. 36, no. 11, pp. 1529–37, 11 1991. [PubMed: 1754623]
- [43]. Chappard C, Laugier P, Fournier B, Roux C, and Berger G, "Assessment of the relationship between broadband ultrasound attenuation and bone mineral density at the calcaneus using BUA imaging and DXA," *Osteoporos Int*, vol. 7, no. 4, pp. 316–22, 1997. [PubMed: 9373564]
- [44]. Wear KA, "The effect of phase cancellation on estimates of calcaneal broadband ultrasound attenuation in vivo," *IEEE Trans Ultrason Ferroelectr Freq Control*, vol. 54, no. 7, pp. 1352–9, 7 2007. [PubMed: 17718324]
- [45]. Chaffai S, Padilla F, Berger G, and Laugier P, "In vitro measurement of the frequency-dependent attenuation in cancellous bone between 0.2 and 2 MHz," *J Acoust Soc Am*, vol. 108, no. 3 Pt 1, pp. 1281–9, 9 2000. [PubMed: 11008828]
- [46]. Wear KA, "Ultrasonic attenuation in human calcaneus from 0.2 to 1.7 MHz," *IEEE Trans Ultrason Ferroelectr Freq Control*, vol. 48, no. 2, pp. 602–8, 3 2001. [PubMed: 11370374]
- [47]. Strelitzki R and Evans JA, "An investigation of the measurement of broadband ultrasonic attenuation in trabecular bone," *Ultrasonics*, vol. 34, no. 8, pp. 785–91, 12 1996. [PubMed: 9010461]
- [48]. Wear KA, "Nonlinear attenuation and dispersion in human calcaneus in vitro: statistical validation and relationships to microarchitecture," *J Acoust Soc Am*, vol. 137, no. 3, pp. 1126–33, 3 2015. [PubMed: 25786928]

- [49]. Hakulinen MA et al., "Prediction of density and mechanical properties of human trabecular bone in vitro by using ultrasound transmission and backscattering measurements at 0.2-6.7 MHz frequency range," *Phys Med Biol*, vol. 50, no. 8, pp. 1629–42, 4 21 2005. [PubMed: 15815086]
- [50]. Laugier P, Droin P, Laval-Jeantet AM, and Berger G, "In vitro assessment of the relationship between acoustic properties and bone mass density of the calcaneus by comparison of ultrasound parametric imaging and quantitative computed tomography," *Bone*, vol. 20, no. 2, pp. 157–65, 2 1997. [PubMed: 9028541]
- [51]. Wear KA, Stuber AP, and Reynolds JC, "Relationships of ultrasonic backscatter with ultrasonic attenuation, sound speed and bone mineral density in human calcaneus," *Ultrasound Med Biol*, vol. 26, no. 8, pp. 1311–6, 10 2000. [PubMed: 11120369]
- [52]. Chaffai S, Peyrin F, Nuzzo S, Porcher R, Berger G, and Laugier P, "Ultrasonic characterization of human cancellous bone using transmission and backscatter measurements: relationships to density and microstructure," *Bone*, vol. 30, no. 1, pp. 229–37, 1 2002. [PubMed: 11792590]
- [53]. Wear KA, Nagaraja S, Dreher ML, and Gibson SL, "Relationships of quantitative ultrasound parameters with cancellous bone microstructure in human calcaneus in vitro," *J Acoust Soc Am*, vol. 131, no. 2, pp. 1605–12, 2 2012. [PubMed: 22352530]
- [54]. McKelvie ML, Fordham J, Clifford C, and Palmer SB, "In vitro comparison of quantitative computed tomography and broadband ultrasonic attenuation of trabecular bone," *Bone*, vol. 10, no. 2, pp. 101–4, 1989. [PubMed: 2669899]
- [55]. Nicholson PH et al., "Do quantitative ultrasound measurements reflect structure independently of density in human vertebral cancellous bone?," *Bone*, vol. 23, no. 5, pp. 425–31, 11 1998. [PubMed: 9823448]
- [56]. Jenson F, Padilla F, Bousson V, Bergot C, Laredo JD, and Laugier P, "In vitro ultrasonic characterization of human cancellous femoral bone using transmission and backscatter measurements: relationships to bone mineral density," *J Acoust Soc Am*, vol. 119, no. 1, pp. 654–63, 1 2006.
- [57]. Padilla F, Jenson F, Bousson V, Peyrin F, and Laugier P, "Relationships of trabecular bone structure with quantitative ultrasound parameters: in vitro study on human proximal femur using transmission and backscatter measurements," *Bone*, vol. 42, no. 6, pp. 1193–202, 6 2008. [PubMed: 18396124]
- [58]. Hoffmeister BK, Whitten SA, Kaste SC, and Rho JY, "Effect of collagen and mineral content on the high-frequency ultrasonic properties of human cancellous bone," *Osteoporos Int*, vol. 13, no. 1, pp. 26–32, 1 2002. [PubMed: 11878452]
- [59]. Dencks S, Barkmann R, Padilla F, Laugier P, Schmitz G, and Gluer CC, "Model-based estimation of quantitative ultrasound variables at the proximal femur," *IEEE Trans Ultrason Ferroelectr Freq Control*, vol. 55, no. 6, pp. 1304–15, 2008. [PubMed: 18599418]
- [60]. Barkmann et al., "A device for in vivo measurements of quantitative ultrasound variables at the human proximal femur," *IEEE Trans Ultrason Ferroelectr Freq Control*, vol. 55, no. 6, pp. 1197–204, 2008. [PubMed: 18599408]
- [61]. Gluer CC, Vahlensieck M, Faulkner KG, Engelke K, Black D, and Genant HK, "Site-matched calcaneal measurements of broad-band ultrasound attenuation and single X-ray absorptiometry: do they measure different skeletal properties?," *J Bone Miner Res*, vol. 7, no. 9, pp. 1071–9, 9 1992. [PubMed: 1414499]
- [62]. Waud CE, Lew R, and Baran DT, "The relationship between ultrasound and densitometric measurements of bone mass at the calcaneus in women," *Calcif Tissue Int*, vol. 51, no. 6, pp. 415–8, 12 1992. [PubMed: 1451008]
- [63]. Toyras J, Kroger H, and Jurvelin JS, "Bone properties as estimated by mineral density, ultrasound attenuation, and velocity," *Bone*, vol. 25, no. 6, pp. 725–31, 12 1999.
- [64]. Langton CM and Langton DK, "Comparison of bone mineral density and quantitative ultrasound of the calcaneus: site-matched correlation and discrimination of axial BMD status," *Br J Radiol*, vol. 73, no. 865, pp. 31–5, 1 2000. [PubMed: 10721317]
- [65]. Toyras J, Nieminen MT, Kroger H, and Jurvelin JS, "Bone mineral density, ultrasound velocity, and broadband attenuation predict mechanical properties of trabecular bone differently," *Bone*, vol. 31, no. 4, pp. 503–7, 10 2002. [PubMed: 12398947]

- [66]. Hodgkinson R, Njeh CF, Whitehead MA, and Langton CM, "The non-linear relationship between BUA and porosity in cancellous bone," *Rhys Med Biol*, vol. 41, no. 11, pp. 2411–20. 11 1996.
- [67]. Serpe L and Rho JY, "The nonlinear transition period of broadband ultrasound attenuation as bone density varies," *J Biomech*, vol. 29, no. 7, pp. 963–6, 7 1996. [PubMed: 8809627]
- [68]. Han S, Rho J, Medige J, and Ziv I, "Ultrasound velocity and broadband attenuation over a wide range of bone mineral density," *Osteoporos Int*, vol. 6, no. 4, pp. 291–6, 1996. [PubMed: 8883117]
- [69]. Riekkinen O, Hakulinen MA, Lanuni MJ, Jurvelin JS, Kallioniemi A, and Toyras J, "Acoustic properties of trabecular bone—relationships to tissue composition," *Ultrasound Med Biol*, vol. 33, no. 9, pp. 1438–44, 9 2007. [PubMed: 17561333]
- [70]. Ulrich D, van Rietbergen B, Laib A, and Rueggsegger P, "The ability of three-dimensional structural indices to reflect mechanical aspects of trabecular bone," *Bone*, vol. 25, no. 1, pp. 55–60. 7 1999. [PubMed: 10423022]
- [71]. Stauber M and Muller R, "Volumetric spatial decomposition of trabecular bone into rods and plates—a new method for local bone morphometry," *Bone*, vol. 38, no. 4, pp. 475–84, 4 2006. [PubMed: 16338187]
- [72]. Boutroy S, Van Rietbergen B, Somay-Rendu E, Munoz F, Bouxsein ML, and Delmas PD, "Finite element analysis based on in vivo HR-pQCT images of the distal radius is associated with wrist fracture in postmenopausal women," *J Bone Miner Res*, vol. 23, no. 3, pp. 392–9, 3 2008. [PubMed: 17997712]
- [73]. Kaufman JJ, Luo G, and Siffert RS, "3D simulation of ultrasound in the ultra-distal radius," in *Acoustical Imaging*, vol. 31, N A. et al., Ed.: Springer, 2012, pp. 39–43.
- [74]. Cheung AM et al., "High-resolution peripheral quantitative computed tomography for the assessment of bone strength and structure: a review by the Canadian Bone Strength Working Group," *Curr Osteoporos Rep*, vol. 11, no. 2, pp. 136–46, 6 2013. [PubMed: 23525967]
- [75]. Trebacz H and Natali A, "Ultrasound velocity and attenuation in cancellous bone samples from lumbar vertebra and calcaneus," *Osteoporos Int*, vol. 9, no. 2, pp. 99–105, 1999. [PubMed: 10367035]
- [76]. Nicholson PH et al., "Quantitative ultrasound and trabecular architecture in the human calcaneus," *J Bone Miner Res*, vol. 16no. 10 pp. 1886–92. 10 2001. [PubMed: 11585354]
- [77]. Hakulinen MA, Day JS, Toyras J, Weinans H, and Jurvelin JS, "Ultrasonic characterization of human trabecular bone microstructure," *Phys Med Biol*. vol. 51, no. 6, pp. 1633–48. 3 21 2006. [PubMed: 16510968]
- [78]. Keaveny TM and Hayes WC, "A 20-year perspective on the mechanical properties of trabecular bone," *J Biomech Eng*, vol. 115, no. 4B, pp. 534–42, 11 1993. [PubMed: 8302037]
- [79]. Morgan EF, Bayraktar HH, and Keaveny TM, "Trabecular bone modulus-density relationships depend on anatomic site," *J Biomech*, vol. 36, no. 7, pp. 897–904, 7 2003. [PubMed: 12757797]
- [80]. Bevill G and Keaveny TM, "Trabecular bone strength predictions using finite element analysis of micro-scale images at limited spatial resolution," *Bone*, vol. 44, no. 4, pp. 579–84. 4 2009. [PubMed: 19135184]
- [81]. Wang J et al., "Trabecular plates and rods determine elastic modulus and yield strength of human trabecular bone," *Bone*, vol. 72 pp. 71–80. 3 2015. [PubMed: 25460571]
- [82]. Oftadeh R, Perez-Viloria M, Villa-Camacho JC, Vaziri A, and Nazarian A, "Biomechanics and mechanobiology of trabecular bone: a review," *J Biomech Eng*, vol. 137, no. 1, 1 2015.
- [83]. Hakulinen MA, Toyras J, Saarakkala S, Hirvonen J, Kroger H, and Jurvelin JS, "Ability of ultrasound backscattering to predict mechanical properties of bovine trabecular bone," *Ultrasound Med Biol*, vol. 30, no. 7, pp. 919–27. 7 2004. [PubMed: 15313324]
- [84]. Bevill G, Eswaran SK, Farahmand F, and Keaveny TM, "The influence of boundary conditions and loading mode on high-resolution finite element-computed trabecular tissue properties." *Bone*, vol. 44 no. 4 pp. 573–8. 4 2009. [PubMed: 19110082]
- [85]. Althomali MAM, Wille ML, Shortell MP and Langton CM, "Estimation of mechanical stiffness by finite element analysis of ultrasound computed tomography (UCT-FEA); a comparison with



X-ray  $\mu$ CT based FEA in cancellous bone replica models,” *Appl. Acoust.*, vol. 133, pp. 8–15. 2018.

- [86]. Bouxsein ML and Radloff SE, “Quantitative ultrasound of the calcaneus reflects the mechanical properties of calcaneal trabecular bone,” *J Bone Miner Res.*, vol. 12, no. 5, pp. 839–46. 5 1997. [PubMed: 9144351]
- [87]. Wear KA, Nagaraja S, Dreher ML, Sadoughi S, Zhu S, and Keaveny TM, “Relationships among ultrasonic and mechanical properties of cancellous bone in human calcaneus in vitro,” *Bone.* vol. 103, pp. 93–101, 10 2017. [PubMed: 28666970]
- [88]. Riekkinen O, Hakulinen MA, Toyras J, and Jurvelin JS, “Spatial variation of acoustic properties is related with mechanical properties of trabecular bone,” *Phys Med Biol.*, vol. 52, no. 23, pp. 6961–8, 12 7 2007. [PubMed: 18029987]
- [89]. Nicholson PH and Bouxsein ML, “Quantitative ultrasound does not reflect mechanically induced damage in human cancellous bone,” *J Bone Miner Res.*, vol. 15, no. 12, pp. 2467–72. 12 2000. [PubMed: 11127211]
- [90]. Nicholson PF, “Ultrasound and the biomechanical competence of bone,” *IEEE Trans Ultrason Ferroelectr Freq Control.*, vol. 55, no. 7, pp. 1539–45, 7 2008. [PubMed: 18986944]
- [91]. Busse LJ and Miller JG, “Detection of spatially nonuniform ultrasonic radiation with phase sensitive (piezoelectric) and phase insensitive (acoustoelectric) receivers,” *J. Acoust. Soc. Am.*, vol. 70, no. 5, pp. 1377–1386, 1981.
- [92]. Petley GW, Robins PA, and Aindow JD, “Broadband ultrasonic attenuation: are current measurement techniques inherently inaccurate?,” *Br J Radiol.*, vol. 68, no. 815, pp. 1212–4, 11 1995. [PubMed: 8542228]
- [93]. Strelitzki R, Metcalfe SC, Nicholson PH, Evans JA, and Paech V, “On the ultrasonic attenuation and its frequency dependence in the os calcis assessed with a multielement receiver,” *Ultrasound Med Biol.*, vol. 25, no. 1, pp. 133–41, 1 1999. [PubMed: 10048810]
- [94]. Wear KA, “The effect of phase cancellation on estimates of broadband ultrasound attenuation and backscatter coefficient in human calcaneus in vitro,” *IEEE Trans Ultrason Ferroelectr Freq Control.*, vol. 55, no. 2, pp. 384–90, 2 2008. [PubMed: 18334344]
- [95]. Cheng J, Serra-Hsu F, Tian Y, Lin W, and Qin YX, “Effects of phase cancellation and receiver aperture size on broadband ultrasonic attenuation for trabecular bone in vitro,” *Ultrasound Med Biol.*, vol. 37, no. 12, pp. 2116–25, 12 2011. [PubMed: 22033134]
- [96]. Langton CM and Wille ML, “Experimental and computer simulation validation of ultrasound phase interference created by lateral inhomogeneity of transit time in replica bone: marrow composite models,” *Proc Inst Mech Eng H.*, vol. 227, no. 8, pp. 890–5, 8 2013. [PubMed: 23636768]
- [97]. Wille ML, Almualimi MA, and Langton CM, “Pulse-echo ultrasound transit time spectroscopy: A comparison of experimental measurement and simulation prediction,” *Proc Inst Mech Eng H.*, vol. 230, no. 1, pp. 20–9, 1 2016. [PubMed: 26586528]
- [98]. Langton CM, Wille ML, and Flegg MB, “A deconvolution method for deriving the transit time spectrum for ultrasound propagation through cancellous bone replica models,” *Proc Inst Mech Eng H.*, vol. 228, no. 4, pp. 321–9, 4 2014. [PubMed: 24598434]
- [99]. Wille ML, Zapf M, Ruiter NV, Gemmeke H, and Langton CM, “Comparison of active-set method deconvolution and matched-filtering for derivation of an ultrasound transit time spectrum,” *Phys Med Biol.*, vol. 60, no. 12, pp. N251–60, 6 21 2015. [PubMed: 26047163]
- [100]. Wille ML and Langton CM, “Solid volume fraction estimation of bone:marrow replica models using ultrasound transit time spectroscopy,” *Ultrasonics.*, vol. 65, pp. 329–37, 2 2016. [PubMed: 26455950]
- [101]. Alomari AH, Wille ML, and Langton CM, “Bone volume fraction and structural parameters for estimation of mechanical stiffness and failure load of human cancellous bone samples; in-vitro comparison of ultrasound transit time spectroscopy and X-ray  $\mu$ CT,” *Bone.*, vol. 107, pp. 145–153, 2 2018. [PubMed: 29198979]
- [102]. Morse PM and Ingard KU, *Theoretical Acoustics.* Princeton, NJ: Princeton University Press, 1968.

- [103]. Laugier P, Giat P, Droin P, Saied A, and Berger G, "Ultrasound images of the os calcis: a new method of assessment of bone status," Proc. IEEE Ultrason. Symp., pp. 989–992, 1993.
- [104]. Strelitzki R, Clarke AJ, and Evans JA, "The measurement of the velocity of ultrasound in fixed trabecular bone using broadband pulses and single-frequency tone bursts," Phys Med Biol, vol. 41, no. 4, pp. 743–53, 4 1996. [PubMed: 8730667]
- [105]. Nicholson PH, Lowet G, Langton CM, Dequeker J, and Van der Perre G, "A comparison of time-domain and frequency-domain approaches to ultrasonic velocity measurement in trabecular bone," Phys Med Biol, vol. 41, no. 11, pp. 2421–35, 11 1996. [PubMed: 8938036]
- [106]. Wear KA, "The effects of frequency-dependent attenuation and dispersion on sound speed measurements: applications in human trabecular bone," IEEE Trans Ultrason Ferroelectr Freq Control, vol. 47, no. 1, pp. 265–73, 2000. [PubMed: 18238539]
- [107]. Wear KA, "The dependence of time-domain speed-of-sound measurements on center frequency, bandwidth, and transit-time marker in human calcaneus in vitro," J Acoust Soc Am, vol. 122, no. 1, pp. 636–44, 7 2007. [PubMed: 17614520]
- [108]. Wear KA, "A method for improved standardization of in vivo calcaneal time-domain speed-of-sound measurements," IEEE Trans Ultrason Ferroelectr Freq Control, vol. 55, no. 7, pp. 1473–9, 7 2008. [PubMed: 18986936]
- [109]. Le LH, "An investigation of pulse-timing techniques for broadband ultrasonic velocity determination in cancellous bone: a simulation study," Phys Med Biol, vol. 43, no. 8, pp. 2295–308, 8 1998. [PubMed: 9725605]
- [110]. Ragozzino M, "Analysis of the error in measurement of ultrasound speed in tissue due to waveform deformation by frequency-dependent attenuation," Ultrasonics, vol. 19, no. 3, pp. 135–8, 5 1981. [PubMed: 7222263]
- [111]. Njeh CF, Hodgskinson R, Currey JD, and Langton CM, "Orthogonal relationships between ultrasonic velocity and material properties of bovine cancellous bone," Med Eng Phys, vol. 18, no. 5, pp. 373–81, 7 1996. [PubMed: 8818135]
- [112]. Njeh CF and Langton CM, "The effect of cortical endplates on ultrasound velocity through the calcaneus: an in vitro study," Br J Radiol, vol. 70, no. 833, pp. 504–10, 5 1997. [PubMed: 9227233]
- [113]. Njeh CF, Kuo CW, Langton CM, Atrah HI, and Boivin CM, "Prediction of human femoral bone strength using ultrasound velocity and BMD: an in vitro study," Osteoporos Int, vol. 7, no. 5, pp. 471–7, 1997. [PubMed: 9425506]
- [114]. Hoffmeister BK, Whitten SA, and Rho JY, "Low-megahertz ultrasonic properties of bovine cancellous bone," Bone, vol. 26, no. 6, pp. 635–42, 6 2000. [PubMed: 10831936]
- [115]. Hoffmeister BK, Auwarter JA, and Rho JY, "Effect of marrow on the high frequency ultrasonic properties of cancellous bone," Phys Med Biol, vol. 47, no. 18, pp. 3419–27, 9 21 2002. [PubMed: 12375829]
- [116]. Hodgskinson R, Njeh CF, Currey JD, and Langton CM, "The ability of ultrasound velocity to predict the stiffness of cancellous bone in vitro," Bone, vol. 21, no. 2, pp. 183–90, 8 1997. [PubMed: 9267694]
- [117]. Du H, Mohanty K, and Muller M, "Microstructural characterization of trabecular bone using ultrasonic backscattering and diffusion parameters," J Acoust Soc Am, vol. 141, no. 5, p. EL445, 5 2017. [PubMed: 28599551]
- [118]. Hoffmeister BK, Huber MT, Viano AM, and Huang J, "Characterization of a polymer, open-cell rigid foam that simulates the ultrasonic properties of cancellous bone," J Acoust Soc Am, vol. 143, no. 2, p. 911, 2 2018. [PubMed: 29495707]
- [119]. Mizuno K, Somiya H, Kubo T, Matsukawa M, Otani T, and Tsujimoto T, "Influence of cancellous bone microstructure on two ultrasonic wave propagations in bovine femur: an in vitro study," J Acoust Soc Am, vol. 128, no. 5, pp. 3181–9, 11 2010. [PubMed: 21110613]
- [120]. Alves JM, Xu W, Lin D, Siffert RS, Ryaby JT, and Kaufman JJ, "Ultrasonic assessment of human and bovine trabecular bone: a comparison study," IEEE Trans Biomed Eng, vol. 43, no. 3, pp. 249–58, 3 1996. [PubMed: 8682537]
- [121]. Haiat G et al., "In vitro speed of sound measurement at intact human femur specimens," Ultrasound Med Biol, vol. 31, no. 7, pp. 987–96, 7 2005. [PubMed: 15972205]

- [122]. Mizuno K, Matsukawa M, Otani T, Laugier P, and Padilla F, "Propagation of two longitudinal waves in human cancellous bone: an in vitro study," *J Acoust Soc Am*, vol. 125, no. 5, pp. 3460–6, 5 2009. [PubMed: 19425685]
- [123]. Mizuno K, Matsukawa M, Otani T, Takada M, Mano I, and Tsujimoto T, "Effects of structural anisotropy of cancellous bone on speed of ultrasonic fast waves in the bovine femur," *IEEE Trans Ultrason Ferroelectr Freq Control*, vol. 55, no. 7, pp. 1480–7, 7 2008. [PubMed: 18986937]
- [124]. Haiat G et al., "Optimal prediction of bone mineral density with ultrasonic measurements in excised human femur," *Calcif Tissue Int*, vol. 77, no. 3, pp. 186–92, 9 2005. [PubMed: 16151672]
- [125]. Goossens L et al., "The correlation between the SOS in trabecular bone and stiffness and density studied by finite-element analysis," *IEEE Trans Ultrason Ferroelectr Freq Control*, vol. 55, no. 6, pp. 1234–42, 2008. [PubMed: 18599411]
- [126]. Cavani F et al., "Influence of density, elasticity, and structure on ultrasound transmission through trabecular bone cylinders," *IEEE Trans Ultrason Ferroelectr Freq Control*, vol. 55, no. 7, pp. 1465–72, 7 2008. [PubMed: 18986935]
- [127]. Zagzebski JA, Rossman PJ, Mesina C, Mazess RB, and Madsen EL, "Ultrasound transmission measurements through the os calcis," *Calcif Tissue Int*, vol. 49, no. 2, pp. 107–11, 8 1991. [PubMed: 1913288]
- [128]. Nicholson PH and Boussein ML, "Effect of temperature on ultrasonic properties of the calcaneus in situ," *Osteoporos Int*, vol. 13, no. 11, pp. 888–92, 11 2002. [PubMed: 12415436]
- [129]. Lee KI, Roh HS, and Yoon SW, "Correlations between acoustic properties and bone density in bovine cancellous bone from 0.5 to 2 MHz," *J Acoust Soc Am*, vol. 113, no. 5, pp. 2933–8, 5 2003. [PubMed: 12765411]
- [130]. Haiat G, Padilla F, Cleveland RO, and Laugier P, "Effects of frequency-dependent attenuation and velocity dispersion on in vitro ultrasound velocity measurements in intact human femur specimens," *IEEE Trans Ultrason Ferroelectr Freq Control*, vol. 53, no. 1, pp. 39–51, 1 2006. [PubMed: 16471431]
- [131]. Haiat G, Padilla F, Barkmann R, Gluer CC, and Laugier P, "Numerical simulation of the dependence of quantitative ultrasonic parameters on trabecular bone microarchitecture and elastic constants," *Ultrasonics*, vol. 44 Suppl 1, pp. e289–94, 12 22 2006. [PubMed: 16859726]
- [132]. Qin YX et al., "Prediction of trabecular bone qualitative properties using scanning quantitative ultrasound," *Acta Astronaut*, vol. 92, no. 1, pp. 79–88, 11 2013. [PubMed: 23976803]
- [133]. Alves JM, Ryaby JT, Kaufman JJ, Magee FP, and Siffert RS, "Influence of marrow on ultrasonic velocity and attenuation in bovine trabecular bone," *Calcif Tissue Int*, vol. 58, no. 5, pp. 362–7, 5 1996. [PubMed: 8661972]
- [134]. Luo G et al., "Computational methods for ultrasonic bone assessment," *Ultrasound Med Biol*, vol. 25, no. 5, pp. 823–30, 6 1999. [PubMed: 10414899]
- [135]. Cardoso L, Teboul F, Sedel L, Oddou C, and Meunier A, "In vitro acoustic waves propagation in human and bovine cancellous bone," *J Bone Miner Res*, vol. 18, no. 10, pp. 1803–12, 10 2003. [PubMed: 14584891]
- [136]. Njeh CF et al., "Comparison of six calcaneal quantitative ultrasound devices: precision and hip fracture discrimination," *Osteoporos Int*, vol. 11, no. 12, pp. 1051–62, 2000. [PubMed: 11256897]
- [137]. Otani T et al., "Attempt at standardization of bone quantitative ultrasound in Japan," *J Med Ultrason (2001)*, vol. 45, no. 1, pp. 3–13, 1 2018. [PubMed: 28884290]
- [138]. Wear KA, "A numerical method to predict the effects of frequency-dependent attenuation and dispersion on speed of sound estimates in cancellous bone," *J Acoust Soc Am*, vol. 109, no. 3, pp. 1213–8, 3 2001. [PubMed: 11303934]
- [139]. Kolsky H, *Stress waves in solids*. New York: Dover, 1963.
- [140]. Ashman RB, Corin JD, and Turner CH, "Elastic properties of cancellous bone: measurement by an ultrasonic technique," *J Biomech*, vol. 20, no. 10, pp. 979–86, 1987. [PubMed: 3693379]
- [141]. Turner CH and Eich M, "Ultrasonic velocity as a predictor of strength in bovine cancellous bone," *Calcif Tissue Int*, vol. 49, no. 2, pp. 116–9, 8 1991. [PubMed: 1913290]

- [142]. Wear KA, "Cancellous bone analysis with modified least squares Prony's method and chirp filter: phantom experiments and simulation," *J Acoust Soc Am*, vol. 128, no. 4, pp. 2191–203, 10 2010. [PubMed: 20968389]
- [143]. Waters KR and Hoffmeister BK, "Kramers-Kronig analysis of attenuation and dispersion in trabecular bone," *J Acoust Soc Am*, vol. 118, no. 6, pp. 3912–20, 12 2005. [PubMed: 16419833]
- [144]. Lin W, Mittra E, and Qin YX, "Determination of ultrasound phase velocity in trabecular bone using time dependent phase tracking technique," *J Biomech Eng*, vol. 128, no. 1, pp. 24–9, 2 2006. [PubMed: 16532614]
- [145]. O'Donnell M, Jaynes ET, and Miller JG, "Kramers–Kronig relationship between ultrasonic attenuation and phase velocity," *J Acoust Soc Am*, vol. 69, pp. 696–701, 1981.
- [146]. Groopman AM et al., "Conventional, Bayesian, and Modified Prony's methods for characterizing fast and slow waves in equine cancellous bone," *J Acoust Soc Am*, vol. 138, no. 2, pp. 594–604, 8 2015. [PubMed: 26328678]
- [147]. Bauer AQ, Marutyan KR, Holland MR, and Miller JG, "Is the Kramers-Kronig relationship between ultrasonic attenuation and dispersion maintained in the presence of apparent losses due to phase cancellation?," *J Acoust Soc Am*, vol. 122, no. 1, pp. 222–8, 7 2007. [PubMed: 17614481]
- [148]. Strelitzki R and Evans JA, "On the measurement of the velocity of ultrasound in the os calcis using short pulses," *Euro. J. Ultrasound*, vol. 4, pp. 205–213, 1996.
- [149]. Wear KA, "Measurements of phase velocity and group velocity in human calcaneus," *Ultrasound Med Biol*, vol. 26, no. 4, pp. 641–6, 5 2000. [PubMed: 10856627]
- [150]. Wear KA, "Group velocity, phase velocity, and dispersion in human calcaneus in vivo," *J Acoust Soc Am*, vol. 121, no.4, pp. 2431–7, 4 2007. [PubMed: 17471754]
- [151]. Lee KI, "Correlations of group velocity, phase velocity, and dispersion with bone density in bovine trabecular bone," *J Acoust Soc Am*, vol. 130, no. 6, pp. EL399–404, 12 2011. [PubMed: 22225133]
- [152]. Lee KI, "Velocity dispersion and backscatter in marrow-filled and water-filled trabecular bone samples in vitro," *J Acoust Soc Am*, vol. 144, no. 5, p. EL386, 11 2018. [PubMed: 30522272]
- [153]. Chen PJ and Chen T, "Measurements of acoustic dispersion on calcaneus using split spectrum processing technique," *Med Eng Phys*, vol. 28, no. 2, pp. 187–93, 3 2006. [PubMed: 15939657]
- [154]. Marutyan KR, Holland MR, and Miller JG, "Anomalous negative dispersion in bone can result from the interference of fast and slow waves," *J Acoust Soc Am*, vol. 120, no. 5 Pt 1, pp. EL55–61, 11 2006. [PubMed: 17139755]
- [155]. Bauer AQ, Marutyan KR, Holland MR, and Miller JG, "Negative dispersion in bone: the role of interference in measurements of the apparent phase velocity of two temporally overlapping signals," *J Acoust Soc Am*, vol. 123, no. 4, pp. 2407–14, 4 2008. [PubMed: 18397043]
- [156]. Anderson CC, Marutyan KR, Holland MR, Wear KA, and Miller JG, "Interference between wave modes may contribute to the apparent negative dispersion observed in cancellous bone," *J Acoust Soc Am*, vol. 124, no. 3, pp. 1781–9, 9 2008. [PubMed: 19045668]
- [157]. Nelson AM et al., "Determining attenuation properties of interfering fast and slow ultrasonic waves in cancellous bone," *J Acoust Soc Am*, vol. 130, no. 4, pp. 2233–40, 10 2011. [PubMed: 21973378]
- [158]. Biot MA, "The theory of propagation of elastic waves in fluid-saturated porous solid. I. Higher frequency range," *J. Acoust. Soc. Am*, vol. 28, pp. 179–191, 1956.
- [159]. Biot MA, "The theory of propagation of elastic waves in fluid-saturated porous solid. I. Low frequency range," *J. Acoust. Soc. Am*, vol. 28, pp. 168–178, 1956.
- [160]. Haiat G, Lhemery A, Renaud F, Padilla F, Laugier P, and Naili S, "Velocity dispersion in trabecular bone: influence of multiple scattering and of absorption," *J Acoust Soc Am*, vol. 124, no. 6, pp. 4047–58, 12 2008. [PubMed: 19206827]
- [161]. Wear KA, "The dependencies of phase velocity and dispersion on trabecular thickness and spacing in trabecular bone-mimicking phantoms," *J Acoust Soc Am*, vol. 118, no. 2, pp. 1186–92, 8 2005. [PubMed: 16158673]

- [162]. Wear KA, "The dependencies of phase velocity and dispersion on volume fraction in cancellous-bone-mimicking phantoms," *J Acoust Soc Am*, vol. 125, no. 2, pp. 1197–201, 2 2009. [PubMed: 19206892]
- [163]. Hughes ER, Leighton TG, Petley GW, and White PR, "Ultrasonic propagation in cancellous bone: a new stratified model," *Ultrasound Med Biol*, vol. 25, no. 5, pp. 811–21, 6 1999. [PubMed: 10414898]
- [164]. Lin W, Qin YX, and Rubin C, "Ultrasonic wave propagation in trabecular bone predicted by the stratified model," *Ann Biomed Eng*, vol. 29, no. 9, pp. 781–90, 9 2001. [PubMed: 11599586]
- [165]. Wear KA, "A stratified model to predict dispersion in trabecular bone," *IEEE Trans Ultrason Ferroelectr Freq Control*, vol. 48, no. 4, pp. 1079–83, 7 2001. [PubMed: 11477766]
- [166]. Pakula M, Padilla F, and Laugier P, "Influence of the filling fluid on frequency-dependent velocity and attenuation in cancellous bones between 0.35 and 2.5 MHz," *J Acoust Soc Am*, vol. 126, no. 6, pp. 3301–10, 12 2009. [PubMed: 20000944]
- [167]. Hans D et al., "Ultrasound velocity of trabecular cubes reflects mainly bone density and elasticity," *Calcif Tissue Int*, vol. 64, no. 1, pp. 18–23, 1 1999. [PubMed: 9868278]
- [168]. Guipieri S et al., "Ultrasound Speed of Sound Measurements in Trabecular Bone Using the Echographic Response of a Metallic Pin," *Ultrasound Med Biol*, vol. 41, no. 11, pp. 2966–76, 11 2015. [PubMed: 26320667]
- [169]. Haire TJ and Langton CM, "Biot theory: a review of its application to ultrasound propagation through cancellous bone," *Bone*, vol. 24, no. 4, pp. 291–5, 4 1999. [PubMed: 10221540]
- [170]. Lee KI, Roh HS, and Yoon SW, "Acoustic wave propagation in bovine cancellous bone: application of the Modified Biot-Attenborough model," *J Acoust Soc Am*, vol. 114, no. 4 Pt 1, pp. 2284–93, 10 2003. [PubMed: 14587625]
- [171]. Fellah ZE, Chapelon JY, Berger S, Lauriks W, and Depollier C, "Ultrasonic wave propagation in human cancellous bone: application of Biot theory," *J Acoust Soc Am*, vol. 116, no. 1, pp. 61–73, 7 2004. [PubMed: 15295965]
- [172]. Langton CM and Njeh CF, "Quantitative Ultrasound," in *The Physical Measurement of Bone*, Langton M and Njeh CF, Eds. London, U.K: Institute of Physics, 2004, pp. 412–474.
- [173]. Hosokawa and A Otani T, "Ultrasonic wave propagation in bovine cancellous bone," *J Acoust Soc Am*, vol. 101, no. 1, pp. 558–62, 1 1997. [PubMed: 9000743]
- [174]. Kaczmarek M, Kubik J, and Pakula M, "Short ultrasonic waves in cancellous bone," *Ultrasonics*, vol. 40, no. 1–8, pp. 95–100, 5 2002. [PubMed: 12160076]
- [175]. Hosokawa A and Otani T, "Acoustic anisotropy in bovine cancellous bone," *J Acoust Soc Am*, vol. 103, no. 5 Pt 1, pp. 2718–22, 5 1998. [PubMed: 9604363]
- [176]. Yamashita K, Fujita F, Mizuno K, Mano I, and Matsukawa M, "Two-wave propagation imaging to evaluate the structure of cancellous bone," *IEEE Trans Ultrason Ferroelectr Freq Control*, vol. 59, no. 6, pp. 1160–6, 6 2012. [PubMed: 22711411]
- [177]. Lin L, Cheng J, Lin W, and Qin YX, "Prediction of trabecular bone principal structural orientation using quantitative ultrasound scanning," *J Biomech*, vol. 45, no. 10, pp. 1790–5, 6 26 2012. [PubMed: 22560370]
- [178]. Mizuno K, Nagatani Y, Yamashita K, and Matsukawa M, "Propagation of two longitudinal waves in a cancellous bone with the closed pore boundary," *J Acoust Soc Am*, vol. 130, no. 2, pp. EL122–7, 8 2011. [PubMed: 21877770]
- [179]. Nagatani Y, Mizuno K, and Matsukawa M, "Two-wave behavior under various conditions of transition area from cancellous bone to cortical bone," *Ultrasonics*, vol. 54, no. 5, pp. 1245–50, 7 2014. [PubMed: 24315036]
- [180]. Mano I, Horii K, Fujita F, Nagatani Y, Matsukawa M, and Otani T, "Influence of the circumferential wave on the fast and slow wave propagation in small distal radius bone," *Jpn. J. Appl. Phys*, vol. 53, pp. 07KF07–1–3, 2014.
- [181]. Hachiken T, Nakanishi S, and Matsukawa M, "Effect of medullary cavity in cancellous bone on two-wave phenomenon," *Jpn. J. Appl. Phys*, vol. 55, pp. 07KF16–1–5, 2016.
- [182]. Fujita F, Mizuno K, and Matsukawa M, "An experimental study on the ultrasonic wave propagation in cancellous bone: waveform changes during propagation," *J Acoust Soc Am*, vol. 134, no. 6, p. 4775, 12 2013. [PubMed: 25669289]

- [183]. Nagatani Y, Mizuno K, Saeki T, Matsukawa M, Sakaguchi T, and Hosoi H, "Numerical and experimental study on the wave attenuation in bone--FDTD simulation of ultrasound propagation in cancellous bone," *Ultrasonics*, vol. 48, no. 6–7, pp. 607–12, 11 2008. [PubMed: 18589470]
- [184]. Meziere F et al., "Experimental observation of ultrasound fast and slow waves through three-dimensional printed trabecular bone phantoms," *J Acoust Soc Am*, vol. 139, no. 2, pp. EL13–18, 2 2016. [PubMed: 26936578]
- [185]. Lashkari B, Manbachi A, Mandelis A, and Cobbold RS, "Slow and fast ultrasonic wave detection improvement in human trabecular bones using Golay code modulation," *J Acoust Soc Am*, vol. 132, no. 3, pp. EL222–8, 9 2012. [PubMed: 22979836]
- [186]. Yamamoto T et al., "Measurement of human trabecular bone by novel ultrasonic bone densitometry based on fast and slow waves," *OsteoporosInt*, vol. 20, no. 7, pp. 1215–24, 7 2009.
- [187]. Sai H et al., "Novel ultrasonic bone densitometry based on two longitudinal waves: significant correlation with pQCT measurement values and age-related changes in trabecular bone density, cortical thickness, and elastic modulus of trabecular bone in a normal Japanese population," *Osteoporos Int*, vol. 21, no. 10, pp. 1781–90, 10 2010. [PubMed: 20514480]
- [188]. Breban S et al., "Trabecular and cortical bone separately assessed at radius with a new ultrasound device, in a young adult population with various physical activities," *Bone*, vol. 46, no. 6, pp. 1620–5, 6 2010. [PubMed: 20230926]
- [189]. McKelvie ML and Palmer SB, "The interaction of ultrasound with cancellous bone," *Phys Med Biol*, vol. 36, no. 10, pp. 1331–40, 10 1991. [PubMed: 1745661]
- [190]. Williams JL, "Ultrasonic wave propagation in cancellous and cortical bone: prediction of some experimental results by Biot's theory," *J Acoust Soc Am*, vol. 91, no. 2, pp. 1106–12, 2 1992. [PubMed: 1556311]
- [191]. Hughes ER, Leighton TG, Petley GW, White PR, and Chivers RC, "Estimation of critical and viscous frequencies for Biot theory in cancellous bone," *Ultrasonics*, vol. 41, no. 5, pp. 365–8, 7 2003. [PubMed: 12788218]
- [192]. Roh H, Lee KI, and Yoon SW, "Acoustic characterization of a non-rigid porous medium with circular cylindrical pores," *J. Korean Phys. Soc*, vol. 43, no. 1, pp. 55–65, 2003.
- [193]. Mohamed MM, Shaat LT, and Mahmoud AN, "Propagation of ultrasonic waves through demineralized cancellous bone," *IEEE Trans Ultrason Ferroelectr Freq Control*, vol. 50, no. 3, pp. 279–88, 3 2003. [PubMed: 12699161]
- [194]. Attenborough K, Shin HC, Qin Q, Fagan MJ, and Langton CM, "Measurements of tortuosity in stereolithographical bone replicas using audiofrequency pulses," *J Acoust Soc Am*, vol. 118, no. 5, pp. 2779–82, 11 2005. [PubMed: 16334655]
- [195]. Sebaa N et al., "Ultrasonic characterization of human cancellous bone using the Biot theory: inverse problem," *J Acoust Soc Am*, vol. 120, no. 4, pp. 1816–24, 10 2006. [PubMed: 17069280]
- [196]. Hughes ER, Leighton TG, White PR, and Petley GW, "Investigation of an anisotropic tortuosity in a biot model of ultrasonic propagation in cancellous bone," *J Acoust Soc Am*, vol. 121, no. 1, pp. 568–74, 1 2007. [PubMed: 17297810]
- [197]. Lee KI, Humphrey VF, Leighton TG, and Yoon SW, "Predictions of the modified Biot-Attenborough model for the dependence of phase velocity on porosity in cancellous bone," *Ultrasonics*, vol. 46, pp. 323–320, 2007. [PubMed: 17573089]
- [198]. Pakula M, Padilla F, Laugier P, and Kaczmarek M, "Application of Biot's theory to ultrasonic characterization of human cancellous bones: determination of structural, material, and mechanical properties," *J Acoust Soc Am*, vol. 123, no. 4, pp. 2415–23, 4 2008. [PubMed: 18397044]
- [199]. Fellah ZA et al., "Application of the biot model to ultrasound in bone: direct problem," *IEEE Trans Ultrason Ferroelectr Freq Control*, vol. 55, no. 7, pp. 1508–15, 7 2008. [PubMed: 18986940]
- [200]. Sebaa N et al., "Application of the Biot model to ultrasound in bone: inverse problem," *IEEE Trans Ultrason Ferroelectr Freq Control*, vol. 55, no. 7, pp. 1516–23, 7 2008. [PubMed: 18986941]

- [201]. Cardoso L, Meunier A, and Oddou C, "In vitro acoustic wave propagation in human and bovine cancellous bone as predicted by Biot's theory," *J. Mech. Med. & Biol.*, vol. 8, no. 2, pp. 183–201, 2008.
- [202]. Aygun H, Attenborough K, Postema M, Lauriks W, and Langton CM, "Predictions of angle dependent tortuosity and elasticity effects on sound propagation in cancellous bone," *J Acoust Soc Am*, vol. 126, no. 6, pp. 3286–90, 12 2009. [PubMed: 20000942]
- [203]. Nguyen V, Naili S, and Sansalone V, "Simulation of ultrasonic wave propagation in anisotropic cancellous bone immersed in fluid," *Wave Motion*, vol. 47, pp. 117–129, 2010.
- [204]. Aygun H, Attenborough K, Lauriks W, and Langton CM, "Ultrasonic wave propagation in stereo-lithographical bone replicas," *J Acoust Soc Am*, vol. 127, no. 6, pp. 3781–9, 6 2010. [PubMed: 20550276]
- [205]. Aygun H, Attenborough K, Lauriks W, Rubini PA, and Langton CM, "Wave propagation in stereo-lithographical (STL) bone replicas at oblique incidence," *Appl. Acoust*, vol. 72, pp. 458–463, 2011.
- [206]. Buchanan JL, Gilbert RP, and Ou MJ, "Wavelet decomposition of transmitted ultrasound wave through a 1-D muscle-bone system," *J Biomech*, vol. 44, no. 2, pp. 352–8, 1 11 2011. [PubMed: 21092969]
- [207]. Buchanan JL, Gilbert RP, and Ou MJ, "Recovery of the parameters of cancellous bone by inversion of effective velocities, and transmission and reflection coefficients," *Inverse Problems in Science and Engineering.*, vol. 27, pp. 1–23, 2011.
- [208]. Cardoso L and Cowin SC, "Fabric dependence of quasi-waves in anisotropic porous media," *J Acoust Soc Am*, vol. 129, no. 5, pp. 3302–16, 5 2011. [PubMed: 21568431]
- [209]. Cowin SC and Cardoso L, "Fabric dependence of wave propagation in anisotropic porous media," *Biomech Model Mechanobiol*, vol. 10, no. 1, pp. 39–65, 2 2011. [PubMed: 20461539]
- [210]. Buchanan JL, Gilbert RP, and Ou MJ, "Transfer functions for a one-dimensional fluid-poroelastic system subject to an ultrasonic pulse," *Nonlinear Analysis: Real World Applications*, vol. 13, pp. 1030–1043, 2012.
- [211]. Gilbert RP, Guyenne P, and Ou MY, "A quantitative ultrasound model of the bone with blood as the interstitial fluid," *Math. & Comp. Modelling*, vol. 55, no. 9–10, pp. 2019–2039, 2012.
- [212]. Fellah M, Fellah ZE, Mitri FG, Ogam E, and Depollier C, "Transient ultrasound propagation in porous media using Biot theory and fractional calculus: application to human cancellous bone," *J Acoust Soc Am*, vol. 133, no. 4, pp. 1867–81, 4 2013. [PubMed: 23556556]
- [213]. Drelich R, Pakula M, and Kaczmarek M, "Identification of Drag Parameters of Flow in High Permeability Materials by U-Tube Method," *Transp Porous Med*, vol. 101, pp. 69–79, 2014.
- [214]. Morin C and Hellmich C, "A multiscale poromicromechanical approach to wave propagation and attenuation in bone," *Ultrasonics*, vol. 54, no. 5, pp. 1251–69, 7 2014. [PubMed: 24457030]
- [215]. Meziere F, Muller M, Bossy E, and Derode A, "Measurements of ultrasound velocity and attenuation in numerical anisotropic porous media compared to Biot's and multiple scattering models," *Ultrasonics*, vol. 54, no. 5, pp. 1146–54, 7 2014. [PubMed: 24125533]
- [216]. Lee KI, "Dependences of Ultrasonic Properties on the Propagation Angle with Respect to the Trabecular Alignment in Trabecular Bone," *J. Korean Phys. Soc.*, vol. 64, no. 12, pp. 1802–1807, 2014.
- [217]. aygun H and Barlow C, "Ultrasonic wave propagation through porous ceramics at different angles of propagation," *Appl. Acoust*, vol. 88, pp. 6–11, 2015.
- [218]. Gilbert RP, Guyenne P, and Shoushani M, "Recovery of parameters of cancellous bone by acoustic interrogation," *Inverse Problems in Science and Engineering.*, pp. 1–33, 2015.
- [219]. Cardoso L and Schaffler MB, "Changes of elastic constants and anisotropy patterns in trabecular bone during disuse-induced bone loss assessed by poroelastic ultrasound," *J Biomech Eng*, vol. 137, no. 1, 1 2015.
- [220]. Cowin SC and Cardoso L, "Fabric dependence of bone ultrasound," *Acta Bioeng Biomech*, vol. 12, no. 2, pp. 3–23, 2010.
- [221]. Wear KA, Laib A, Stuber AP, and Reynolds JC, "Comparison of measurements of phase velocity in human calcaneus to Biot theory," *J Acoust Soc Am*, vol. 117, no. 5, pp. 3319–24, 5 2005. [PubMed: 15957798]

- [222]. Marutyan KR, Bretthorst GL, and Miller JG, "Bayesian estimation of the underlying bone properties from mixed fast and slow mode ultrasonic signals," *J Acoust Soc Am*, vol. 121, no. 1, pp. EL8–15, 1 2007. [PubMed: 17297820]
- [223]. Hoffman JJ, Nelson AM, Holland MR, and Miller JG, "Cancellous bone fast and slow waves obtained with Bayesian probability theory correlate with porosity from computed tomography," *J Acoust Soc Am*, vol. 132, no. 3, pp. 1830–7, 9 2012. [PubMed: 22978910]
- [224]. Anderson CC et al., "Inverse problems in cancellous bone: estimation of the ultrasonic properties of fast and slow waves using Bayesian probability theory," *J Acoust Soc Am*, vol. 128, no. 5, pp. 2940–8, 11 2010. [PubMed: 21110589]
- [225]. Wear KA, "Decomposition of two-component ultrasound pulses in cancellous bone using modified least squares prony method--phantom experiment and simulation," *Ultrasound Med Biol*, vol. 36, no. 2, pp. 276–87, 2 2010. [PubMed: 20113862]
- [226]. Dencks S and Schmitz G, "Estimation of multipath transmission parameters for quantitative ultrasound measurements of bone," *IEEE Trans Ultrason Ferroelectr Freq Control*, vol. 60, pp. 1884–1895, 2013. [PubMed: 24658719]
- [227]. Wear KA, "Estimation of fast and slow wave properties in cancellous bone using Prony's method and curve fitting," *J Acoust Soc Am*, vol. 133, no. 4, pp. 2490–501, 4 2013. [PubMed: 23556613]
- [228]. Wear K, Nagatani Y, Mizuno K, and Matsukawa M, "Fast and slow wave detection in bovine cancellous bone in vitro using bandlimited deconvolution and Prony's method," *J Acoust Soc Am*, vol. 136, no. 4, pp. 2015–24, 10 2014. [PubMed: 25324100]
- [229]. Taki H, Nagatani Y, Matsukawa M, Mizuno K, and Sato T, "Fast characterization of two ultrasound longitudinal waves in cancellous bone using an adaptive beamforming technique," *J Acoust Soc Am*, vol. 137, no. 4, pp. 1683–92, 4 2015. [PubMed: 25920821]
- [230]. Taki H, Nagatani Y, Matsukawa M, Kanai H, and Izumi SI, "Fast decomposition of two ultrasound longitudinal waves in cancellous bone using a phase rotation parameter for bone quality assessment: Simulation study," *J Acoust Soc Am*, vol. 142, no. 4, p. 2322, 10 2017. [PubMed: 29092537]
- [231]. Maruo S and Hosokawa A, "A generalized harmonic analysis of ultrasound waves propagating in cancellous bone," *Jpn. J. Appl. Phys*, vol. 53, pp. 07KF06–1–07KF06–6, 2014.
- [232]. Nagatani Y and Tachibana RO, "Multichannel instantaneous frequency analysis of ultrasound propagating in cancellous bone," *J Acoust Soc Am*, vol. 135, no. 3, pp. 1197–206, 3 2014. [PubMed: 24606262]
- [233]. Wear KA, "Time-domain separation of interfering waves in cancellous bone using bandlimited deconvolution: simulation and phantom study," *J Acoust Soc Am*, vol. 135, no. 4, pp. 2102–12, 4 2014. [PubMed: 25235007]
- [234]. Wear KA, "Ultrasonic scattering from cancellous bone: a review," *IEEE Trans Ultrason Ferroelectr Freq Control*, vol. 55, no. 7, pp. 1432–41, 7 2008. [PubMed: 18986932]
- [235]. Padilla F and Wear K, "Scattering by Trabecular Bone," in *Bone Quantitative Ultrasound*, Laugier P and Haiat G, Eds. Dordrecht: Springer, 2011.
- [236]. Wear KA and Armstrong DW 3rd, "Relationships among calcaneal backscatter, attenuation, sound speed, hip bone mineral density, and age in normal adult women," *J Acoust Soc Am*, vol. 110, no. 1, pp. 573–8, 7 2001. [PubMed: 11508981]
- [237]. O'Donnell M and Miller JG, "Quantitative broadband ultrasonic backscatter: An approach to nondestructive evaluation in acoustically inhomogeneous materials," *J. Appl. Phys*, vol. 52, no. 2, pp. 1056–1065, 1981.
- [238]. Campbell JA and Waag RC, "Normalization of ultrasonic scattering measurements to obtain average differential scattering cross sections for tissues," *J Acoust Soc Am*, vol. 74, no. 2, pp. 393–9, 8 1983. [PubMed: 6619417]
- [239]. Lizzi FL, Greenebaum M, Feleppa EJ, Elbaum M, and Coleman DJ, "Theoretical framework for spectrum analysis in ultrasonic tissue characterization," *J Acoust Soc Am*, vol. 73, no. 4, pp. 1366–73, 4 1983. [PubMed: 6853848]



- [240]. Madsen EL, Insana MF, and Zagzebski JA, "Method of data reduction for accurate determination of acoustic backscatter coefficients," *J Acoust Soc Am*, vol. 76, no. 3, pp. 913–23, 9 1984. [PubMed: 6491053]
- [241]. Chen X, Phillips D, Schwarz KQ, Mottley JG, and Parker KJ, "The measurement of backscatter coefficient from a broadband pulse-echo system: a new formulation," *IEEE Trans Ultrason Ferroelectr Freq Control*, vol. 44, no. 2, pp. 515–25, 1997. [PubMed: 18244149]
- [242]. Wear KA, "Fundamental precision limitations for measurements of frequency dependence of backscatter: applications in tissue-mimicking phantoms and trabecular bone," *J Acoust Soc Am*, vol. 110, no. 6, pp. 3275–82, 12 2001. [PubMed: 11785828]
- [243]. Padilla F, Jenson F, and Laugier P, "Estimation of trabecular thickness using ultrasonic backscatter," *Ultrasonic Imaging*, vol. 28, pp. 3–22, 2006. [PubMed: 16924879]
- [244]. Padilla F, Jenson F, and Laugier P, "Influence of the precision of spectral backscatter measurements on the estimation of scatterers size in cancellous bone," *Ultrasonics*, vol. 44 Suppl 1, pp. e57–60, 12 22 2006. [PubMed: 16904147]
- [245]. Burckhardt CB, "Speckle in Ultrasound B-Mode Scans," *IEEE Trans Son. Ultrason*, vol. SU-25, no. 1, pp. 1–6, 1978.
- [246]. Wagner RF, Smith SW, Sandrik JM, and Lopez H, "Statistics of speckle in ultrasound B-scans," *IEEE Trans Son. Ultrason*, vol. 30, no. 3, pp. 156–163, 1983.
- [247]. Wear KA and Garra BS, "Assessment of bone density using ultrasonic backscatter," *Ultrasound Med Biol*, vol. 24, no. 5, pp. 689–95, 6 1998. [PubMed: 9695272]
- [248]. Litniewski J, Nowicki A, and Lewin PA, "Semi-empirical bone model for determination of trabecular structure properties from backscattered ultrasound," *Ultrasonics*, vol. 49, no. 6–7, pp. 505–13, 6 2009. [PubMed: 19232659]
- [249]. Wear KA et al., "Interlaboratory comparison of ultrasonic backscatter coefficient measurements from 2 to 9 MHz," *J Ultrasound Med*, vol. 24, no. 9, pp. 1235–50, 9 2005. [PubMed: 16123184]
- [250]. Lavarello RJ, Ghoshal G, and Oelze ML, "On the estimation of backscatter coefficients using single-element focused transducers," *J Acoust Soc Am*, vol. 129, no. 5, pp. 2903–11, 5 2011. [PubMed: 21568393]
- [251]. Wear KA, "Measurement of dependence of backscatter coefficient from cylinders on frequency and diameter using focused transducers--with applications in trabecular bone," *J Acoust Soc Am*, vol. 115, no. 1, pp. 66–72, 1 2004. [PubMed: 14758996]
- [252]. Hoffmeister BK, McPherson JA, Smathers MR, Spinolo PL, and Sellers ME, "Ultrasonic backscatter from cancellous bone: the apparent backscatter transfer function," *IEEE Trans Ultrason Ferroelectr Freq Control*, vol. 62, no. 12, pp. 2115–25, 12 2015. [PubMed: 26683412]
- [253]. Hoffmeister BK, "Frequency dependence of apparent ultrasonic backscatter from human cancellous bone," *Phys Med Biol*, vol. 56, no. 3, pp. 667–83, 2 7 2011. [PubMed: 21220842]
- [254]. Liu C et al., "Signal of Interest Selection Standard for Ultrasonic Backscatter in Cancellous Bone Evaluation," *Ultrasound Med Biol*, vol. 41, no. 10, pp. 2714–21, 10 2015. [PubMed: 26210784]
- [255]. Li B et al., "Effect of spectral estimation on ultrasonic backscatter parameters in measurements of cancellous bones," *IEEE Access*, vol. in press, 2019.
- [256]. Hoffmeister BK et al., "Ultrasonic characterization of human cancellous bone in vitro using three different apparent backscatter parameters in the frequency range 0.6–15.0 mhz," *IEEE Trans Ultrason Ferroelectr Freq Control*, vol. 55, no. 7, pp. 1442–52, 7 2008. [PubMed: 18986933]
- [257]. Hoffmeister BK, Wilson AR, Gilbert MJ, and Sellers ME, "A backscatter difference technique for ultrasonic bone assessment," *J Acoust Soc Am*, vol. 132, no. 6, pp. 4069–76, 12 2012. [PubMed: 23231136]
- [258]. Hoffmeister BK, Spinolo PL, Sellers ME, Marshall PL, Viano AM, and Lee SR, "Effect of intervening tissues on ultrasonic backscatter measurements of bone: An in vitro study," *J Acoust Soc Am*, vol. 138, no. 4, pp. 2449–57, 10 2015. [PubMed: 26520327]
- [259]. Hoffmeister BK, Viano AM, Fairbanks LC, Ebron SC, McPherson JA, and Huber MT, "Effect of gate choice on backscatter difference measurements of cancellous bone," *J Acoust Soc Am*, vol. 142, no. 2, p. 540, 8 2017. [PubMed: 28863582]

- [260]. Hoffmeister BK et al., "Ultrasonic backscatter difference measurements of cancellous bone from the human femur: Relation to bone mineral density and microstructure," *J Acoust Soc Am*, vol. 143, no. 6, p. 3642, 6 2018. [PubMed: 29960442]
- [261]. Riekkinen O, Hakulinen MA, Timonen M, Toyras J, and Jurvelin JS, "Influence of overlying soft tissues on trabecular bone acoustic measurement at various ultrasound frequencies," *Ultrasound Med Biol*, vol. 32, no. 7, pp. 1073–83, 7 2006. [PubMed: 16829321]
- [262]. Riekkinen O, Hakulinen MA, Toyras J, and Jurvelin JS, "Dual-frequency ultrasound--new pulse-echo technique for bone densitometry," *Ultrasound Med Biol*, vol. 34, no. 10, pp. 1703–8, 10 2008. [PubMed: 18524463]
- [263]. Karjalainen JP, Toyras J, Riekkinen O, Hakulinen M, and Jurvelin JS, "Ultrasound backscatter imaging provides frequency-dependent information on structure, composition and mechanical properties of human trabecular bone," *Ultrasound Med Biol*, vol. 35, no. 8, pp. 1376–84, 8 2009. [PubMed: 19525060]
- [264]. Wear KA, "Characterization of trabecular bone using the backscattered spectral centroid shift," *IEEE Trans Ultrason Ferroelectr Freq Control*, vol. 50, no. 4, pp. 402–7, 4 2003. [PubMed: 12744396]
- [265]. Liu C, Zhang R, Li Y, Xu F, Ta D, and Wang W, "An Ultrasonic Backscatter Instrument for Cancellous Bone Evaluation in Neonates," *Engineering*, vol. 1, no. 3, pp. 336–343, 2015.
- [266]. Karjalainen J, Toyras J, Riekkonen T, Jurvelin JS, and Riekkinen O, "Dual-frequency ultrasound technique minimizes errors induced by soft tissue in ultrasound bone densitometry," *Acta Radiol*, vol. 49, no. 9, pp. 1038–41, 11 2008. [PubMed: 18728919]
- [267]. Malo MK, Karjalainen JP, Isaksson H, Riekkinen O, Jurvelin JS, and Toyras J, "Numerical analysis of uncertainties in dual frequency bone ultrasound technique," *Ultrasound Med Biol*, vol. 36, no. 2, pp. 288–94, 2 2010. [PubMed: 20113863]
- [268]. Malo MK, Karjalainen JP, Riekkinen O, Isaksson H, Jurvelin JS, and Toyras J, "Effects of non-optimal focusing on dual-frequency ultrasound measurements of bone," *IEEE Trans Ultrason Ferroelectr Freq Control*, vol. 58, no. 6, pp. 1182–8, 6 2011. [PubMed: 21693400]
- [269]. Liu C, Ta D, Le LH, and Wang W, "The analysis and compensation of cortical thickness effect on ultrasonic backscatter signals in cancellous bone," *J. Appl. Phys.*, vol. 116, pp. 124903-1-6, 2014.
- [270]. Hoffmeister BK, Holt AP, and Kaste SC, "Effect of the cortex on ultrasonic backscatter measurements of cancellous bone," *Phys Med Biol*, vol. 56, no. 19, pp. 6243–55, 10 7 2011. [PubMed: 21896966]
- [271]. Kitamura K, Pan H, Ueha S, Kimura S, and Ohtomo N, "Ultrasonic scattering study of cancellous bone for osteoporosis diagnosis," *Jpn. J. Appl. Phys*, vol. 35, pp. 3156–3162, 1996.
- [272]. Kitamura K, Nishikouri H, Ueha S, Kimura S, and Ohtomo N, "Estimation of trabecular bone axis for characterization of cancellous bone using scattered ultrasonic wave," *Jpn. J. Appl. Phys*, vol. 37, pp. 3082–3087, 1998.
- [273]. Strelitzki R, Nicholson PH, and Paech V, "A model for ultrasonic scattering in cancellous bone based on velocity fluctuations in a binary mixture," *Physiol Meas*, vol. 19, no. 2, pp. 189–96, 5 1998. [PubMed: 9626683]
- [274]. Wear KA, "Frequency dependence of ultrasonic backscatter from human trabecular bone: theory and experiment," *J Acoust Soc Am*, vol. 106, no. 6, pp. 3659–64, 12 1999. [PubMed: 10615704]
- [275]. Chaffai S, Roberjot V, Peyrin F, Berger G, and Laugier P, "Frequency dependence of ultrasonic backscattering in cancellous bone: autocorrelation model and experimental results," *J Acoust Soc Am*, vol. 108, no. 5 Pt 1, pp. 2403–11, 11 2000. [PubMed: 11108380]
- [276]. Nicholson PH, Strelitzki R, Cleveland RO, and Bouxsein ML, "Scattering of ultrasound in cancellous bone: predictions from a theoretical model," *J Biomech*, vol. 33, no. 4, pp. 503–6, 4 2000. [PubMed: 10768401]
- [277]. Luppe F, Conoir JM, and Franklin H, "Scattering by a fluid cylinder in a porous medium: application to trabecular bone," *J Acoust Soc Am*, vol. 111, no. 6, pp. 2573–82, 6 2002. [PubMed: 12083188]

- [278]. Luppe F, Conoir JM, and Franklin H, "Multiple scattering in a trabecular bone: influence of the marrow viscosity on the effective properties," *J Acoust Soc Am*, vol. 113, no. 5, pp. 2889–92, 5 2003. [PubMed: 12765405]
- [279]. Faran JJ, "Sound scattering by solid cylinders and spheres," *J. Acoust. Soc. Am*, vol. 23, pp. 405–418, 1951.
- [280]. Wear KA and Harris GR, "Frequency dependence of backscatter from thin, oblique, finite-length cylinders measured with a focused transducer-with applications in cancellous bone," *J Acoust Soc Am*, vol. 124, no. 5, pp. 3309–14, 11 2008. [PubMed: 19045813]
- [281]. Ta D, Wang W, Huang K, Wang Y, and Le LH, "Analysis of frequency dependence of ultrasonic backscatter coefficient in cancellous bone," *J Acoust Soc Am*, vol. 124, no. 6, pp. 4083–90, 12 2008. [PubMed: 19206830]
- [282]. Huang K, Ta D, Wang W, and Le LH, "Simplified inverse filter tracking algorithm for estimating the mean trabecular bone spacing," *IEEE Trans Ultrason Ferroelectr Freq Control*, vol. 55, no. 7, pp. 1453–64, 7 2008. [PubMed: 18986934]
- [283]. Litniewski J, Cieslik L, Wojcik J, and Nowicki A, "Statistics of the envelope of ultrasonic backscatter from human trabecular bone," *J Acoust Soc Am*, vol. 130, no. 4, pp. 2224–32, 10 2011. [PubMed: 21973377]
- [284]. Jenson F, Padilla F, and Laugier P, "Prediction of frequency-dependent ultrasonic backscatter in cancellous bone using statistical weak scattering model," *Ultrasound Med Biol*, vol. 29, no. 3, pp. 455–64, 3 2003. [PubMed: 12706197]
- [285]. Deligianni DD and Apostolopoulos KN, "Characterization of dense bovine cancellous bone tissue microstructure by ultrasonic backscattering using weak scattering models," *J Acoust Soc Am*, vol. 122, no. 2, pp. 1180–90, 8 2007. [PubMed: 17672664]
- [286]. Wear KA, Padilla F, and Laugier P, "Comparison of the Faran Cylinder Model and the Weak Scattering Model for predicting the frequency dependence of backscatter from human cancellous femur in vitro," *J Acoust Soc Am*, vol. 124, no. 3, pp. 1408–10, 9 2008. [PubMed: 19045632]
- [287]. Sehgal CM and Greenleaf JF, "Scattering of ultrasound by tissues," *Ultrason Imaging*, vol. 6, no. 1, pp. 60–80, 1 1984. [PubMed: 6540912]
- [288]. Sehgal CM, "Quantitative relationship between tissue composition and scattering of ultrasound," *J Acoust Soc Am*, vol. 94, no. 4, pp. 1944–52, 10 1993. [PubMed: 8227740]
- [289]. Padilla F, Peyrin F, and Laugier P, "Prediction of backscatter coefficient in trabecular bones using a numerical model of three-dimensional microstructure," *J Acoust Soc Am*, vol. 113, no. 2, pp. 1122–9, 2 2003. [PubMed: 12597205]
- [290]. Lee KI and Choi MJ, "Frequency-dependent attenuation and backscatter coefficients in bovine trabecular bone from 0.2 to 1.2 MHz," *J. Acoust. Soc. Am*, vol. 131, no. 1, pp. EL67–EL73, 2012. [PubMed: 22280732]
- [291]. Lee KI, "Correlations of the frequency dependence of the ultrasonic backscatter coefficient with the bone volume fraction and the trabecular thickness in bovine trabecular bone: Application of the binary mixture model," *J. Acoust. Soc. Am*, vol. 145, pp. EL393–EL399, 2019. [PubMed: 31153347]
- [292]. Roberjot V, Laugier P, Droin P, Giat P, and Berger G, "Measurement of integrated backscatter coefficient of trabecular bone," in *IEEE Ultrason. Symp.*, 1996, vol. 2, pp. 1123–1126.
- [293]. Wear KA and Armstrong DW, "The relationship between ultrasonic backscatter and bone mineral density in human calcaneus," *IEEE Trans Ultrason Ferroelectr Freq Control*, vol. 47, no. 4, pp. 777–80, 2000. [PubMed: 18238608]
- [294]. Garra BS, Locher M, Felker S, and Wear KA, "Measurements of ultrasonic backscattered spectral centroid shift from spine in vivo: methodology and preliminary results," *Ultrasound Med Biol*, vol. 35, no. 1, pp. 165–8, 1 2009. [PubMed: 18723270]
- [295]. Jiang YQ et al., "Analysis of apparent integrated backscatter coefficient and backscattered spectral centroid shift in Calcaneus in vivo for the ultrasonic evaluation of osteoporosis," *Ultrasound Med Biol*, vol. 40, no. 6, pp. 1307–17, 6 2014. [PubMed: 24642217]
- [296]. Liu C et al., "Measurement of the Human Calcaneus In Vivo Using Ultrasonic Backscatter Spectral Centroid Shift," *J Ultrasound Med*, vol. 35, no. 10, pp. 2197–208, 10 2016. [PubMed: 27562978]

- [297]. Malo MK, Toyras J, Karjalainen JP, Isaksson H, Riekkinen O, and Jurvelin JS, "Ultrasound backscatter measurements of intact human proximal femurs--relationships of ultrasound parameters with tissue structure and mineral density," *Bone*, vol. 64, pp. 240–5, 7 2014. [PubMed: 24769331]
- [298]. Hoffmeister BK, Jones CI 3rd, Caldwell GJ, and Kaste SC, "Ultrasonic characterization of cancellous bone using apparent integrated backscatter," *Phys Med Biol*, vol. 51, no. 11, pp. 2715–27, 6 7 2006. [PubMed: 16723761]
- [299]. Liu C et al. , "Relationships of Ultrasonic Backscatter With Bone Densities and Microstructure in Bovine Cancellous Bone," *IEEE Trans Ultrason Ferroelectr Freq Control*, vol. 65, no. 12, pp. 2311–2321, 12 2018. [PubMed: 30575524]
- [300]. Wear KA and Laib A, "The dependence of ultrasonic backscatter on trabecular thickness in human calcaneus: theoretical and experimental results," *IEEE Trans Ultrason Ferroelectr Freq Control*, vol. 50, no. 8, pp. 979–86, 8 2003. [PubMed: 12952089]
- [301]. Wojcik J, Litniewski J, and Nowicki A, "Modeling and analysis of multiple scattering of acoustic waves in complex media: application to the trabecular bone," *J Acoust Soc Am*, vol. 130, no. 4, pp. 1908–18, 10 2011. [PubMed: 21973345]
- [302]. Derode A, Mamou V, Padilla F, Jenson F, and Laugier P, "Dynamic coherent backscattering in a heterogeneous absorbing medium: Application to human trabecular bone characterization," *Appl. Phys. Lett.*, vol. 87, pp. 114101-1-3, 2005.
- [303]. Aubry A, Derode A, and Padilla F, "Local measurements of the diffusion constant in multiple scattering media: Application to human trabecular bone imaging," *Appl. Phys. Lett.*, vol. 92, pp. 124101–124103, 2008.
- [304]. Wear KA, "Anisotropy of ultrasonic backscatter and attenuation from human calcaneus: implications for relative roles of absorption and scattering in determining attenuation," *J Acoust Soc Am*, vol. 107, no. 6, pp. 3474–9, 6 2000. [PubMed: 10875391]
- [305]. Kaufman JJ, Luo G, and Siffert RS, "On the relative contributions of absorption and scattering to ultrasound attenuation in trabecular bone: a simulation study," in *IEEE Int'l Ultrasonics Symp*, 2003, pp. 1519–1523.
- [306]. Bossy E, Padilla F, Peyrin F, and Laugier P, "Three-dimensional simulation of ultrasound propagation through trabecular bone structures measured by synchrotron microtomography," *Phys Med Biol*, vol. 50, no. 23, pp. 5545–56, 12 7 2005. [PubMed: 16306651]
- [307]. Bossy E, Laugier P, Peyrin F, and Padilla F, "Attenuation in trabecular bone: A comparison between numerical simulation and experimental results in human femur," *J Acoust Soc Am*, vol. 122, no. 4, pp. 2469–75, 10 2007. [PubMed: 17902882]
- [308]. Aula AS, Toyras J, Hakulinen MA, and Jurvelin JS, "Effect of bone marrow on acoustic properties of trabecular bone--3D finite difference modeling study," *Ultrasound Med Biol*, vol. 35, no. 2, pp. 308–18, 2 2009. [PubMed: 19010590]
- [309]. Wear KA, "Mechanisms for attenuation in cancellous-bone-mimicking phantoms," *IEEE Trans Ultrason Ferroelectr Freq Control*, vol. 55, no. 11, pp. 2418–25, 11 2008. [PubMed: 19049921]
- [310]. Ahuja AS, "Effect of particle viscosity on propagation of sound in suspensions and emulsions," *J. Acoust. Soc. Am*, vol. 51, no. 1, pp. 182–191, 1972.
- [311]. Ahuja AS, "Formulation of wave equation for calculating velocity of sound in suspensions," *J. Acoust. Soc. Am*, vol. 51, no. 3, pp. 916–919, 1972.
- [312]. Ahuja AS and Hendee WR, "Effects of particle shape and orientation on propagation of sound in suspensions," *J. Acoust. Soc. Am*, vol. 63, no. 4, pp. 1074–1080, 1978.
- [313]. Mottley JG and Miller JG, "Anisotropy of the ultrasonic attenuation in soft tissues: measurements in vitro," *J Acoust Soc Am*, vol. 88, no. 3, pp. 1203–10, 9 1990. [PubMed: 2229659]
- [314]. Hosokawa A, "Simulation of ultrasound propagation through bovine cancellous bone using elastic and Biot's finite-difference time-domain methods," *J Acoust Soc Am*, vol. 118, no. 3 Pt 1, pp. 1782–9, 9 2005. [PubMed: 16240836]
- [315]. Gluer CC, Wu CY, and Genant HK, "Broadband ultrasound attenuation signals depend on trabecular orientation: an in vitro study," *Osteoporos Int*, vol. 3, no. 4, pp. 185–91, 7 1993. [PubMed: 8338973]

- [316]. Hosokawa A, "Numerical investigation of ultrasound refraction caused by oblique orientation of trabecular network in cancellous bone," *IEEE Trans Ultrason Ferroelectr Freq Control*, vol. 58, no. 7, pp. 1389–96, 7 2011. [PubMed: 21768023]
- [317]. Nicholson PH and Boussein ML, "Bone marrow influences quantitative ultrasound measurements in human cancellous bone," *Ultrasound Med Biol*, vol. 28, no. 3, pp. 369–75, 3 2002. [PubMed: 11978417]
- [318]. Lee KI, "Ultrasonic properties in marrow-filled and water-filled bovine femoral trabecular bones in vitro," *J Acoust Soc Am*, vol. 132, no. 4, pp. EL296–302, 10 2012. [PubMed: 23039568]
- [319]. Kawasaki S et al., "Ultrasonic wave properties of human bone marrow in the femur and tibia," *J Acoust Soc Am*, vol. 138, no. 1, pp. EL83–7, 7 2015. [PubMed: 26233067]
- [320]. Kubo T, Fujimori K, Cazier N, Saeki T, and Matsukawa M, "Properties of ultrasonic waves in bovine bone marrow," *Ultrasound Med Biol*, vol. 37, no. 11, pp. 1923–9, 11 2011. [PubMed: 21963039]
- [321]. Clarke AJ, Evans JA, Truscott JG, Milner R, and Smith MA, "A phantom for quantitative ultrasound of trabecular bone," *Phys Med Biol*, vol. 39, no. 10, pp. 1677–87, 10 1994. [PubMed: 15551538]
- [322]. Strelitzki R, Evans JA, and Clarke AJ, "The influence of porosity and pore size on the ultrasonic properties of bone investigated using a phantom material," *Osteoporos Int*, vol. 7, no. 4, pp. 370–5, 1997. [PubMed: 9373573]
- [323]. Langton CM, Whitehead MA, Langton DK, and Langley G, "Development of a cancellous bone structural model by stereolithography for ultrasound characterisation of the calcaneus," *Med Eng Phys*, vol. 19, no. 7, pp. 599–604, 10 1997. [PubMed: 9457693]
- [324]. Lee KI and Choi MJ, "Phase velocity and normalized broadband ultrasonic attenuation in Polyacetal cuboid bone-mimicking phantoms," *J Acoust Soc Am*, vol. 121, no. 6, pp. EL263–9, 6 2007. [PubMed: 17552579]
- [325]. Le LH, Zhang C, Ta D, and Lou E, "Measurement of tortuosity in aluminum foams using airborne ultrasound," *Ultrasonics*, vol. 50, no. 1, pp. 1–5, 1 2010. [PubMed: 19720388]
- [326]. Zhang C, Le LH, Zheng R, Ta D, and Lou E, "Measurements of ultrasonic phase velocities and attenuation of slow waves in cellular aluminum foams as cancellous bone-mimicking phantoms," *J Acoust Soc Am*, vol. 129, no. 5, pp. 3317–26, 5 2011. [PubMed: 21568432]
- [327]. Ji Q, Le LH, Filipow LJ, and Jackson SA, "Ultrasonic wave propagation in water-saturated aluminum foams," *Ultrasonics*, vol. 36, pp. 759–765, 1998.
- [328]. Lee KI, "Relationships of linear and nonlinear ultrasound parameters with porosity and trabecular spacing in trabecular-bone-mimicking phantoms," *J Acoust Soc Am*, vol. 140, no. 6, p. EL528, 12 2016. [PubMed: 28040043]
- [329]. Lee KI, "Dependences of quantitative ultrasound parameters on frequency and porosity in water-saturated nickel foams," *J Acoust Soc Am*, vol. 135, no. 2, pp. EL61–7, 2 2014. [PubMed: 25234916]
- [330]. Lee KI, "Dependences of ultrasonic properties on frequency and trabecular spacing in trabecular-bone-mimicking phantoms," *J Acoust Soc Am*, vol. 137, no. 2, pp. EL194–9, 2 2015. [PubMed: 25698050]
- [331]. Wydra A and Maev RG, "A novel composite material specifically developed for ultrasound bone phantoms: cortical, trabecular and skull," *Phys Med Biol*, vol. 58, no. 22, pp. N303–19, 11 21 2013. [PubMed: 24171934]
- [332]. Kaufman JJ, Luo G, and Siffert RS, "Ultrasound simulation in bone," *IEEE Trans Ultrason Ferroelectr Freq Control*, vol. 55, no. 6, pp. 1205–18, 2008. [PubMed: 18599409]
- [333]. Kaufman JJ, Luo G, and Siffert RS, "A portable real-time ultrasonic bone densitometer," *Ultrasound Med Biol*, vol. 33, no. 9, pp. 1445–52, 9 2007. [PubMed: 17587486]
- [334]. Padilla F, Bossy E, Haiat G, Jenson F, and Laugier P, "Numerical simulation of wave propagation in cancellous bone," *Ultrasonics*, vol. 44 Suppl 1, pp. e239–43, 12 22 2006.
- [335]. Haiat G, Padilla F, Peyrin F, and Laugier P, "Variation of ultrasonic parameters with microstructure and material properties of trabecular bone: a 3D model simulation," *J Bone Miner Res*, vol. 22, no. 5, pp. 665–74, 5 2007. [PubMed: 17295606]

- [336]. Haiat G, Padilla F, and Laugier P, "Sensitivity of qus parameters to controlled variations of bone strength assessed with a cellular model," *IEEE Trans Ultrason Ferroelectr Freq Control*, vol. 55, no. 7, pp. 1488–96, 7 2008. [PubMed: 18986938]
- [337]. Saade RG, Tsoukas G, and Caminis J, "Understanding velocity of sound in trabecular bone via computer simulations," *Comput Biol Med*, vol. 36, pp. 439–447, 2006. [PubMed: 16125163]
- [338]. Laugier P, Haiat G, and Padilla F, "Computer simulations of ultrasonic propagation in trabecular bone," *Comput Biol Med*, vol. 37, no. 12, pp. 1827–8, 12 2007. [PubMed: 17599821]
- [339]. Hosokawa A, "Ultrasonic pulse waves in cancellous bone analyzed by finite-difference time-domain methods," *Ultrasonics*, vol. 44 Suppl 1, pp. e227–31, 12 22 2006. [PubMed: 16844171]
- [340]. Hosokawa A, "Numerical analysis of variability in ultrasound propagation properties induced by trabecular microstructure in cancellous bone," *IEEE Trans Ultrason Ferroelectr Freq Control*, vol. 56, no. 4, pp. 738–47, 4 2009. [PubMed: 19406702]
- [341]. Hosokawa A, "Effect of porosity distribution in the propagation direction on ultrasound waves through cancellous bone," *IEEE Trans Ultrason Ferroelectr Freq Control*, vol. 57, no. 6, pp. 1320–8, 6 2010. [PubMed: 20529708]
- [342]. Hosokawa A, "Development of a numerical cancellous bone model for finite-difference time-domain simulations of ultrasound propagation," *IEEE Trans Ultrason Ferroelectr Freq Control*, vol. 55, no. 6, pp. 1219–33, 2008. [PubMed: 18599410]
- [343]. Hosokawa A, "Numerical investigation of reflection properties of fast and slow longitudinal waves in cancellous bone," *IEEE Trans Ultrason Ferroelectr Freq Control*, vol. 60, no. 5, pp. 1030–5, 5 2013. [PubMed: 23661139]
- [344]. Hosokawa A, "Numerical investigation of ultrasound reflection and backscatter measurements in cancellous bone on various receiving areas," *Ultrasonics*, vol. 54, no. 5, pp. 1237–44, 7 2014. [PubMed: 24128942]
- [345]. Hosokawa A, "Numerical Analysis of Ultrasound Backscattered Waves in Cancellous Bone Using a Finite-Difference Time-Domain Method: Isolation of the Backscattered Waves From Various Ranges of Bone Depths," *IEEE Trans Ultrason Ferroelectr Freq Control*, vol. 62, no. 6, pp. 1201–10, 6 2015. [PubMed: 26263571]
- [346]. Nagatani Y, Mizuno K, Saeki T, Matsukawa M, Sakaguchi T, and Hosoi H, "Propagation of fast and slow waves in cancellous bone: Comparative study of simulation and experiment," *Acoust. Sci. & Tech*, vol. 30, no. 4, pp. 257–264, 2009.
- [347]. Nagatani Y, Imaizumi H, Fukuda T, Matsukawa M, Watanabe Y, and Otani T, "Applicability of Finite-Difference Time-Domain Method to Simulation of Wave Propagation in Cancellous Bone," *Jpn. J. Appl. Phys*, vol. 45, no. 9A, pp. 7186–7190, 2006.
- [348]. Gilbert RP, Guyenne P, and Li J, "Simulation of a mixture model for ultrasound propagation through cancellous bone using staggered-grid finite differences," *J. Comp. Acoust*, vol. 21, no. 1, p. 1250017, 2013.
- [349]. Meziere F, Muller M, Dobigny B, Bossy E, and Derode A, "Simulations of ultrasound propagation in random arrangements of elliptic scatterers: occurrence of two longitudinal waves," *J Acoust Soc Am*, vol. 133, no. 2, pp. 643–52, 2 2013. [PubMed: 23363084]
- [350]. Vafaeian B, El-Rich M, El-Bialy T, and Adeeb S, "The finite element method for micro-scale modeling of ultrasound propagation in cancellous bone," *Ultrasonics*, vol. 54, no. 6, pp. 1663–76, 8 2014. [PubMed: 24656933]
- [351]. Vafaeian B, Le LH, Tran TN, El-Rich M, El-Bialy T, and Adeeb S, "Micro-scale finite element modeling of ultrasound propagation in aluminum trabecular bone-mimicking phantoms: A comparison between numerical simulation and experimental results," *Ultrasonics*, vol. 68, pp. 17–28, 5 2016. [PubMed: 26894840]
- [352]. Calle S, Moreschi H, Renaud G, and Defontaine M, "Ultrasound propagation in trabecular bone: a numerical study of the influence of microcracks," *Ultrasonics*, vol. 54, no. 5, pp. 1231–6, 7 2014. [PubMed: 24041497]
- [353]. Cleveland RO, Johnson PA, Muller M, Talmant M, Padilla F, and Laugier P, "Modeling nonlinear ultrasound propagation in bone," in *17th Intl. Symp. Nonlinear Acoust.*, 2006, vol. 838, p. 333.
- [354]. Matsukawa M, "Bone ultrasound," *Jpn. J. Appl. Phys*, vol. 58, p. SG0802, 2019.

- [355]. Bumrerraj S and Katz JL, "Scanning acoustic microscopy study of human cortical and trabecular bone," *Ann Biomed Eng*, vol. 29, no. 12, pp. 1034–42, 12 2001. [PubMed: 11853252]
- [356]. Litniewski J, "Determination of the elasticity coefficient for a single trabecula of a cancellous bone: scanning acoustic microscopy approach," *Ultrasound Med Biol*, vol. 31, no. 10, pp. 1361–6, 10 2005. [PubMed: 16223639]
- [357]. Turner CH, Rho J, Takano Y, Tsui TY, and Pharr GM, "The elastic properties of trabecular and cortical bone tissues are similar: results from two microscopic measurement techniques," *J Biomech*, vol. 32, no. 4, pp. 437–41, 4 1999. [PubMed: 10213035]
- [358]. Raum K et al., "Variations of microstructure, mineral density and tissue elasticity in B6/C3H mice," *Bone*, vol. 41, no. 6, pp. 1017–24, 12 2007. [PubMed: 17931992]
- [359]. Rupin F et al., "Adaptive remodeling of trabecular bone core cultured in 3-D bioreactor providing cyclic loading: an acoustic microscopy study," *Ultrasound Med Biol*, vol. 36, no. 6, pp. 999–1007, 6 2010. [PubMed: 20510189]
- [360]. Matsukawa M, Tsubota R, Kawabe M, and Fukui K, "Application of a micro-Brillouin scattering technique to characterize bone in the GHz range," *Ultrasonics*, vol. 54, no. 5, pp. 1155–61, 7 2014. [PubMed: 24139301]
- [361]. Tsubota R, Fukui K, and Matsukawa M, "Local ultrasonic wave velocities in trabeculae measured by micro-Brillouin scattering," *J Acoust Soc Am*, vol. 135, no. 2, pp. EL109–14, 2 2014. [PubMed: 25234913]
- [362]. Kawabe M et al., "Comparative investigation of elastic properties in a trabecula using micro-Brillouin scattering and scanning acoustic microscopy," *J Acoust Soc Am*, vol. 132, no. 1, pp. EL54–60, 7 2012. [PubMed: 22779573]
- [363]. Ojanen X, Toyras J, Inkinen SI, Malo MK, Isaksson H, and Jurvelin JS, "Differences in acoustic impedance of fresh and embedded human trabecular bone samples-Scanning acoustic microscopy and numerical evaluation," *J Acoust Soc Am* vol. 140, no. 3, p. 1931, 9 2016. [PubMed: 27914413]
- [364]. Beyer RT, "The Parameter B / A," in *Nonlinear Acoustics*, Hamilton MF and Blackstock DT, Eds. First ed San Diego, CA: Academic Press, 1998.
- [365]. Engan HE, Ingebrigtsen KA, Oygarden KG, Hagen EK, and Hoff L, "Nonlinear Ultrasound Detection of Osteoporosis," in *IEEE Intl. Ultrasonics Symp*, 2006, pp. 2096–2099.
- [366]. Lee KI, "Feasibility of Bone Assessment by Using the Nonlinear Parameter in Trabecular Bone," *J. Korean Phys. Soc*, vol. 62, no. 8, pp. 1108–1113, 2013.
- [367]. Lee KI, "Correlations of linear and nonlinear ultrasound parameters with density and microarchitectural parameters in trabecular bone," *J Acoust Soc Am*, vol. 134, no. 5, pp. EL381–6, 11 2013. [PubMed: 24181979]
- [368]. Lee KI, "Feasibility of a Nonlinear Acoustic Method for the Assessment of Bone Status and Osteoporosis in Trabecular Bone," *J. Korean Phys. Soc*, vol. 73, no. 12, pp. 1849–1854, 2018.
- [369]. Calle S, Remenieras JP, Bou Matar O, Defontaine M, and Patat F, "Application of nonlinear phenomena induced by focused ultrasound to bone imaging," *Ultrasound Med Biol*, vol. 29, no. 3, pp. 465–72, 3 2003. [PubMed: 12706198]
- [370]. Renaud G, Calle S, Remenieras JP, and Defontaine M, "Exploration of trabecular bone nonlinear elasticity using time-of-flight modulation," *IEEE Trans Ultrason Ferroelectr Freq Control*, vol. 55, no. 7, pp. 1497–507, 7 2008. [PubMed: 18986939]
- [371]. Zacharias K, Balabanidou E, Hatzokos I, Rekanos IT, and Trochidis A, "Microdamage evaluation in human trabecular bone based on nonlinear ultrasound vibro-modulation (NUVM)," *J Biomech*, vol. 42, no. 5, pp. 581–6, 3 26 2009. [PubMed: 19243780]

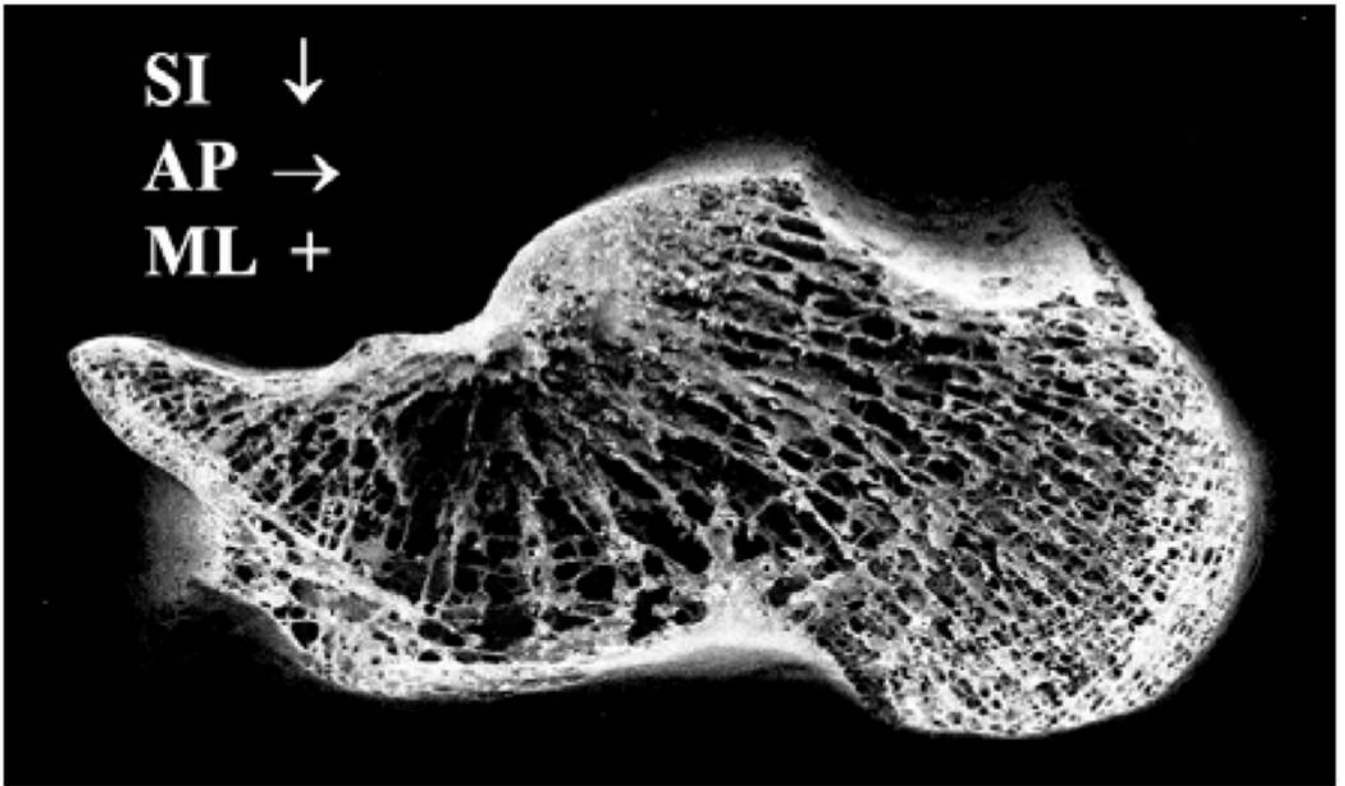
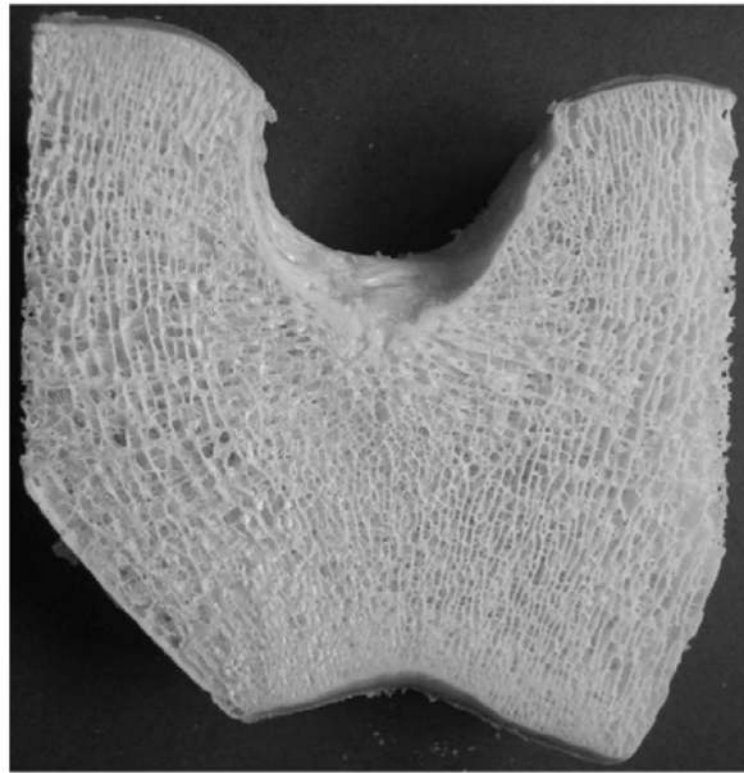


**Fig. 1.** Human calcaneus with lateral cortical endplates removed. Three orientations for ultrasound propagation are shown: superoinferior (SI), anteroposterior (AP), and mediolateral (ML). The most common orientation for ultrasound measurements *in vitro* and *in vivo* is ML.





(a)



(b)

**Fig. 2.** (a) human femurs. (b) cut slice showing cancellous bone corresponding to dashed box in (a). Reprinted with permission from M. Pakula *et al.*, Influence of the filling fluid on frequency-dependent velocity and attenuation in cancellous bones between 0.35 and 2.5 MHz, *J. Acoust. Soc. Am.*, 126, 3301-3310, 2009. Copyright 2009, Acoustical Society of America.

Power fit Attenuation= $-0.078+4.64 f^{1.49}$   $R^2 = 0.995$

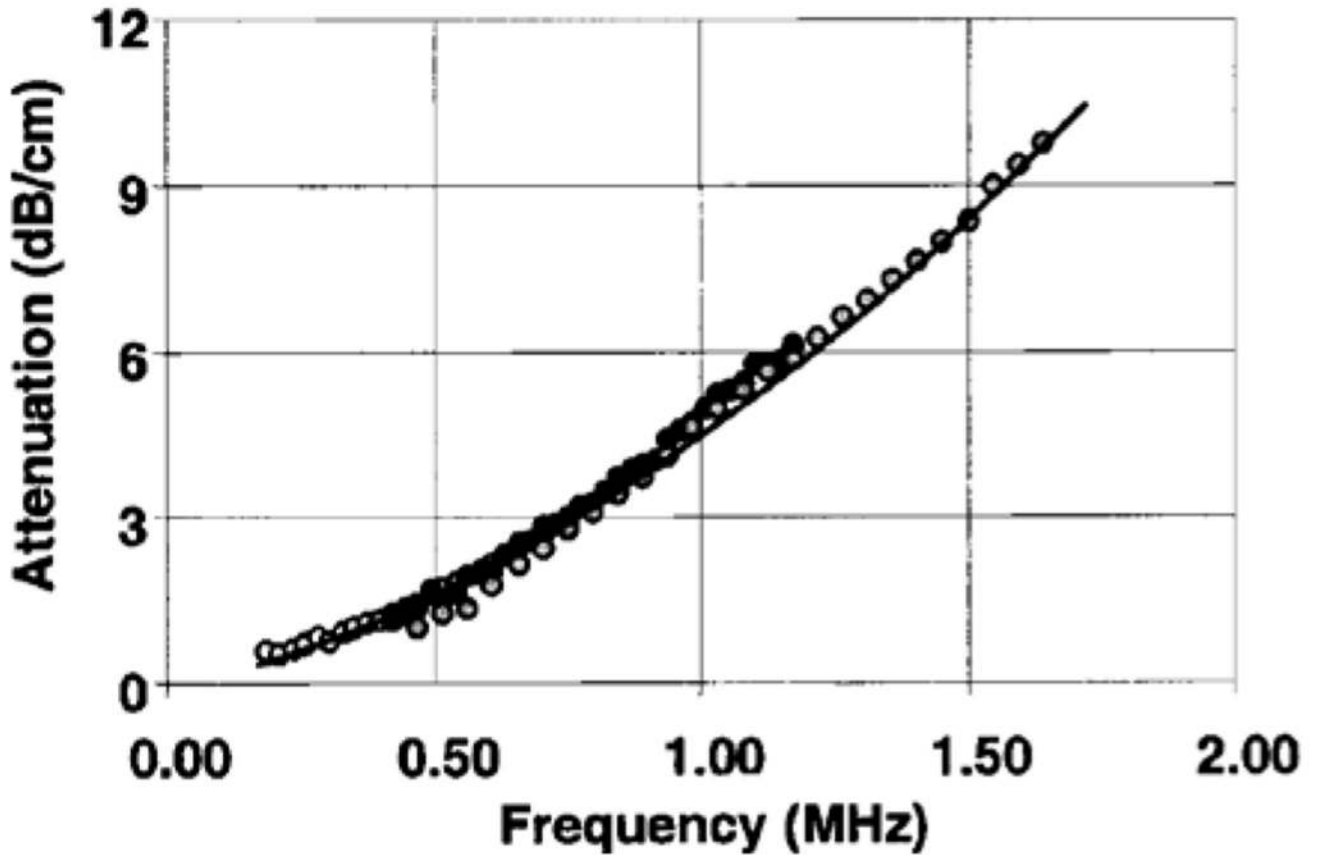
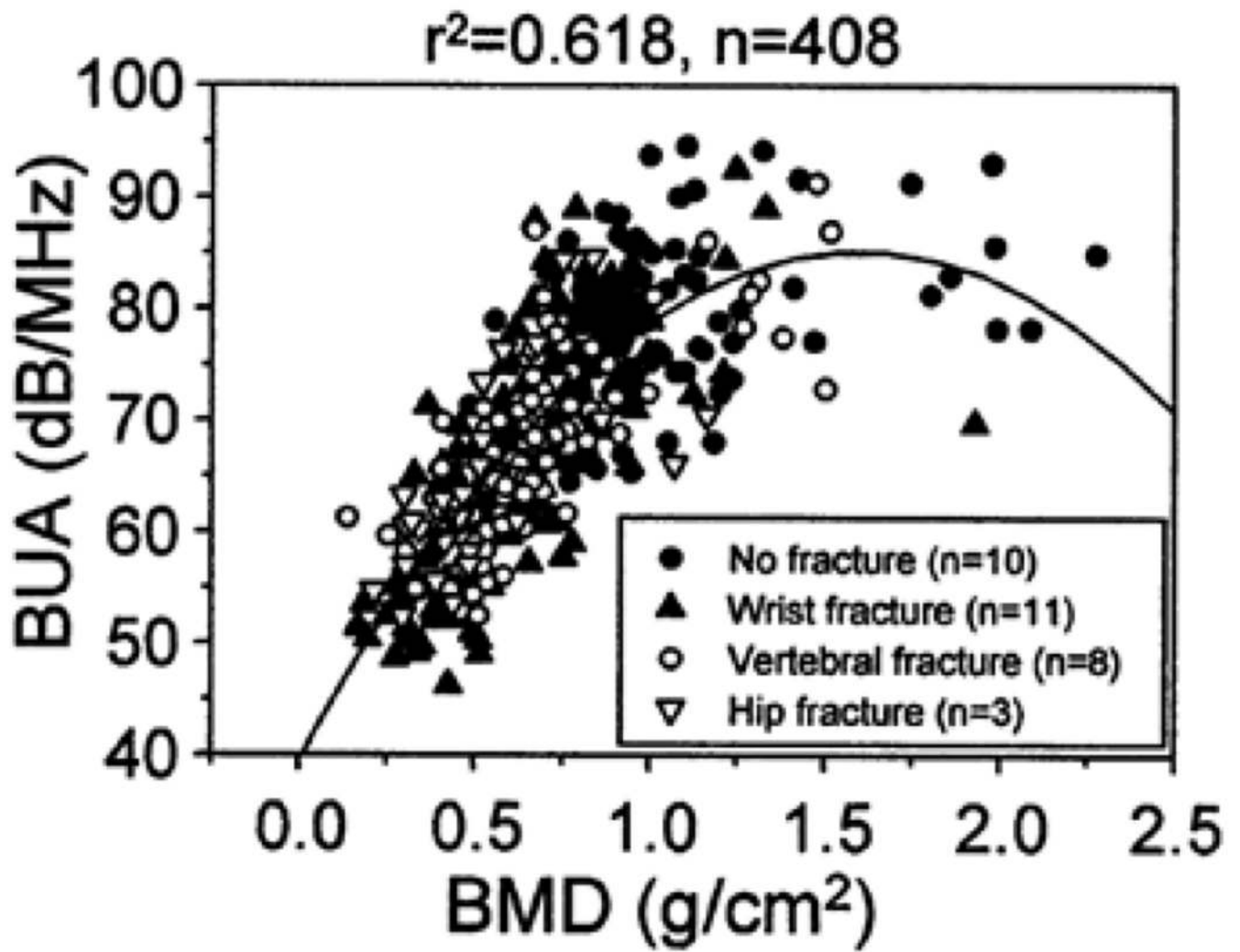
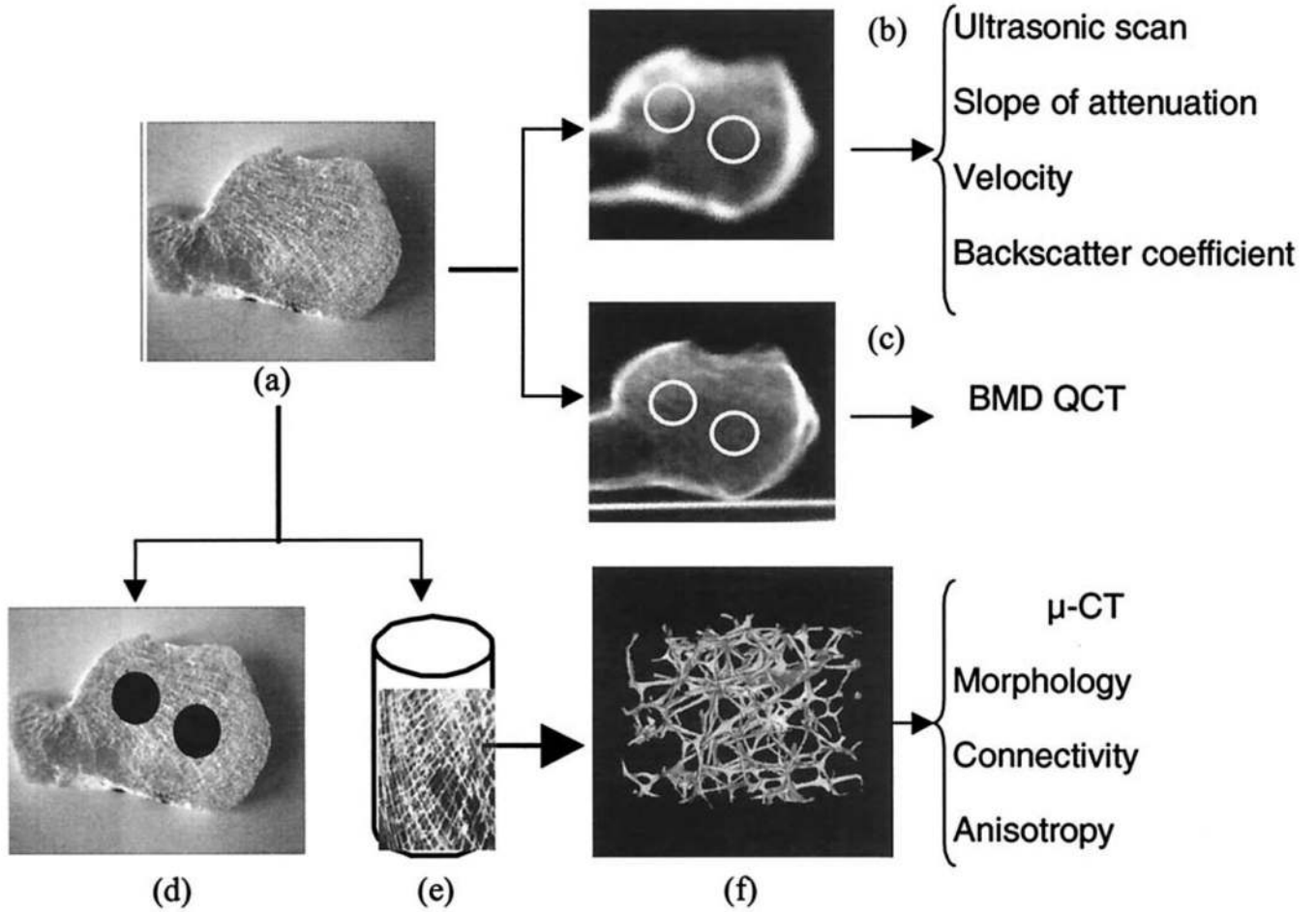


Fig. 3.

Attenuation coefficient of human cancellous calcaneus *in vitro* from 0.2-1.7 MHz. Although attenuation seems linear with frequency over a clinical bandwidth (*e.g.*, 300-700 kHz), it may be nonlinear over a broader bandwidth. Reprinted with permission from S. Chaffai *et al.*, In vitro measurement of the frequency-dependent attenuation in cancellous bone between 0.2 and 2 MHz, *J. Acoust. Soc. Am.*, 108, 1281-1289, 2000. Copyright 2000, Acoustical Society of America.



**Fig. 4.** BUA vs. areal BMD in human calcaneus *in vivo*. Reprinted, with permission from *Bone*, 31, Toyras *et al.*, Bone mineral density, ultrasound velocity, and broadband attenuation predict mechanical properties of trabecular bone differently, 503-5-7, Copyright (2002), with permission from Elsevier.



**Fig. 5.**

Steps for ultrasound and  $\mu$ CT analysis of cancellous calcaneus. Reprinted from *Bone*, 30, S. Chaffai *et al.*, Ultrasonic characterization of human cancellous bone using transmission and backscatter measurements: relationships to density and microstructure, 229-237, Copyright (2002), with permission from Elsevier.

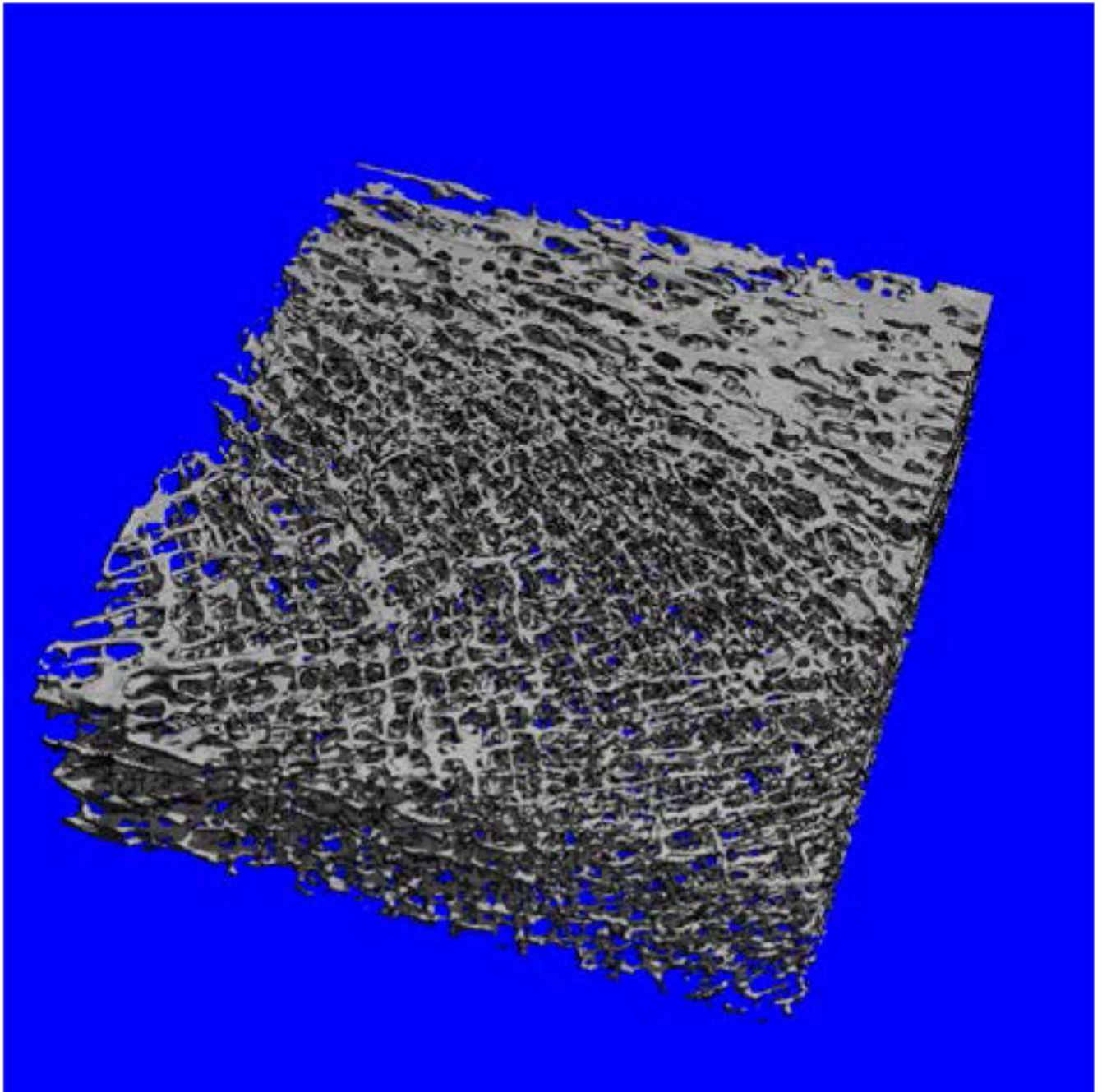


**Fig. 6.**  
 $\mu$ CT reconstruction of rectangular volume from human calcaneus with cortical endplates removed. © 2003 IEEE. Reprinted, with permission, from K. A. Wear and A. Laib, The dependence of ultrasonic backscatter on trabecular thickness in human calcaneus, *IEEE Trans Ultrason., Ferroelectr., and Freq. Contr.*, 50(8). 979-986. 2003.

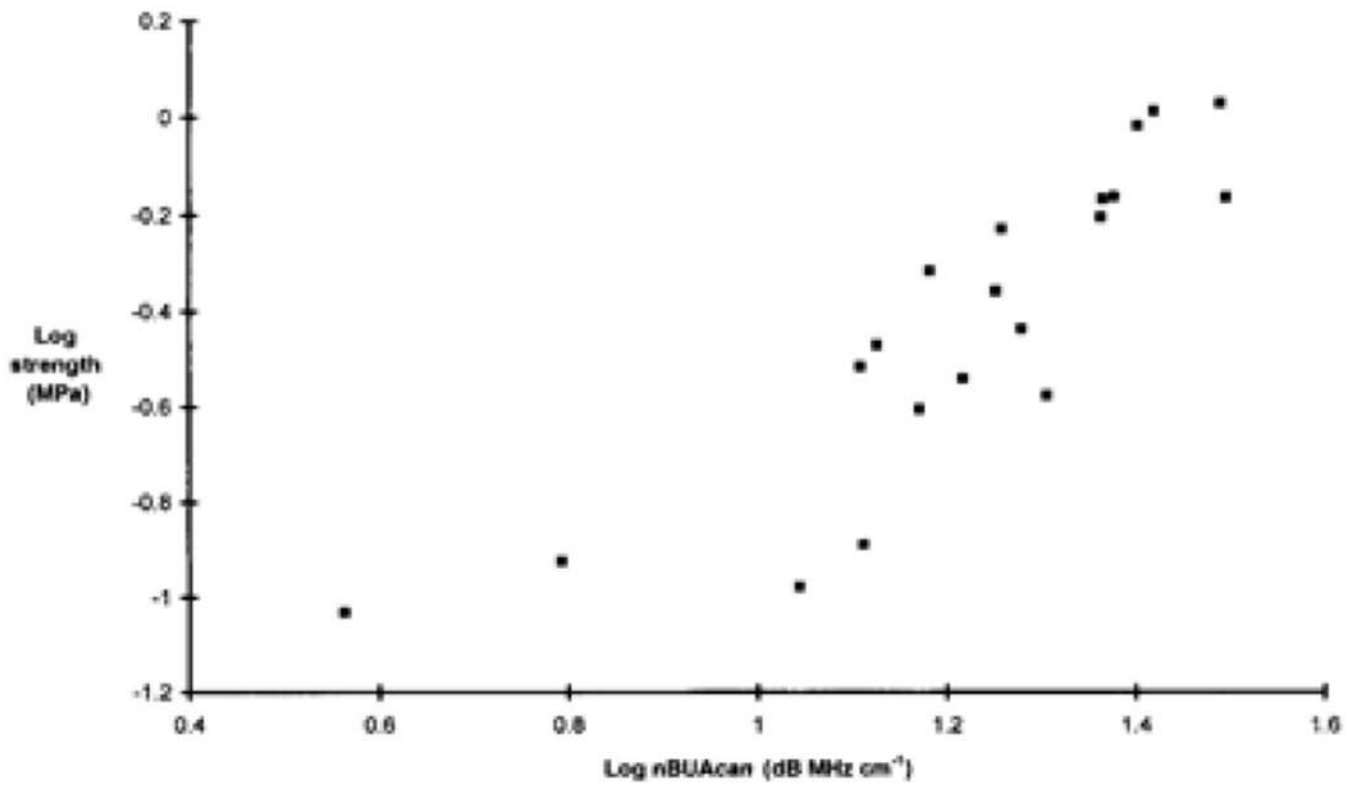


**Fig. 7.** Log strength vs log nBUA in human calcaneus *in vitro*. Reprinted with permission from *Bone*, 18, C. M. Langton *et al.*, Prediction of mechanical properties of the human calcaneus by broadband ultrasonic attenuation, 495-503, Copyright (1996), with permission from Elsevier.

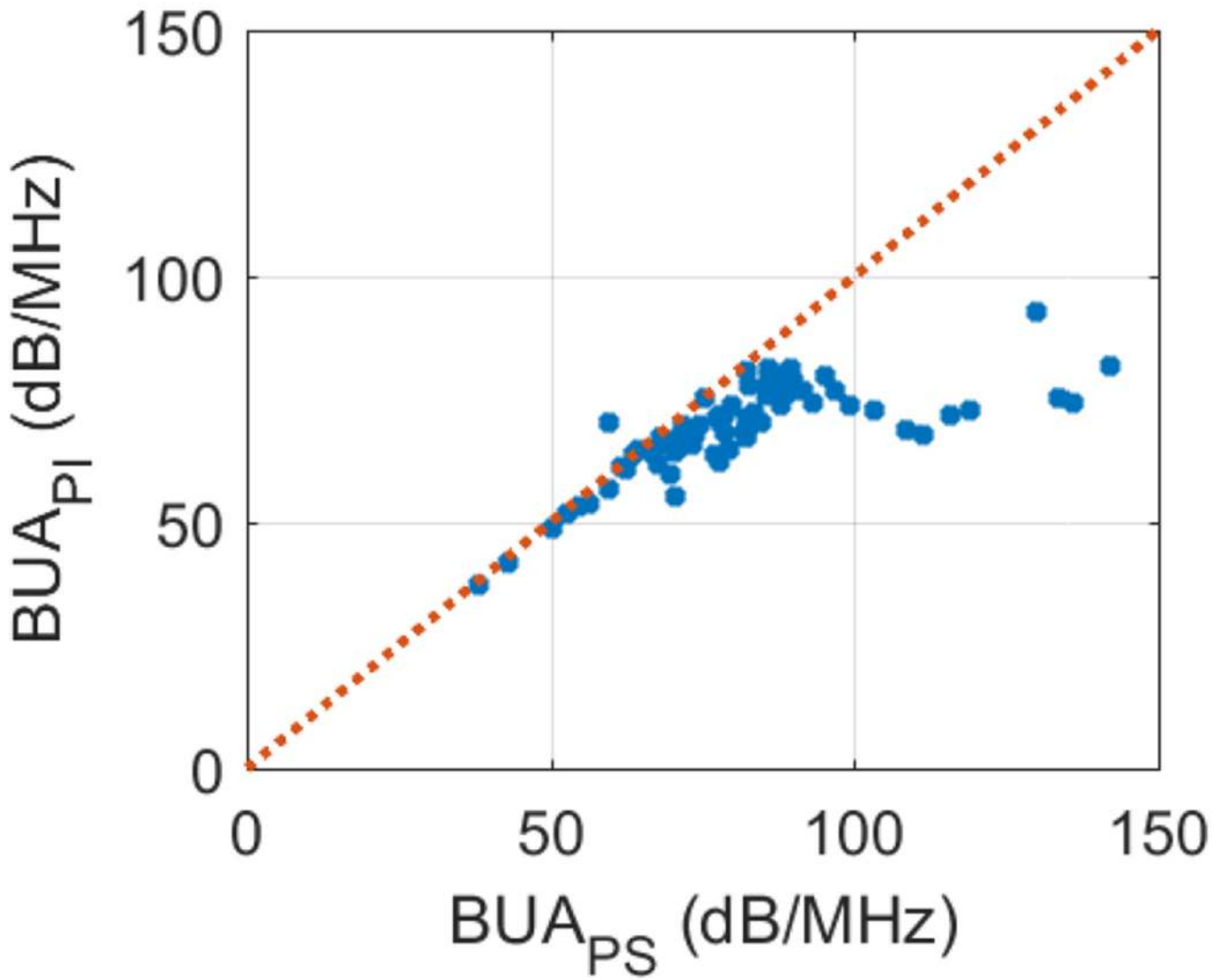


**Fig. 8.**

Phase insensitive (PI) vs. phase sensitive (PS) BUA in 73 women. © 2007 IEEE. Reprinted, with permission, from K. A. Wear, The effect of phase cancellation on estimates of calcaneal broadband ultrasound attenuation in vivo, *IEEE Trans Ultrason., Ferroelectr., and Freq. Contr.*, 54(7), 1353-1359, 2007.

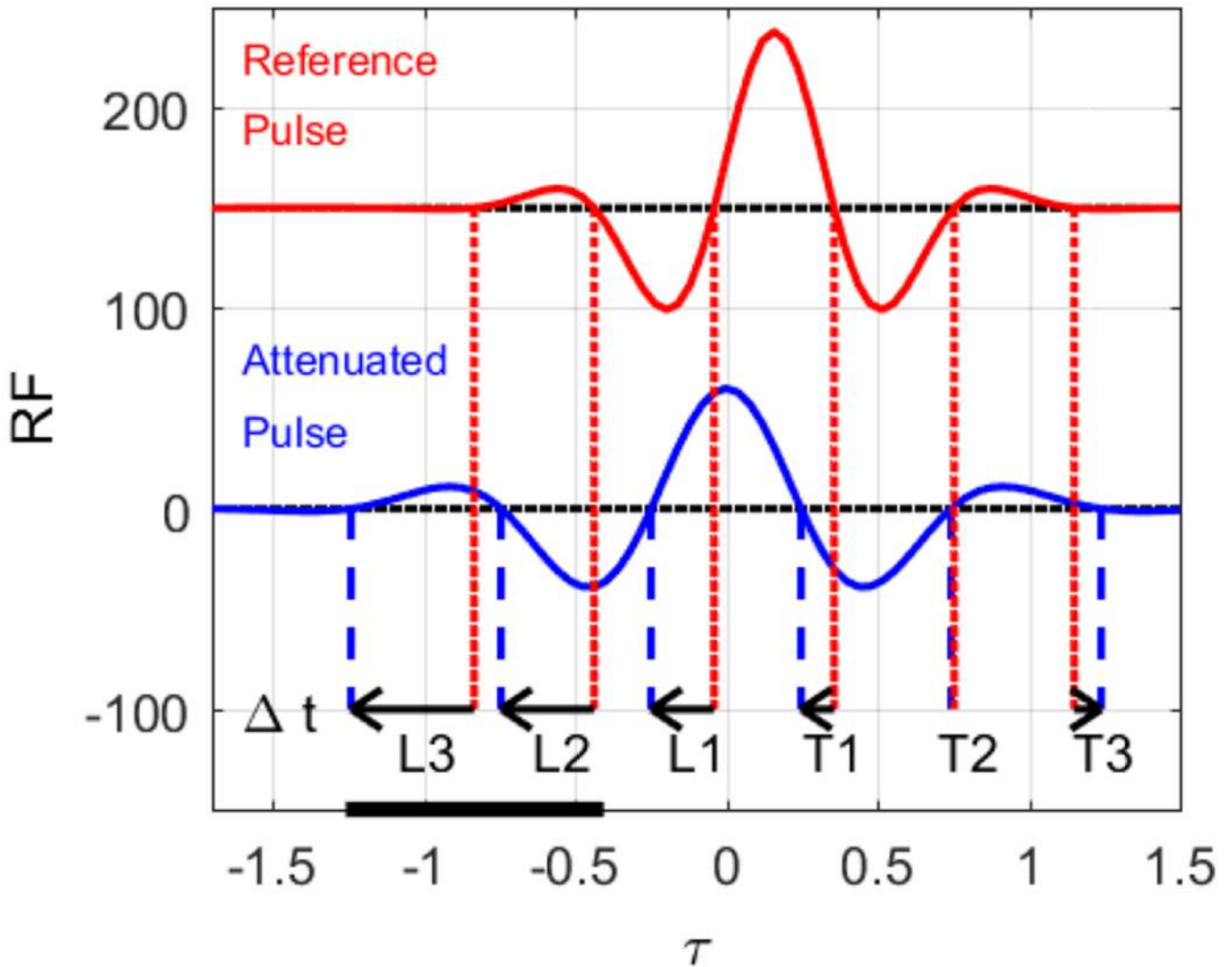


**Fig. 9.**

The effect of frequency-dependent attenuation and transit-time marker location on transit-time differential,  $\Delta t$ . Zero-crossing markers are labeled with an L for leading half or a T for trailing half and are numbered outward from the pulse center. The values for  $\Delta t$  for each marker location are shown by the black arrows. The variation in  $\Delta t$  with marker location is due to the fact that the attenuated pulse is stretched in time as a consequence of the low-pass filtering effect of frequency-dependent attenuation. The black bar on the time axis represents the mean  $\pm$  one standard deviation of marker locations used in 43 papers. See Table I. © 2008 IEEE. Reprinted, with permission, from K. A. Wear, A method for improved standardization of in vivo calcaneal time-domain speed-of-sound measurements, *IEEE Trans Ultrason., Ferroelectr., and Freq. Contr.*, 55(7), 1473-1479, 2008.



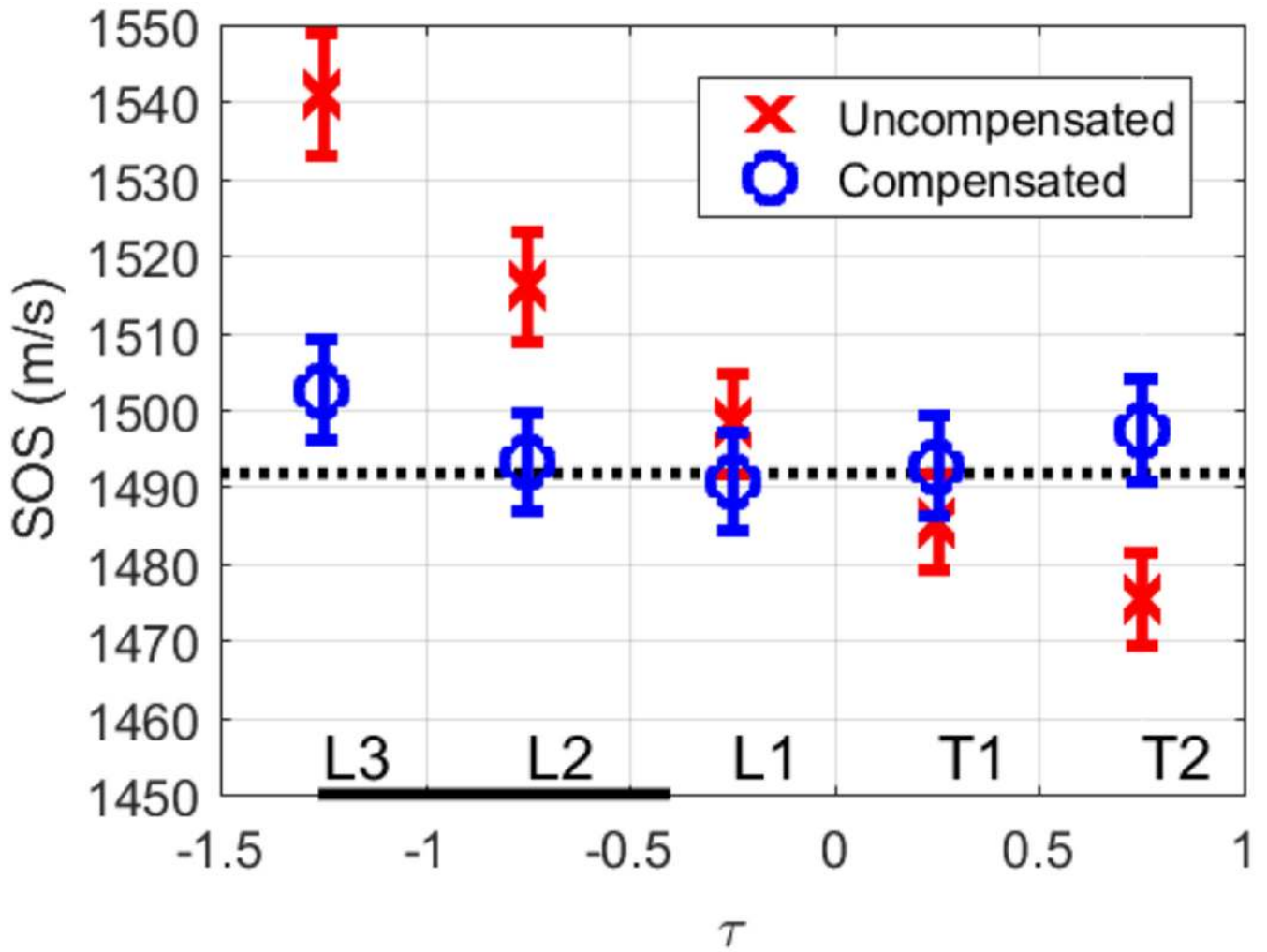


**Fig. 10.**

Average values for SOS from 73 women computed from 5 different transit-time markers. The x's were not compensated. The o's were compensated using (3). The black bar on the time axis represents the mean  $\pm$  one standard deviation of marker locations used in 43 papers. See Table I. © 2008 IEEE. Reprinted, with permission, from K. A. Wear, A method for improved standardization of in vivo calcaneal time-domain speed-of-sound measurements, *IEEE Trans Ultrason., Ferroelectr., and Freq. Contr.*, 55(7), 1473-1479. 2008.

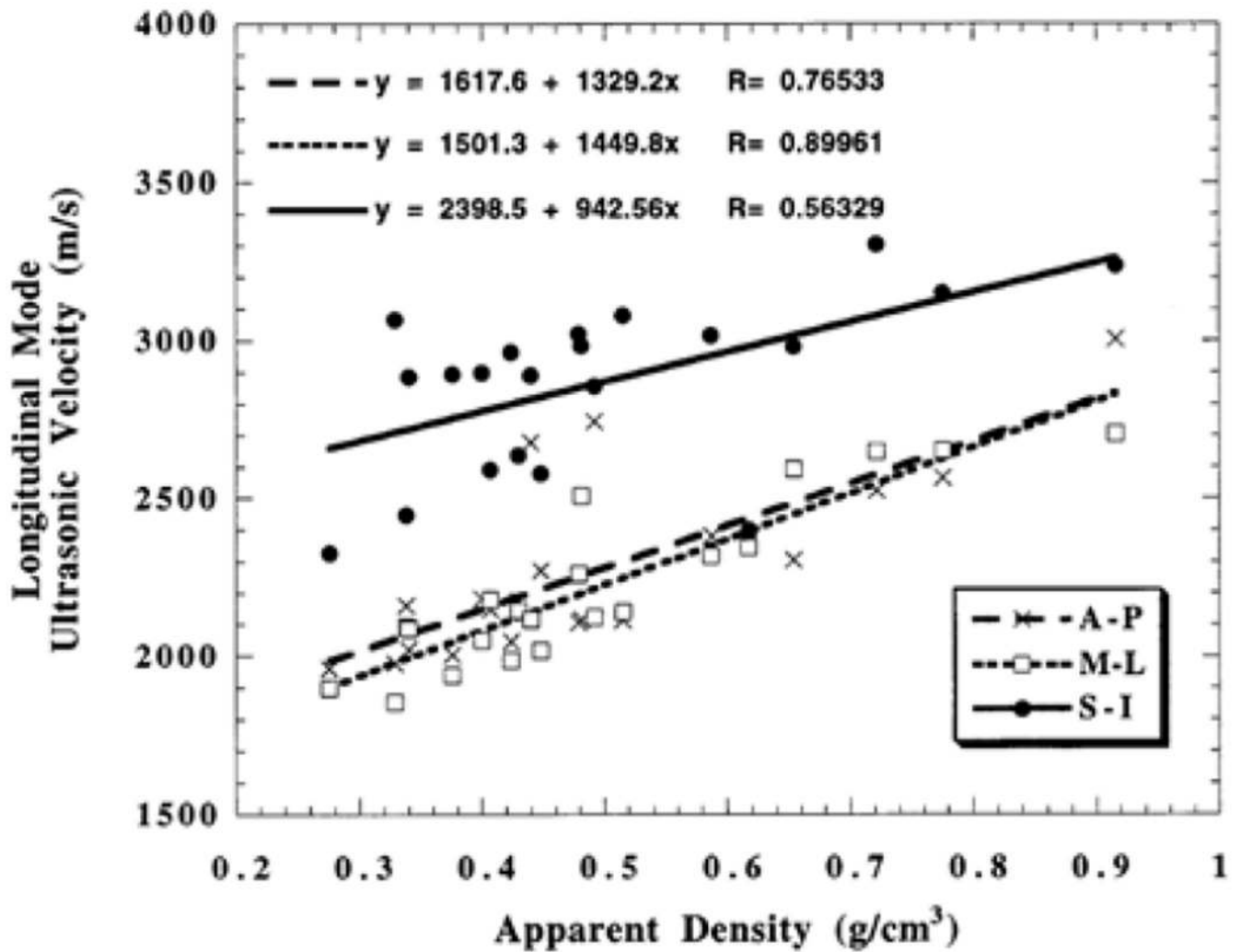


**Fig. 11.** Speed of sound vs. apparent density of bovine cancellous tibia *in vitro* in three orientations: anteroposterior (AP), mediolateral (ML), and superoinferior (SI). Reprinted from *Bone*, 26, B. K. Hoffmeister *et al.*, Low-megahertz ultrasonic properties of bovine cancellous bone, 635-642 Copyright (2000), with permission from Elsevier.

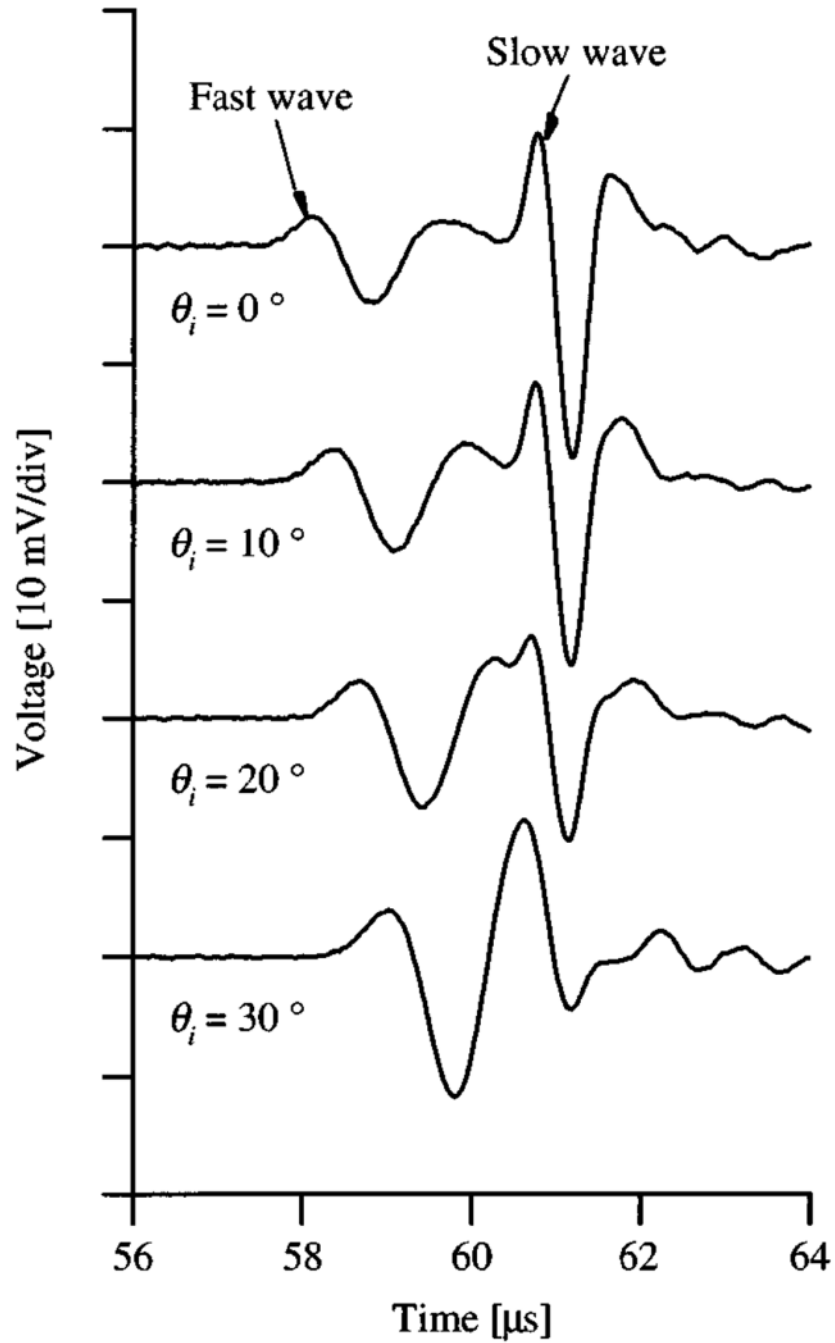


**Fig. 12.**

Fast and slow waves as a function of the angle between ultrasound propagation and main trabecular direction. Reprinted with permission from A. Hosokawa and T. Otani, *Acoustic anisotropy in bovine cancellous bone*, *J. Acoust. Soc. Am.*, 103(5), 2718-2722, 1998. Copyright 1998, Acoustical Society of America.

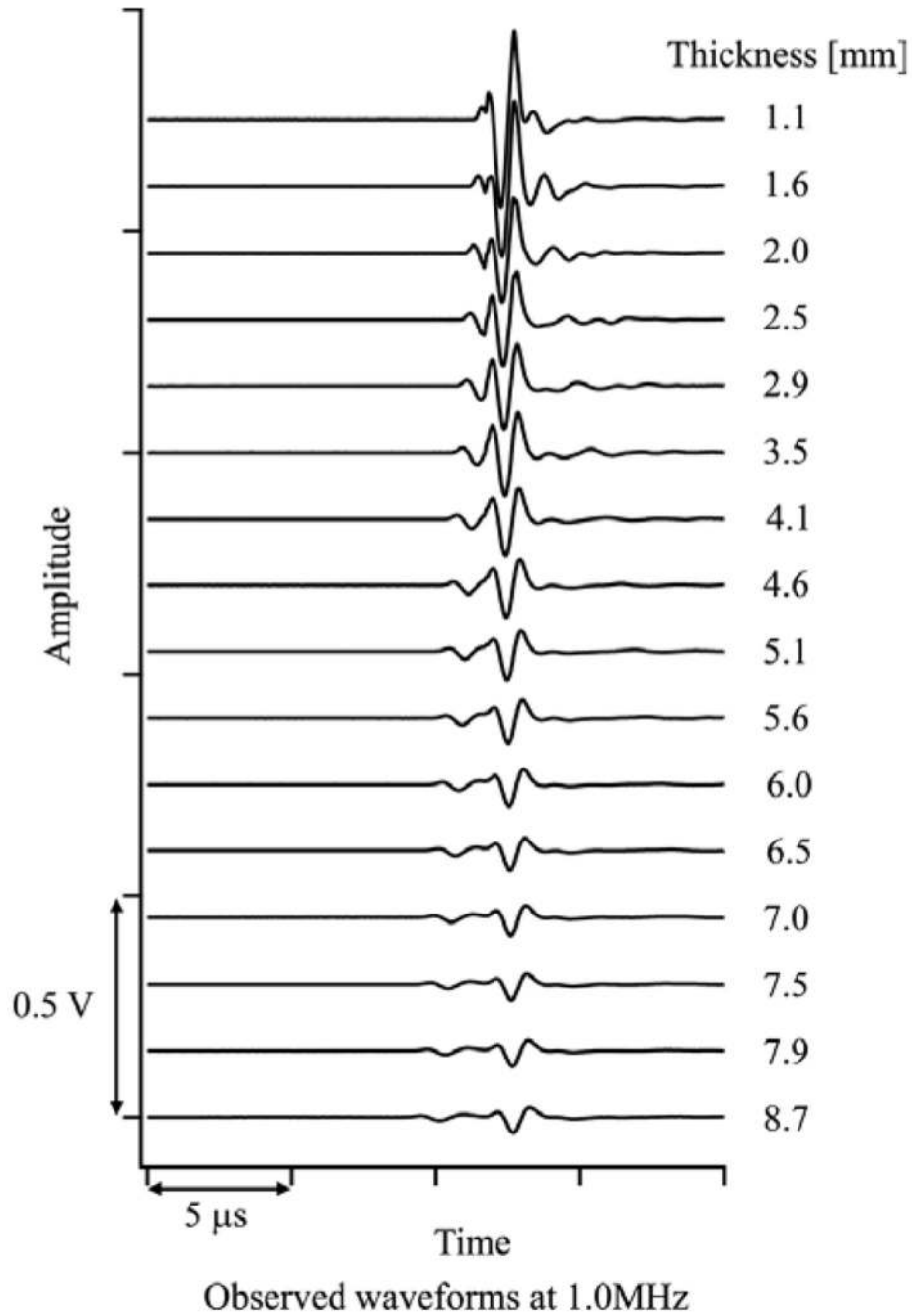


**Fig. 13.**

Through-transmitted signal from equine cancellous bone as a function of sample thickness from 1.1 to 8.7 mm. As the sample gets thicker, fast and slow wave magnitudes decrease due to attenuation and temporal separation between fast and slow waves increases due to longer propagation paths at different velocities. Reprinted with permission from F. Fujita *et al.*, An experimental study on the ultrasonic wave propagation in cancellous bone: Waveform changes during propagation, *J. Acoust. Soc. Am.*, 134(6), 4775-4781, 2013. Copyright 2013, Acoustical Society of America.



**Fig. 14.** Acquisition of backscatter data from human calcaneus *in vivo* using a standoff pad. Reprinted with permission from K. A. Wear and D. W. Armstrong III, Relationships among calcaneal backscatter, attenuation, sound speed, hip bone mineral density, and age in normal adult women, *J. Acoust. Soc. Am.*, 110(1), 573-578, 2001. Copyright 2001, Acoustical Society of America.

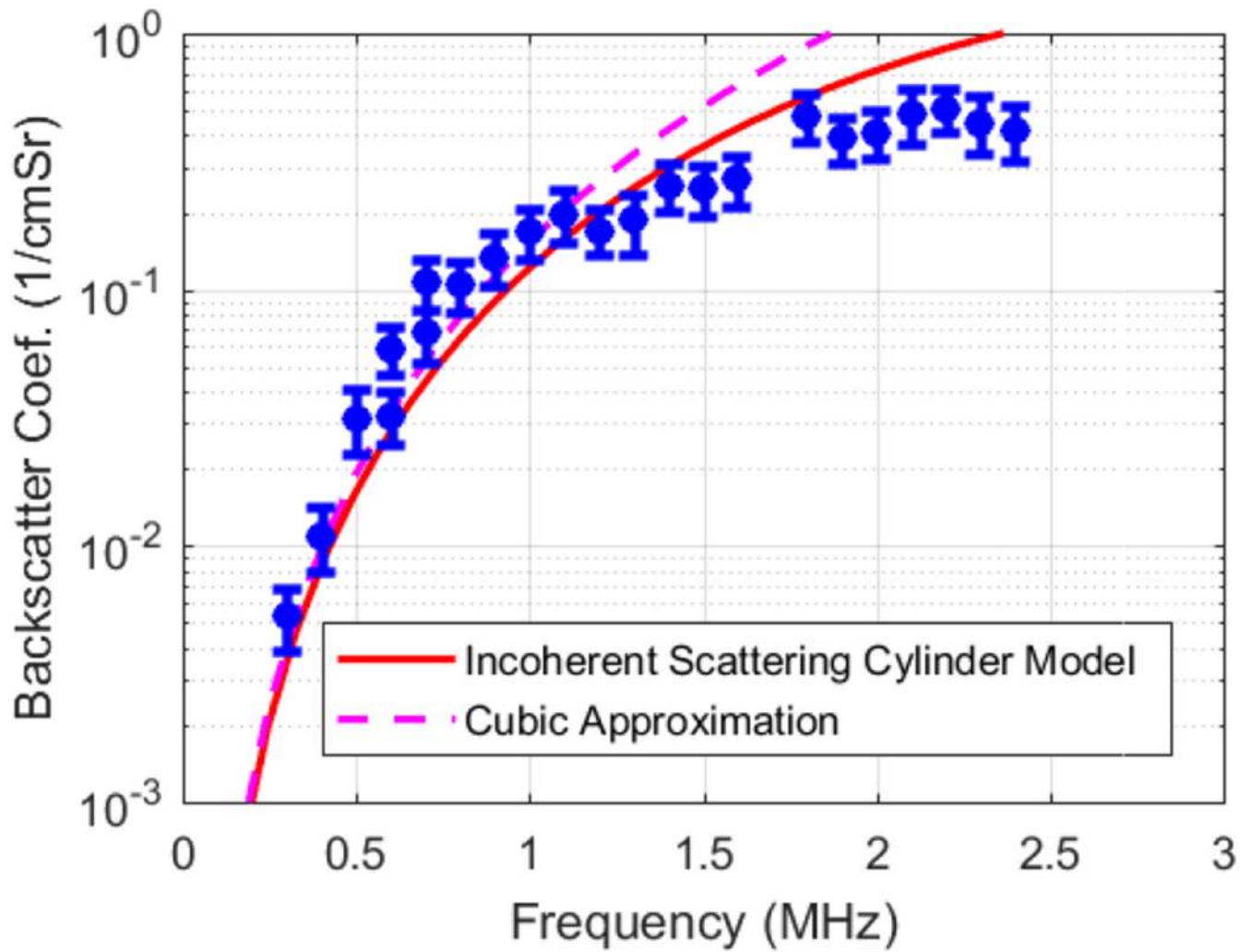


**Fig. 15.** Backscatter coefficient vs. frequency measured from 16 human calcaneus samples *in vitro*. Reprinted with permission from K. A. Wear, Frequency dependence of ultrasonic backscatter from human trabecular bone: theory and experiment, *J. Acoust. Soc. Am.*, 106(6), 3659-3664, 1999. Copyright 1999, Acoustical Society of America.

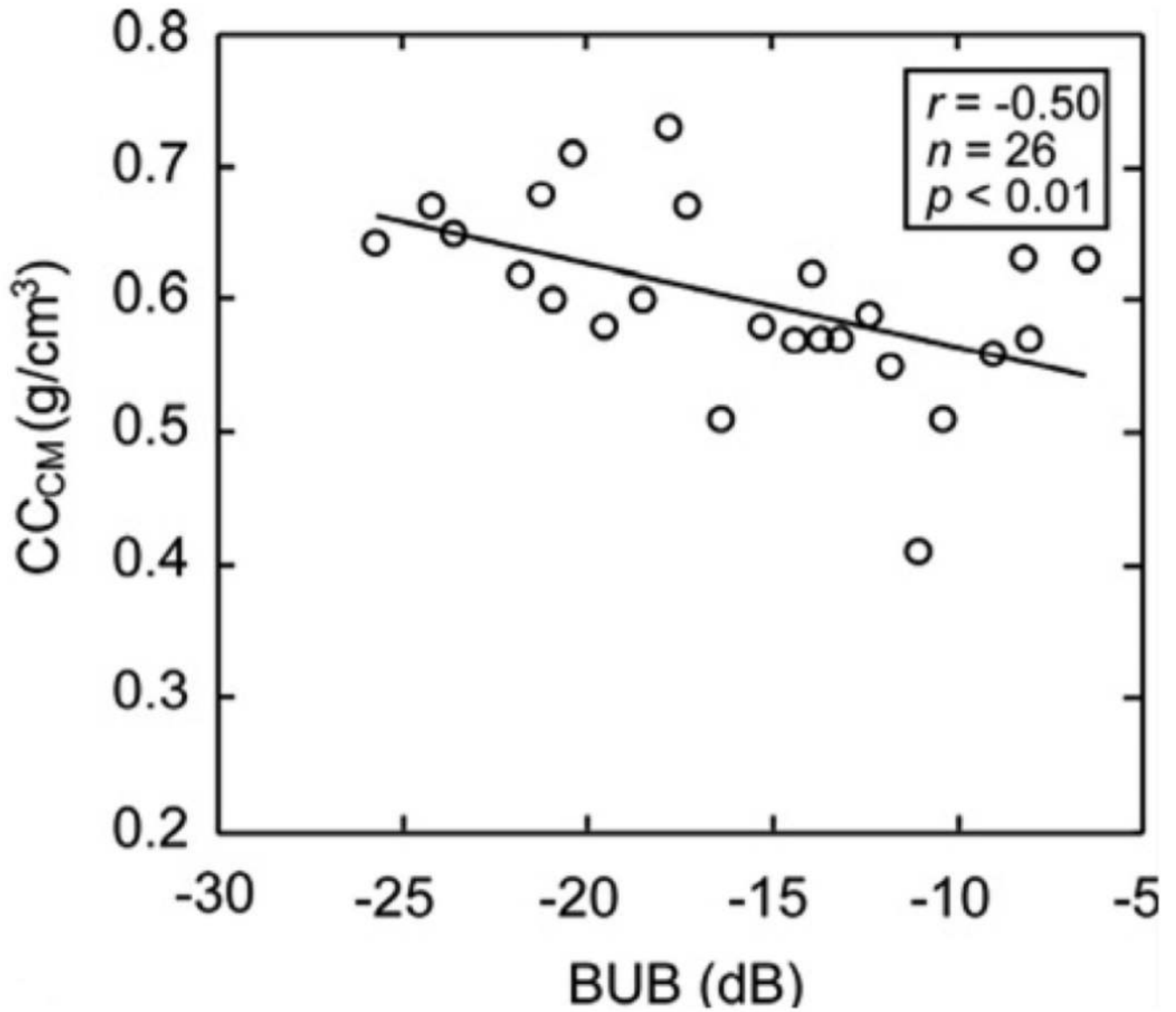


**Fig. 16.** Collagen content (CC) vs. broadband ultrasonic backscatter (BUB). Reprinted from *Ultrasound in Med. & Biol.*, 33, Riekkinen *et al.*, Acoustic properties of trabecular bone—relationships to tissue composition, 1438-1444, Copyright (2007), with permission from Elsevier.

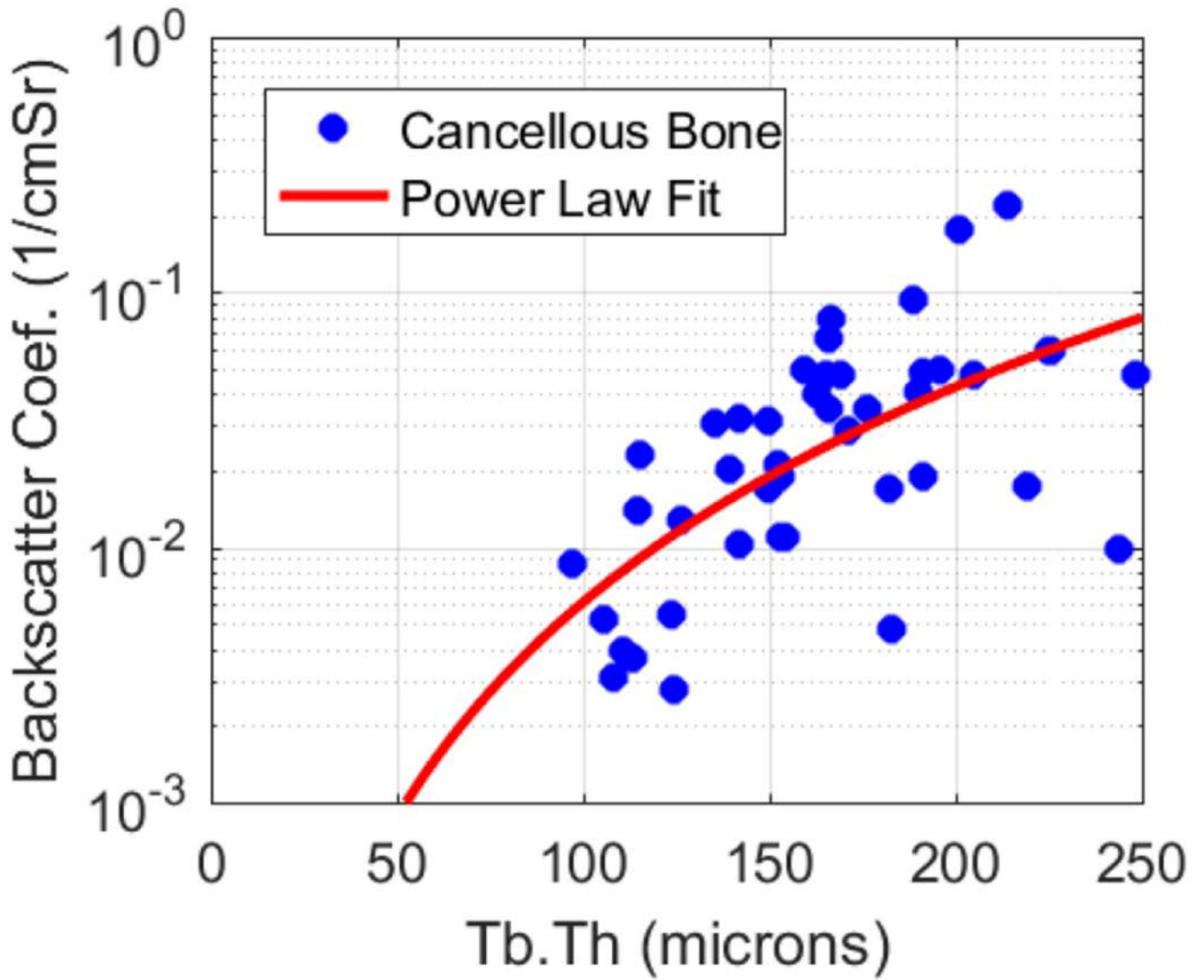


**Fig. 17.**

Backscatter coefficient vs. mean trabecular thickness Tb.Th (measured with  $\mu$ CT) measured from 43 human cancellous femur samples *in vitro*. © 2003 IEEE. Reprinted, with permission, from K. A. Wear and A. Laib, The dependence of ultrasonic backscatter on trabecular thickness in human calcaneus, *IEEE Trans Ultrason., Ferroelectr., and Freq. Contr.*, 50(8), 979-986. 2003.



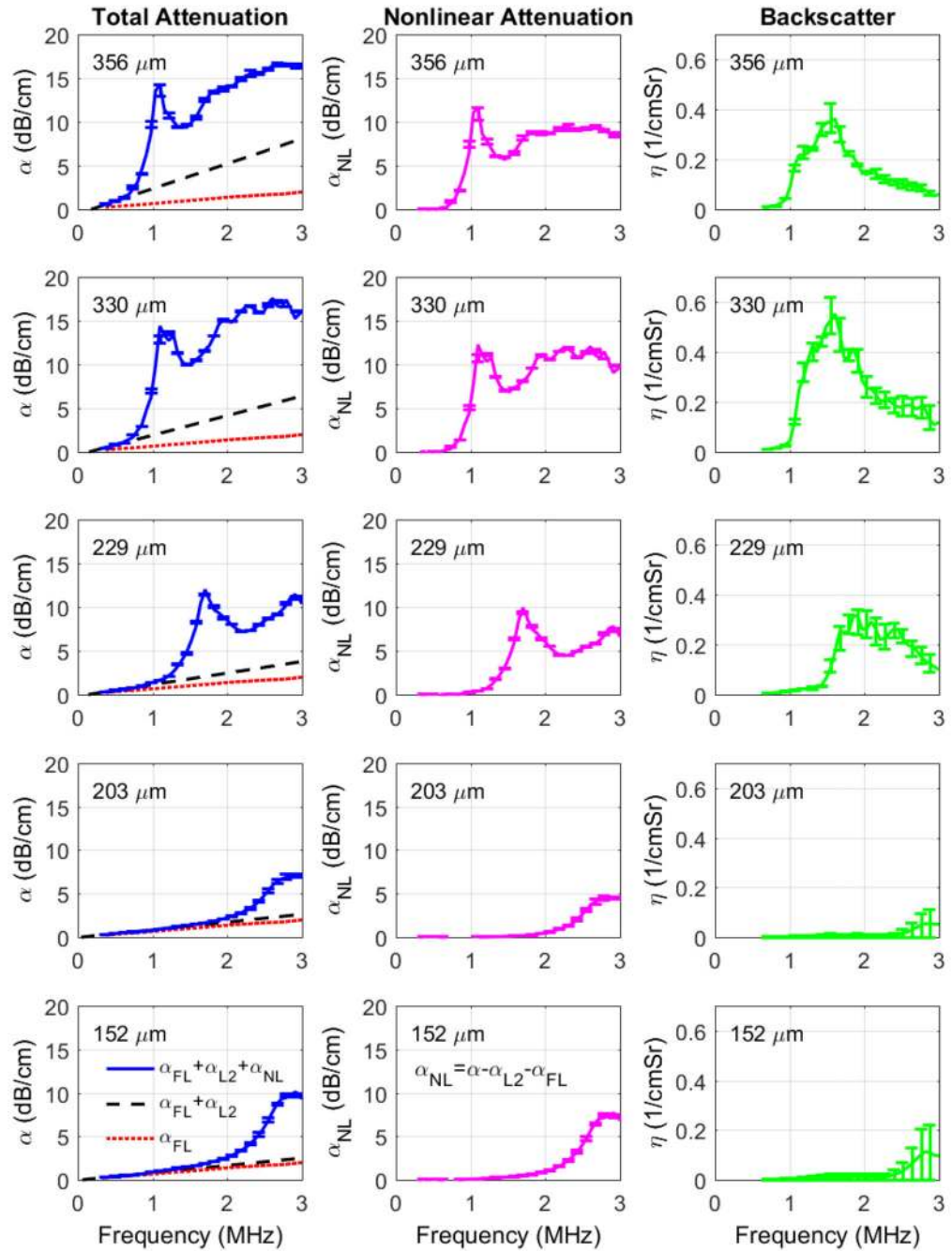


**Fig. 18.**

Total attenuation (left column), nonlinear component of attenuation (middle column) and backscatter coefficient (right column) for 5 phantoms containing nylon filaments (simulating trabeculae) suspended in a soft-tissue-mimicking fluid (simulating marrow). The left panel shows measurements of attenuation coefficient vs. frequency. The red dotted lines correspond to frequency-dependent attenuation coefficients measured from the reference phantom (i.e., phantom without nylon filaments). The black dashed lines correspond to linear fits of attenuation coefficient vs. frequency at low frequencies. The middle panel

shows the nonlinear component of attenuation coefficient,  $\alpha_{\text{NL}}(f)$  which is the difference between  $\alpha(f)$  (left panel) and the low-frequency linear fit to  $\alpha(f)$  (left panel, black dashed line). The right panel shows measurements of backscatter coefficient,  $\eta(f)$ . © 2008 IEEE. Reprinted, with permission, from K. A. Wear, Mechanisms for attenuation in cancellous-bone-mimicking phantoms, *IEEE Trans Ultrason., Ferroelectr., and Freq. Contr.*, 55(11), 2418-2425. 2008.



**Fig. 19.** Aluminum foam sample to mimic cancellous bone. Reprinted with permission from C. Zhang *et al.*, Measurements of ultrasonic phase velocities and attenuation of slow waves in cellular aluminum foams as cancellous bone-mimicking phantoms, *J. Acoust. Soc. Am.*, 129(5), 3317-3326, 2011. Copyright 2011, Acoustical Society of America.

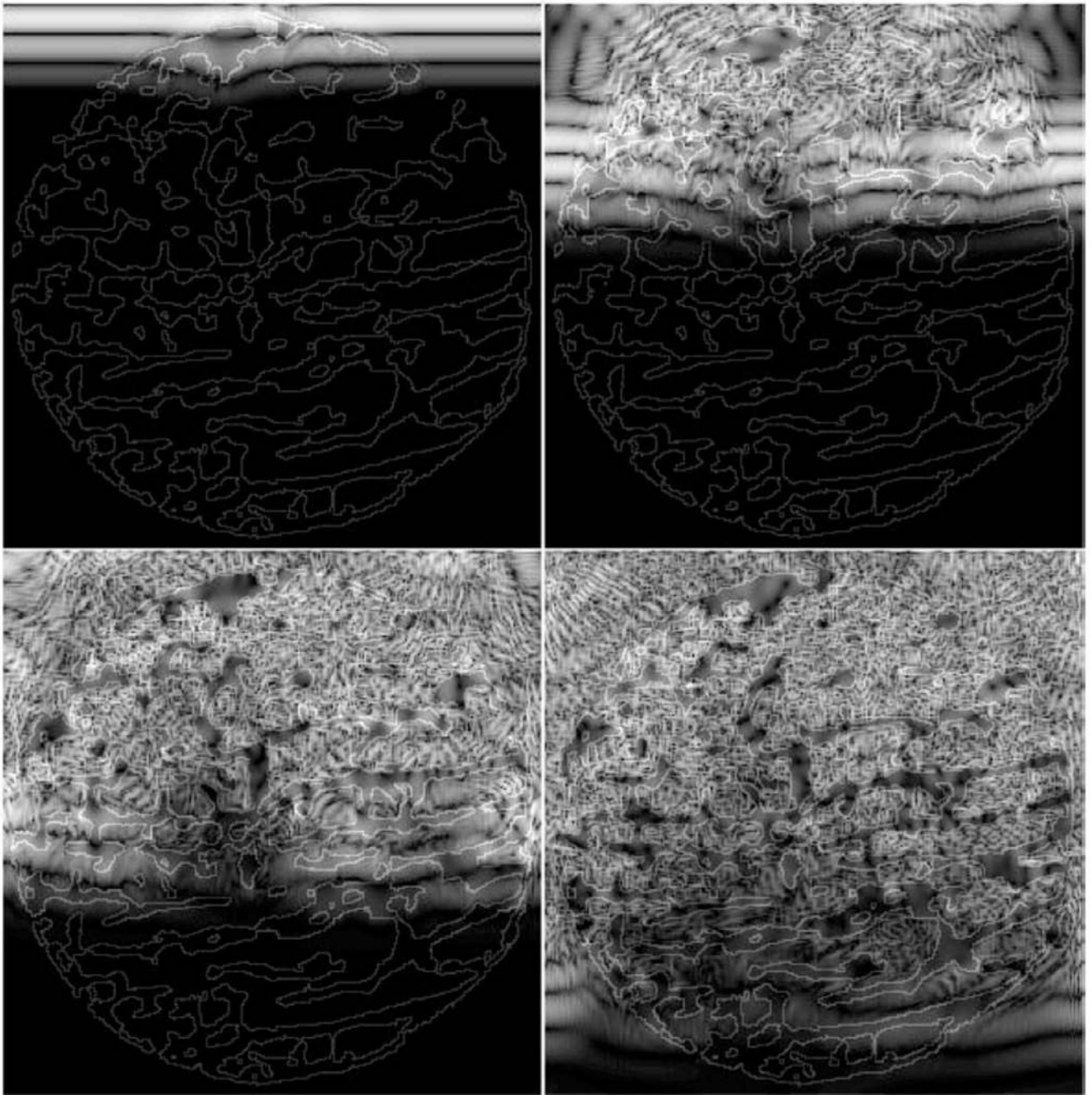


**Fig. 20.** Snapshots of waves propagating through cancellous bone, showing ballistic and scattered components. © 2008 IEEE. Reprinted, with permission, from J. J. Kaufman, Ultrasound Simulation in Bone, *IEEE Trans Ultrason., Ferroelectr., and Freq. Contr.*, 55(6), 1205-1218, 2008.

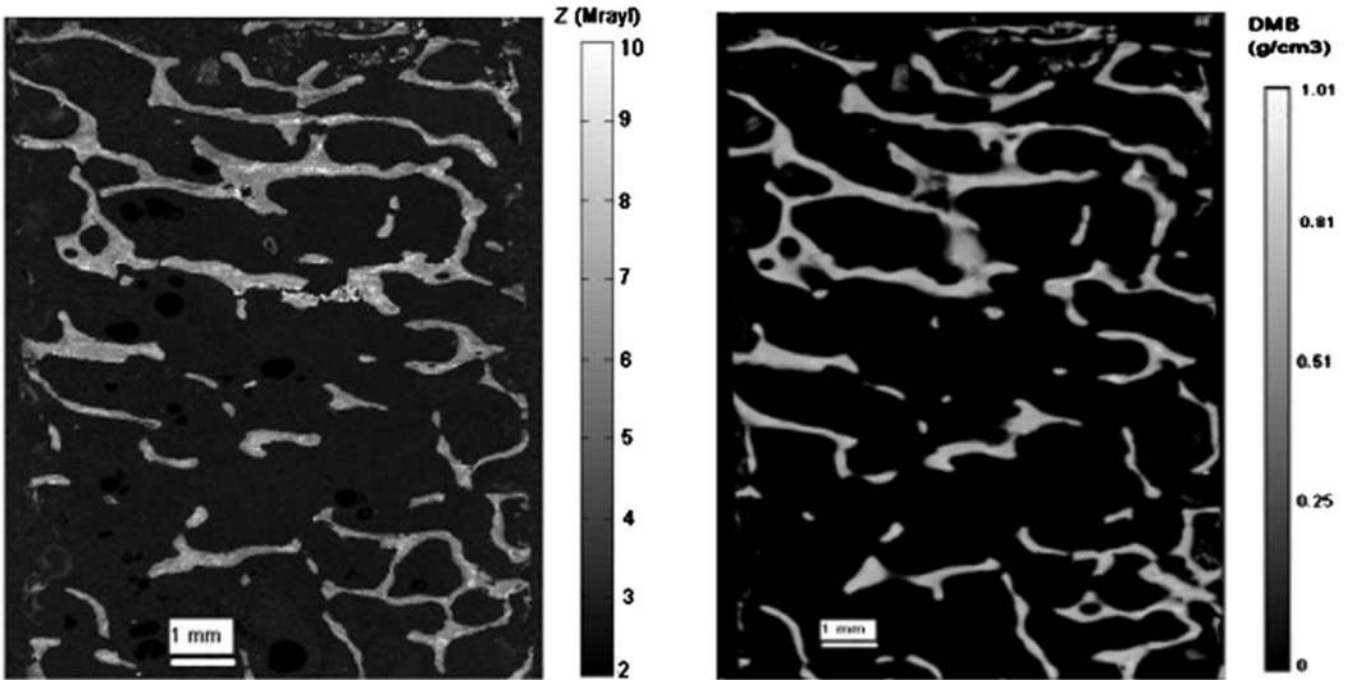


**Fig. 21.** Site-matched acoustic impedance measured with acoustic microscopy (left) and degree of mineralization of bone measured with synchrotron radiation  $\mu$ CT (right) from bovine cancellous sternum. Reprinted from *Ultrasound in Med. & Biol.*, 36, Rupin *et al.* Adaptive remodeling of trabecular bone core cultured in 3-D bioreactor providing cyclic loading: an acoustic microscopy study, 999-1007, Copyright (2010), with permission from Elsevier.

TABLE I.

## ACRONYMS

ABTF	Apparent Backscatter Transfer Function (dB)
AIB	Apparent Integrated Backscatter (dB)
AP	Anteroposterior
BMD	Bone Mineral Density ( $\text{g}/\text{cm}^2$ for areal or projection methods like DXA; $\text{g}/\text{cm}^3$ for volumetric methods like QCT)
BSCS	Backscattered Spectral Centroid Shift (MHz)
BV/TV	Bone Volume Fraction = Bone Volume / Total Volume
BUA	Broadband Ultrasound Attenuation (dB/MHz)
BUB	Broadband Ultrasound Backscatter ( $1/\text{cmSr}$ )
DXA	Dual-energy X-ray Absorptiometry
EDTA	Ethylenediaminetetraacetic acid
FMA	Frequency Modulated Attenuation (dB/cm)
FSAB	Frequency Slope of Apparent Backscatter (dB/MHz)
IRC	Integrated Reflection Coefficient
ML	Mediolateral
MLSP	Modified Least Squares Prony's (method)
MLSP+CF	MLSP plus Curve Fitting
NTD	Net time delay ( $\mu\text{s}$ )
$\mu\text{CT}$	Micro Computed Tomography
nBUA	Normalized BUA= $\text{BUA}/\text{sample thickness}$ (dB/cmMHz)
SOS	Speed of Sound (m/s)
QCT	Quantitative Computed Tomography
QUS	Quantitative Ultrasound
SAGE	Space Alternating Generalized Expectation maximization
SI	Superoinferior
Tb.Th	Mean trabecular thickness ( $\mu\text{m}$ )

**TABLE II.**

## WAVEFORM MARKERS FOR SOS MEASUREMENTS

Marker	$\tau_n$	# References
First detectable deviation from zero (L3)	-1.25	13
3 times noise standard deviation	$\sim -1.2$	1
10% of first rising half cycle	-1.19	4
15% of first rising half cycle	-1.18	1
20% of first rising half cycle	-1.17	3
10% of maximum amplitude	-1.08	1
First maximum	-1	3
"First" zero crossing (L2)	-0.75	17
"Second" zero crossing (L1)	-0.25	3
Envelope maximum	0	7
Mean $\pm$ standard deviation	$-0.83 \pm 0.42$	

$\tau_n$  = offset of waveform time marker from envelope maximum divided by the oscillation period. On the leading half of the pulse,  $\tau_n < 0$ . On the trailing half of the pulse,  $\tau_n > 0$ .